UNIVERSITY OF CALIFORNIA SAN DIEGO

Deciphering the multi-faceted roles of Shp2 in liver tumorigenesis

A dissertation submitted in partial satisfaction of the
requirements for the degree Doctor of Philosophy

in

Biology

by

Jijun Liu

Committee in charge:

Professor Gen-Sheng Feng, Chair
Professor Alexandra Newton
Professor Jing Yang
Professor Ye Zheng
Professor Elena Zuniga

2022

The Dissertation of Jijun Liu is approved, and it is acceptable in quality and form for publication on microfilm and electronically.

University of California San Diego

2022

TABLE OF CONTENTS

LIST OF FIGURES

LIST OF TABLES

ACKNOWLEDGEMENTS

I would like to acknowledge Professor Gen-Sheng Feng for his guidance and support as my thesis advisor and the chair of my committee. I am also grateful for his trust in my capability as an independent scientific researcher. I would like to thank my committee members for their valuable suggestions and generous support.

I would like to acknowledge Yanjie Li, Wendy Chen, Yan Liang, Gaowei Wang, Min Zong, Kota Kaneko, Bing Xin, Li Du, Lydia Chen, Yanyan Long, Kaisa Hanley, Jin Lee and other members and alumni of Feng lab, for the selfless and incalculable help from these kindest and smartest human being.

I would like to acknowledge UCSD School of Medicine Microscopy Core, UCSD Tissue Technology Shared Resource and UCSD Human Embryonic Stem Cell Core Facility for providing resources and technical assistance for conducting experiment and generating data. I would like to acknowledge Dr. N Varki (UCSD) for the pathological examination of tumor samples and Drs. P Sun (Wake Forest) B. Dong (Baylor) for the advice to cell senescence assay.

I would like to acknowledge Dr. David Goeddel, Division of Biological Sciences and Moores Cancer Center of UCSD for awarding me David V. Goeddel Chancellor's Graduate Fellowship and Cancer Biology Research Graduate Fellowship.

I would like to thank my family and friends in San Diego, in other parts of America and on the other side of Pacific Ocean in China, for their immeasurable care, love, companion, trust and encouragement. Especially I am really grateful to have Youtong Huang ("Pangpang"), Ye Zhang ("Yeye") and Wendy Chen ("Wenwen") as my best friends in graduate school. Graduate school years would not have been so smooth and fruitful, without the joy, warmth, laughter, friendship and girl power that they brought to me.

Last but not least, I would like to send my deepest acknowledgement and love to my parents. They have provided me unconditional and enormous love, acceptance, appreciation, encouragement and guidance throughout my life, and they always grant me strength and confidence to try, to mature and to pursue. Without them, I couldn't have gone so far in this journey and become who I am now. Thank you Dedi and Mami.

This dissertation from Chapter 1 through Chapter 5, in part, is a reprint of the material as it appears in Shp2 deletion in hepatocytes suppresses hepatocarcinogenesis driven by oncogenic β-Catenin, PIK3CA and MET. Jacey Jijun Liu, Yanjie Li, Wendy Chen, Yan Liang, Gaowei Wang, Min Zong, Kota Kaneko, Ruiyun Xu, Michael Karin, Gen-Sheng Feng, Journal of Hepatology, 2018. The dissertation author was the primary investigator and author of this paper.

This dissertation from Chapter 1 through Chapter 5, in part, has been accepted for publication of the material as it may appear in Pharmaceutical Shp2 Inhibition Suppresses Primary and Metastasized Liver Tumors by Provoking Hepatic Innate Immunity, Jacey Jijun Liu, Bing Xin, Li Du, Lydia Chen, Yanyan Long, Gen-Sheng Feng, Hepatology, 2022. The dissertation author was the primary investigator and author of this paper.

VITA

2015 Bachelor of Science, Hong Kong University of Science and Technology, Hong Kong, China

2022 Doctor of Philosophy, University of California San Diego

PUBLICATIONS

"Shp2 deletion in hepatocytes suppresses hepatocarcinogenesis driven by oncogenic β-Catenin, PIK3CA and MET" Journal of Hepatology, Volume 69, Issue 1, July 2018, Pages 79-88.

FIELD OF STUDY

Major Field: Biology

Studies in Cancer Biology and Hepatology

Professor Gen-Sheng Feng

ABSTRACT OF THE DISSERTATION

Deciphering multi-faceted roles of Shp2 in liver tumorigenesis

by

Jijun Liu

Doctor of Philosophy in Biology

University of California San Diego, 2022

Professor Gen-Sheng Feng, Chair

Shp2 is an SH2-tyrosine phosphatase acting downstream of receptor tyrosine kinases (RTKs) as a positive regulator of signal transduction. Despite its proto-oncogenic role, recent data demonstrated a liver tumor-suppressing role for Shp2, as ablating Shp2 in hepatocytes aggravated hepatocellular carcinoma (HCC) induced by chemical carcinogen. I further investigated the possible multi-faceted roles of Shp2 by examining the effect of hepatocyte specific ablation of Shp2 on oncogene-induced autochthonous liver tumor formation. Despite the induction of hepatic oxidative and metabolic stresses, Shp2 deletion in hepatocytes suppressed hepatocarcinogenesis

driven by overexpression of oncoproteins Met/β-catenin or Met/PI3K-p110α. Mechanistically, Shp2 loss inhibited proliferative signaling from oncogenic pathways and triggered cell senescence following exogenous expression of the oncogenes. Further, I demonstrated that the catalytic activity of Shp2 was essential for relay of oncogenic signals from RTK in HCC and that chemical inhibition of Shp2 robustly suppressed HCC driven by RTK. However, in contrast to a tumor-promoting hepatic niche generated by genetic deletion of Shp2 in hepatocytes, pharmacological Shp2 inhibition had a tumor-suppressing effect on liver metastasized tumor progression. Mechanistically, the Shp2 inhibitor enhanced an innate anti-tumor immunity by downregulating inflammatory cytokines, suppressing the CCR5 signaling axis and upregulating interferon-β secretion. Collectively, this dissertation study dissected multi-faceted roles of Shp2 in hepatocarcinogenesis, as well as provided preclinical evidence of anti-tumor activity of Shp2 pharmacological inhibition through both cell-autonomous and nonautonomous mechanisms.

Chapter 1. Introduction

1.1. Hepatocellular carcinoma

Hepatocellular carcinoma (HCC), the dominant type of liver cancer, is the seventh most frequently occurring cancer and the second leading cause of cancer-related mortality (1), with an even increasing overall disease burden worldwide in the past decade. Risk factors for HCC includes cirrhosis, viral hepatitis B and C infection, alcohol consumption, fatty liver disease and diabetes, aflatoxin and aristolochic acid (reviewed in (2)). Integrated studies reveal a substantial heterogeneity of HCC molecular pathologies. *TERT*, *CTNNB1* and *TP53* are the most frequently mutated genes in HCC patients but there is a wide variety of genetic alterations have been shown to associate with HCC (3, 4). Moreover, HCC has not shown an addiction to any genetic alterations. Collectively, the heterogeneity of molecular pattern drastically increases the difficulty of developing targeted therapeutics for HCC.

Treatment options vary depending on tumor extent, underlying liver diseases and liver function. For early-stage HCC, curative treatments such as ablation, resection and transplantation should be considered, while locoregional treatments, such as transarterial chemoembolization (TACE) and transarterial radioembolization (TARE), better suit intermediate-stage HCC (5). However, treatment options are limited to systemic therapeutics including kinase and immune checkpoint inhibitors for advanced-stage HCC. So far, systemic therapies are rather limited and of unsatisfactory efficacy, contributing to the high mortality of HCC patients. The first-line systemic drug, sorafenib, prolongs overall survival for only 2-3 months in advanced patients (6, 7), with no other approved kinase inhibitors outperforming sorafenib (8). Immunotherapy has relatively low efficacy on advanced HCC – immune checkpoint inhibitors nivolumab, pembrolizumab, and nivolumab plus ipilimumab have been approved by FDA but only to be used as second-line

treatment after sorafenib (9). Fortunately, the combination of the anti-PDL1 antibody atezolizumab and the VEGF-neutralizing antibody bevacizumab has shown survival advantage superior to sorafenib, which makes this combination a new first-line therapy (10). Despite the new therapy, more efficacious mechanism-based treatment is urgently needed, which requires comprehensive understanding of molecular mechanisms in HCC pathogenesis.

1.2. Protein Tyrosine Phosphatase

Signal transmission through signaling cascades are the most basic mechanism to regulate cellular processes such as proliferation, survival, differentiation and apoptosis etc.. Tyrosyl phosphorylation and dephosphorylation are the most common molecular processes for regulating signal transduction and therefore kinases and phosphatases play critical roles in signaling cascades. Members of protein tyrosine phosphatases (PTPs) superfamily contain a PTP catalytic domain as well as a conserved motif of C-xxxxx-R (C-cysteine, R-Arginine, x-any amino acid) as catalytic site (11). Amino acid residue cysteine initiates a nucleophilic attack on the phosphate group of the substrate as the first step of tyrosine dephosphorylation reaction, followed by transferring of a proton from Asp residue on PTP to now unoccupied tyrosyl group and the exit of dephosphorylated substrate. Finally, the phosphate group leaves and PTP is regenerated (11, 12). Cys-based PTPs are subdivided into three classes and most of Cys-based PTPs reside in Class I depending on a similar topology and catalytic mechanism. Classical PTPs are one of the subclasses reside in Cys-based Class I PTPs and the members of this subclass are of highest homogeneity in sequence and structure of phosphorylated-tyrosine(pTyr) specific PTP domain (13, 14). The function of PTPs in signaling cascades is not simply shutting off the signaling, but rather varies depending on cellular context–positively and negatively regulatory roles of PTPs in cell signaling have been revealed.

1.3. Src homology-2 domain containing phosphatase/Shp2

1.3.1. Shp2 structure

Src homology-2 domain containing phosphatase or Shp2, encoded by gene *PTPN11*, is distributed to Classical non-receptor protein tyrosine phosphatases (NRPTPs) family (11). Shp2 is ubiquitously expressed in various vertebrate cells. Structurally, Shp2 contains two N-terminal Src homology-2 domains (N-SH2 and C-SH2, respectively), followed by pTyr specific PTP domain, and a C terminal tail with tyrosyl phosphorylation sites and a proline-rich motif (15). Phosphatase activity of Shp2 is under regulation by an elegant "molecular switch" mechanism, which was uncovered by biochemical assays and the crystal structure of Shp2 (16-18). Under basal conditions, N-SH2 of Shp2 is docked on PTP domain and blocks substrate access. Upon stimulation of upstream signaling components, a phosphotyrosyl peptide binds to and alters the conformation of N-SH2, followed by the release of PTP domain that allows the entry of substrate (15, 18). The fine-tuned regulation of Shp2 activity by the autoinhibition mechanism enables Shp2 to exert appropriate developmental and physiological functions, whereas disturbance of the mechanism leads to occurrence of several human diseases.

1.3.2. Shp2 functions as protein tyrosine phosphatase

Most of the molecular functions of Shp2, if not all, require its phosphatase activity through PTP domain. PTP domain of Shp2 consists of 4 loops (P-loop, pY-loop, WPD-loop, and Q-loop) which line up the active grove. Besides, each loop is responsible for some specific roles of Shp2 activity, which are executed by specific amino acid residues. Y279 in the pY-loop constricts catalytical site depth, while C459 and R465 on the PTP signature motif (C459-xxxxx-R465) in the P-loop kicks off the nucleophilic attack on substrate and stabilizes the phosphotyrosine-enzyme

complex, respectively (15, 18, 19). Opposed to a more conventional view that sees PTPs as negative regulators of signaling as they remove phosphate groups, Shp2 displays rather positive regulatory role in signaling cascades. The promoting role of Shp2 in Ras/mitogen-activated protein kinase (MAPK) pathway is extensively studied, which accounts for many of Shp2's physiological and pathological roles. Ras/MAPK pathway is a major signaling cascade in mammalian cell that transmits signals emanated from a wide range of cell surface receptors to modulate a variety of cell processes. Evidence at cellular and tissue level is there to support the signal-enhancing function of Shp2 in Ras/MAPK pathway, which include that the absence of Shp2 or catalytically dead Shp2 mutant blunts MAPK activation induced by grow factors, and that hyperactivating Shp2 mutations associated with aberrant MAPK activation are responsible for leukemogenesis (20) and Noonan syndrome (21).

The critical mediatory role of Shp2 catalytic activity in signaling cascade raises great interests in the search for the corresponding substrates of Shp2, the candidates of which are mainly Ras regulators. The following studies mainly examined two hypotheses: (i)Shp2 dephosphorylates and inhibits negative regulator of Ras, or (ii)Shp2 dephosphorylates and activates positive regulator of Ras. Sprouty and p120-RasGAP (Ras GTPase-activating protein) are Ras/MAPK inhibitors whose inhibitory function have been proposed to be impaired, either directly or indirectly, by Shp2-mediated dephosphorylation. Sprouty reduces Ras activity by associating with Growth Factor Receptor Bound Protein 2 (Grb2) and therefore hinders the formation of Grb2/SOS1 Ras-activating complex (22). This inhibitory role of Sprouty has been shown to be impaired by dephosphorylation mediated by Shp2 (23, 24). p120-RasGAP is recruited to phosphorylated receptor or scaffolding protein through its SH2 domains to rapidly inactivate Ras-

GTP, and this interaction can be disturbed by Shp2 via dephosphorylation of the p120-RasGAP docking sites (25-27).

In line with the hypothesis that Shp2 dephosphorylates and attenuates activating function of Ras activators, evidence suggesting a connection between Shp2 and Ras positive mediator emerged in 2002 (28). Following up, Ren et al. and Zhang et al. reported that Shp2 dephosphorylates adaptor protein to impede recruitment of Src inhibitor, C-Terminal Src Kinase (Csk), to the vicinity of Src, though two groups proposed distinct direct substrates for Shp2 (29, 30). Further, Shp2 has been shown to directly dephosphorylate Ras to store its associate with Raf and to activate downstream MAPK signaling cascade (31).

1.3.3. Shp2 functions as scaffolding protein

Through its two SH2 domains and its phosphorylatable tyrosine residue at C-terminus, Shp2 is able to act as a scaffolding protein rather than a phosphatase in order to get involved in signaling events. Shp2 can recruit Grb2/SOS1 complex to activated tyrosine kinase receptor, through phosphorylated Try542 residue, leading to activation of Ras signaling (32). Shp2 also binds to insulin receptor substrate 1 (IRS-1) to bring kinases in proximity of IRS-1 for its phosphorylation at inhibitory serine residue, which provides a mechanism for negative regulation of insulin signaling (33).

1.3.4. The function of Shp2 in development and physiology

The pleiotropic impacts of Shp2 in mammalian cell and its ubiquitous expression pattern across tissues indicate that Shp2 may be involved in multiple developmental and physiologic processes. Indeed, experimental evidence suggests that the requirement of Shp2 in murine embryo

development occurs as early as at blastocyst stage (E6.5), when Shp2 null embryos experience blastocyst inner cell death and fail to maintain trophoblast giant cell (34). Besides, Shp2 is also shown to have regulatory role in the switch from stem cell self-renewal to differentiation, not only in embryonic stem cell but also in many stem cells and progenitors. Due to the embryonic lethality of Shp2 deletion, tissue specific Shp2-deleted models were widely developed and led to discovering a board spectrum of developmental and physiological roles of Shp2 in various tissues (reviewed in Ref.(35)). Notably, Shp2 critically impacts the survival, differentiation and functions of hematopoietic stem cells (36) and blood cell lineages, including T cell development and differentiation (37, 38), mast cell chemotaxis (39), megakaryocyte development and platelet production (40). These functions of Shp2 might confer a causal association on Shp2 mutation with hematological disorder, which will be discussed later.

Shp2 has also been shown to play roles in maintaining metabolic homeostasis. Notably, Shp2 is involved in modulating insulin signaling (33, 41, 42), but this modulator role is dichotomous, depending on cell and tissue types. For example, hepatic Shp2 deficiency improves glucose intolerance and insulin sensitivity (43), while Shp2 loss in skeletal muscle causes insulin resistance and aggravates glucose intolerance (44).

With the discovery of gain-of-function and loss-of-function mutations of Shp2, the connection between these mutations with human diseases has gained great attentions. Germline PTPN11 mutations are found to cause two related, but distinguishable syndromes, namely Noonan Syndrome and Leopard Syndrome. Firstly, Noonan Syndrome (NS) is a genetic disorder which causes developmental defects in the patient, including growth retardation, unusual facial features and cardiac defects. Leopard Syndrome (LS) was first considered a variant of NS due to the phenotypic similarity between LS and NS except for the distinct cardiac defective phenotypes (45,

46). More than 45% of NS are caused by missense Shp2 mutations (45). Most of the NS-associated Shp2 mutations are gain-of-function mutations (47), whereas LS-causing PTPN11 mutations are substantially loss-of-function (48). Notably, animal models mimicking human NS reveal that clinical traits of NS are often linked to Ras/MAPK/Erk hyperactivation, in consistence with Shp2's positive regulatory role in Ras/MAPK signaling (49-51). More interestingly, a significantly higher incidence rate of cancer has been described in *PTPN11*-associated NS (52, 53).

Consistent with the positive regulatory role of Shp2 in Ras/MAPK pathway, in multiple reports mutations in Shp2 are causally linked to development of tumors albeit only for several specific tumor types. Somatic point mutations of Shp2 have been found to cause 35% of cases of juvenile myelomonocytic leukemias (JMML), a rare chronic myeloproliferative/myelodysplastic disorder that occurs in young children. JMML-associated Shp2 mutations are mainly gain-of-function mutations targeting N-SH2 and PTP domain to lift the autoinhibitory conformation and increase Shp2 basal activity (54, 55). Apart from Shp2 mutations, other drivers of JMML involve activating mutations of Nras or Kras and inactivating mutations of RasGAP NF1. Shp2, Ras and NF1 mutations are mainly mutual exclusive, implying that Ras/MAPK pathway exclusively drives JMML (56). Shp2 mutations also occur in childhood acute myeloid leukemia (AML) as well as in some solid tumors such as neuroblastoma and lung cancer, albeit in substantially low frequency (57, 58). Moreover, evidence for implication of abnormal Shp2 activity in development of various tumor types has emerged in the past decade (59-62). In the context of liver, our lab previously showed that Shp2 is required for activation of proliferative signals in liver regeneration (27).

1.3.5. Hepatoprotective function of Shp2

In previous work our lab has generated hepatocyte-specific Shp2 knocked out (*Shp2*$^{hep-/-}$) mouse and shown Shp2 deletion hinders MAPK/Erk pathway activation (27). However, *Shp2*$^{hep-/-}$ mice also exhibit chronic hepatic damages, fibrosis, necrosis, inflammation and spontaneous hepatocellular adenoma (HCA) formation accompanied by steatosis in aged liver, as well as display an aggravated phenotype of HCC driven by chemical carcinogen diethylnitrosamine (DEN) (63). Concurrent deletion of Shp2 and Pten induced a severe phenotype of NASH-associated HCC (64). Simultaneous removal of Shp2 and Ikkβ even induced spontaneous HCC development by causing circadian disorders (65). Thus, the hepatic Shp2 functions appear to be pleiotropic with both pro- and anti-oncogenic effect. Of note, several other conventionally known oncogenes, including Met (66, 67), β-Catenin (68, 69), Stat3 (70, 71) and Jnk (72, 73), demonstrate similar pleiotropic roles specifically in liver, indicating the complexity of liver tumor pathology which is collectively contributed by hepatocyte-autonomous factors and environmental impacts (74).

1.3.6. Discovery and functions of allosteric Shp2 inhibitor

Last generation of Shp2 inhibitors that mainly targeted PTP domain are of poor selectivity, due to the highly conserved sequence of the catalytic site among PTPs, as well as unfavorable cell permeability and oral bioactivity due to the nature of functional chemical groups that the inhibitors are composed of (75, 76). Recent Shp2 inhibitor discovery utilizes the strategy of targeting allosteric pocket and has achieved marked success in discovering highly selective, orally active Shp2 allosteric inhibitors, of which four are currently in clinical trials (JAB-3068, TNO155, RMC-4630, and RLY-1971). The first successful allosteric Shp2 inhibitor, SHP099, was identified by Novartis in 2016, and proven to suppress Ras/MAPK pathway activation and cell growth of RTK-

dependent cancer cell lines (77). It functions through binding to the allosteric pocket surrounded by N-SH2, C-SH2 and PTP domain and locking Shp2 in the auto-inhibitory conformation (77, 78). Beyond SHP099, chemically optimized SHP099 derivatives have emerged with improved potency and capability to overcome resistance conferred by activating PTPN11 mutations.

In consistency with Shp2's cellular function of relaying signals from multiple RTKs to Ras, Shp2 inhibitor is demonstrated to suppress Ras/MAPK-dependent tumor growth by impeding upstream RTK-induced GTP reload on Ras (79-81). Moreover, Shp2 inhibitor re-instates sensitivity to Ras/MAPK pathway inhibitors in resistance-developed Ras-dependent tumors, by shutting down the alternatively activated RTK/Ras pathway bypassing the primary inhibitor (BRAF inhibitor (82), ALF inhibitor (83), MEK inhibitor (81, 84, 85) and etc.). Allosteric Shp2 inhibitor combined with anti-tumor immunity booster also displays promising effects. Shp2 interference augments the proportion of cytotoxic T cell compartment as well as cytotoxic factor secretion, and synergizes with anti-PD-1 treatment in controlling the growth of a murine colon cancer model (86), possibility owing to Shp2 functioning downstream of PD-1. Shp2 inhibitor also synergizes with CSF1R (receptor of the colony-stimulating factor-1) inhibitor to potentiate anti-tumor immunity from the myeloid cell compartment, via shifting macrophage polarization towards M1-type or blocking eat-me-not signal in macrophage (87, 88).

1.4. Tyrosine kinase receptor Met

Met is a cell surface tyrosine kinase receptor bound by ligand Hepatocyte Growth Factor (HGF). Activated by HGF binding, Met then initiates downstream signaling cascade that leads to several biological events, such as cell proliferation, cell invasion and inhibition of apoptosis (reviewed in (66)). Mechanistically, HGF binding triggers Met dimerization and phosphorylation

of two tyrosine residues in its intracellular segment, which provides docking site for SH2 domain-containing proteins, such as Growth Factor Receptor-Bound Protein 2 (Grb2), Grb2-Associated Binding protein 1 (Gab1), Shp2 and etc.(reviewed in (89)). The HGF/Met axis plays a pivotal role in liver tumor development and metastasis. Met overexpression is detected in 20-48% of human HCC samples (90), and is in association with poor prognosis (91, 92). Elevated expression of Met-dependent signature genes is linked to decreased survival and exacerbated metastasis in a cohort of HCC patients (93). Consistently, overexpression of Met efficiently droves HCC development in transgenic mice (94), but ablating Met in hepatocytes also exacerbates HCC development induced by chemical carcinogen diethylnitrosamine (DEN) in mice (95), suggesting complex tumorigenic mechanisms in the liver. Met-targeted therapy is currently an active area of anti-HCC therapeutics research, with selective Met inhibitor tepotinib currently in clinical trial II, which has demonstrated anti-tumor activity against Met-overexpressing advanced HCC (96, 97).

1.5. Suppressor of cytokine signaling-1 (Socs1) and Socs3

Suppressor of cytokine signaling (SOCS) proteins are a family of proteins that mostly function in a classic negative feedback loop to inhibit cytokine signaling. Socs1 and Socs3 belong to this family and both of them consist of a kinase inhibitory region (KIR), responsible for inhibiting JAK directly (98), an SH2 domain, which enables its binding to phosphotyrosine-containing target protein (99), as well as a SOCS box which recruits ubiquitin ligase for ubiquitination and degradation of target proteins (100). The SH2 domain of Socs3 shares similar binding specificity with that of Shp2 and thus the two molecules compete for binding molecular partners (101-104). Socs3 is reported to be involved in liver regeneration and chemically induced hepatocarcinogenesis, mechanistically through its implication in the signal transducer and

activator of transcription 3 (STAT3)- and the mitogenic extracellular signal-regulated kinase 1/2 (Erk1/2)-pathway (105). Furthermore, Socs1 is shown to inhibit Met expression and signaling (106).

1.6. Hydrodynamic transfection

Hydrodynamic transfection, which combines hydrodynamic gene delivery and Sleeping Beauty (SB) transposase-mediated somatic integration, is a mature, widely accepted and utilized *in vivo* transfection method for long-term gene expression. A physiological solution containing plasmid DNA of interest and SB transposase encoding plasmid is prepared for this method. This method features a fast-speed (5-9 seconds) tail vein injection of a substantial volume (2-3ml or equivalent to 10% mouse body weight) of physiological solution, for forcing all the solution to rapidly enter the heart via inferior vena cava. The large volume of solution would over-stretch myocardial fibers and cause cardiac congestion, resulting in backflow of solution into liver specifically, making liver the major organ being transfected (transfection efficiency: 10-40% in liver versus <0.1% in other organs). The hydrodynamic pressure remains with the solution in liver, which permeabilizes capillary endothelium and cell membrane of closely associated parenchymal cells, enabling uptake of plasmids by parenchymal cells, or hepatocytes. Once inside hepatocytes, expressed SB transposase facilitates integration of gene of interest carried by plasmids into hepatocyte genome. Hydrodynamic transfection can transiently transfect 10-40% of hepatocytes and achieve stable, long-term transfection in approximately 2-10% of hepatocytes. By constructing plasmids that work compatibly with SB transposase integration system, overexpression, knockdown and knockout of targeted genes in hepatocyte are made possible in a significantly shorter timeframe than that generation of transgenic mouse. Inevitably, hydrodynamic pressure

leads to liver injury. However, liver usually heals itself in a week. Overall, hydrodynamic transfection is a reliable, flexible and cost-effective in vivo transfection method for generation of novel mouse hepatocarcinogenesis models.

1.7. Acknowledgement

This dissertation from Chapter 1 through Chapter 5, in part, is a reprint of the material as it appears in Shp2 deletion in hepatocytes suppresses hepatocarcinogenesis driven by oncogenic β-Catenin, PIK3CA and MET. Jacey Jijun Liu, Yanjie Li, Wendy Chen, Yan Liang, Gaowei Wang, Min Zong, Kota Kaneko, Ruiyun Xu, Michael Karin, Gen-Sheng Feng, Journal of Hepatology, 2018. The dissertation author was the primary investigator and author of this paper.

This dissertation from Chapter 1 through Chapter 5, in part, has been accepted for publication of the material as it may appear in Pharmaceutical Shp2 Inhibition Suppresses Primary and Metastasized Liver Tumors by Provoking Hepatic Innate Immunity, Jacey Jijun Liu, Bing Xin, Li Du, Lydia Chen, Yanyan Long, Gen-Sheng Feng, Hepatology, 2022. The dissertation author was the primary investigator and author of this paper.

Chapter 2. Results

2.1. Shp2 is required for Met/Cat-induced liver tumorigenesis

Hepatocyte specific Shp2-deleted mouse strain was obtained by crossing *Shp2*$^{flox/flox}$ mice with Albumin-Cre transgenic mice (27). With this *Shp2*$^{hep-/-}$ mouse strain, previous studied conducted in Feng lab demonstrated that hepatic Shp2 deficiency impaired hepatocyte proliferation following partial hepatectomy (27), also triggered HCA development in old mice and exacerbated DEN-induced HCC (63). I first investigated the role of hepatic Shp2 in RTK-driven liver tumorigenesis by comparing the tumor outcome in *WT* versus in *Shp2*$^{hep-/-}$ mouse. Liver tumor was induced by hydrodynamic tail vein injection of two plasmids that encodes human Met and a constitutively active β-catenin truncated mutant, ΔN90-β-catenin (Met/Cat) respectively, together with the Sleeping Beauty (SB) transposase-encoding plasmid. This SB transposase-mediated transfection system delivered by hydrodynamic injection stably transfected the proto-oncogenes into approximately 10% of hepatocytes without transfecting other liver cell types (107). We monitored liver phenotype along the time course and detected multiple tumor nodules in control mice 8 weeks after injection of the oncogenes, but not in *Shp2*$^{hep-/-}$ mouse (Figure 1A). Hepatic Shp2 deficiency resulted in marked reduction of tumor burdens induced by Met/Cat, as evaluated by the liver versus body weight ratios, tumor incidences, and the maximal sizes of tumor lesions (Figure 1B). Histological analysis by experienced histopathologist indicated that the tumors were mainly HCC (Figure 1A). Suppression of Met/Cat-driven liver tumorigenesis by Shp2 depletion in hepatocyte suggested a strong requirement of Shp2 in this oncogene-induced liver tumor formation, which showed sharp contrast to the previous data showing that Shp2 deficiency dramatically aggravated DEN-induced HCC development in the same *Shp2*$^{hep-/-}$ mouse line (63), despite that previously found

physiological features of *Shp2*$^{hep-/-}$ liver including scalloped edges and slightly lumpy surface were also displayed in oncogene-transfected Shp2-depleted liver (Figure 1A).

Fig.1

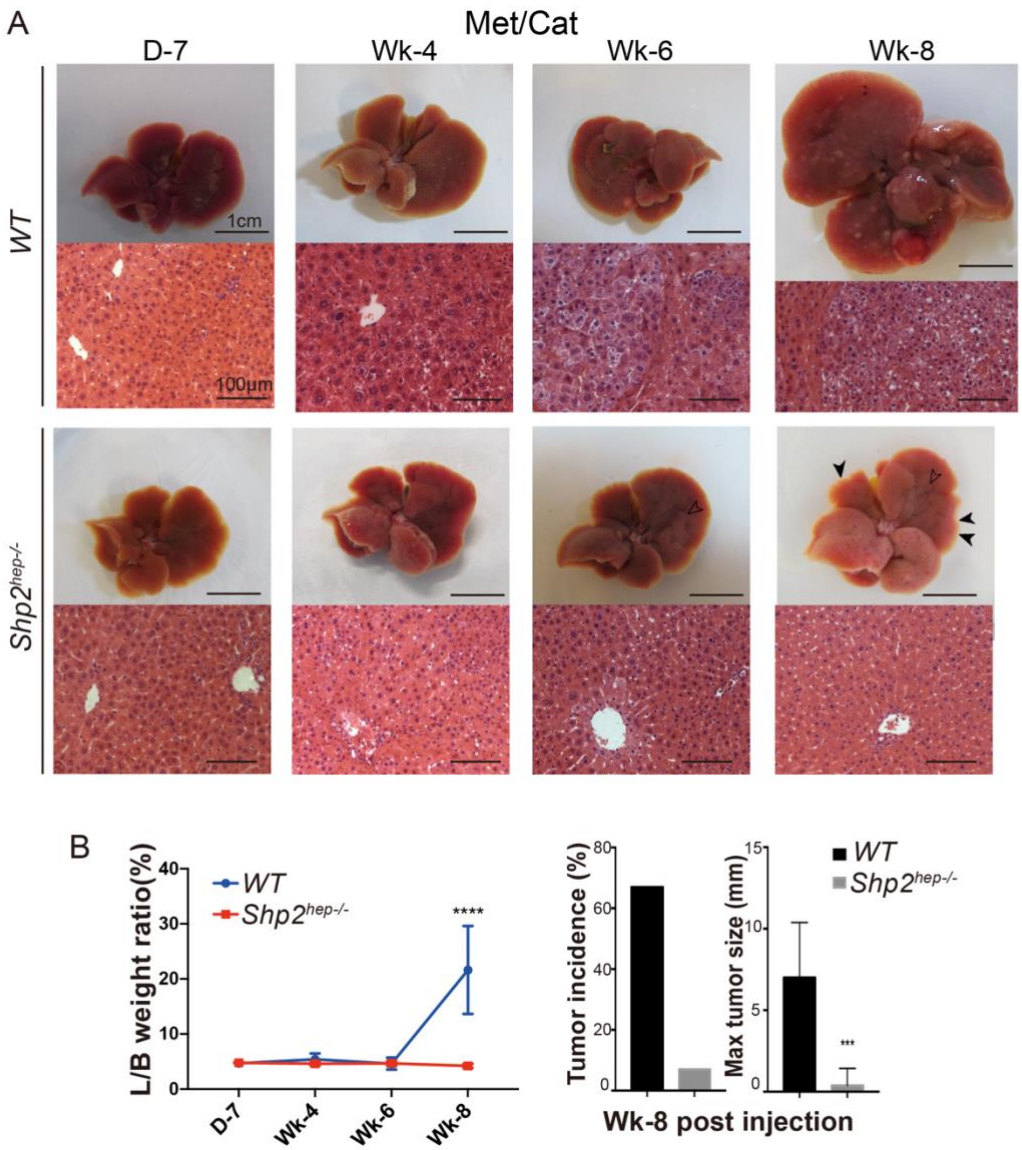

Figure 1. Shp2 deletion suppresses Met/Cat-induced hepatocellular cancer

A. Macroscopic images and H&E staining of mouse liver sections at day 7 and week 4, 6 and 8 post hydrodynamically transfection of Met and ΔN90-β-catenin (Met/Cat). Scale bars: 1 cm (macroscopic); 100 μm (microscopic).

B. Liver versus body (L/B) weight ratios were measured at various time points (n=3, day-7, week 4 and week 6; n=8, week8). Tumor incidences and maximal tumor sizes (n=8) were measured for *WT* and *Shp2*$^{hep-/-}$ mice at week 8 post-injection. Data are mean values ± SD and P values were calculated by unpaired two-tailed Student's T-test, ns or no annotation, not significant, ***P < 0.001, ****P<0.0001.

2.2. Shp2 is also necessary for Met/Pik-induced liver tumorigenesis

We then examined the effect of Shp2 loss on liver tumorigenesis driven by another pair of oncogenes, *MET* and *PIK3CA*^{H1047R} (Met/Pik). *PIK3CA*^{H1047R} encodes for the hyperactive mutant of p110α catalytic subunit of phosphatidylinositol-3-kinase (PI3K), which have been detected in several types of cancer (108). Previous study demonstrated that hydrodynamic delivery of *PIK3CA*^{H1047R} together with *MET* or *NRAS*^{G12V} robustly induced liver tumor accompanied by hepatosteatosis (109). Consistently, we detected liver tumors in *WT* mice at 12 weeks after injection of Met/Pik (Figure 2A). Distinct from Met/Cat-tumor, Met/Pik triggered non-alcoholic fatty liver disease (NAFLD) and diffused liver tumors with undefined nodule boundary. The *Shp2*$^{hep-/-}$ mice were less susceptible to Met/Pik-driven liver tumorigenesis, as evaluated by liver to body weight ratio and pathological analysis (Figure 2A, B). Shp2 deletion also protected liver from Met/Pik-induced NAFLD, as revealed by less lipid droplet accumulation (Figure 2C).

2.3. Shp2 deficiency down-regulates central proliferative signals and Met expression

Given the widely known positive regulatory role of Shp2 for Ras activation, we wondered if Shp2 also plays a regulatory role in the intrinsic oncogenic pathways involved in Met/Cat and Met/Pik. To address this issue, we interrogated the central proliferative signaling events in these two animal tumor models. Immunoblotting of liver lysates demonstrated that exogenous Met/Cat expression induced marked increase of pErk signals (Figure 3A,B), while Met/Pik injection enhanced pAkt levels (Figure 3C,D). However, Shp2 loss suppressed both pErk and pAkt activation, as examined at different time points (Figure 3). We also determined the impact of Shp2 loss on Wnt/β-catenin signaling. Phosphorylation of endogenous β-catenin

at Ser33/Ser37/Thr41, phosphorylation earmarking β-catenin for ubiquitin-mediated degradation (110), was not affected by either oncogenic Met and ΔN90-β-catenin transfection or Shp2 depletion (Figure 3A). However, due to Met/Cat overexpression, hepatocytes expressing β-catenin downstream target glutamine synthetase (GS) expanded beyond the perivenous areas progressively in *WT* but not in *Shp2*$^{hep-/-}$ livers (Figure 3B), indicating overactivation of β-catenin downstream signals.

We then examined the exogenous expression of Met, β-catenin and PIK3CA in the liver at different time points. Exogenous Met- or β-catenin-positive colonies expanded progressively in *WT* livers, but these signals were detected in *Shp2*$^{hep-/-}$ livers only at day 7 but not at week 5 and 8 (Figure 4A). Downregulation of Met expression were observed in *Shp2*$^{hep-/-}$ livers as early as on day 3, and became more observable at week 6, 9 and 12 after Met/Pik injection (Figure 4B), in consistency with Met expression pattern in Met/Cat-transfected *Shp2*$^{hep-/-}$ liver. Similarly, previous experiments demonstrated significantly reduced levels of c-Kit and PDGFRβ, cell surface tyrosine kinase receptors (RTKs), in Shp2-deficient hematopoietic cells and fibroblasts, respectively (111, 112). Therefore, the Shp2 function in mediating RTK signaling is at least in part contributed by its ability to sustain the upstream RTK expression or stability, with the underlying mechanism to be elucidated.

Fig.2

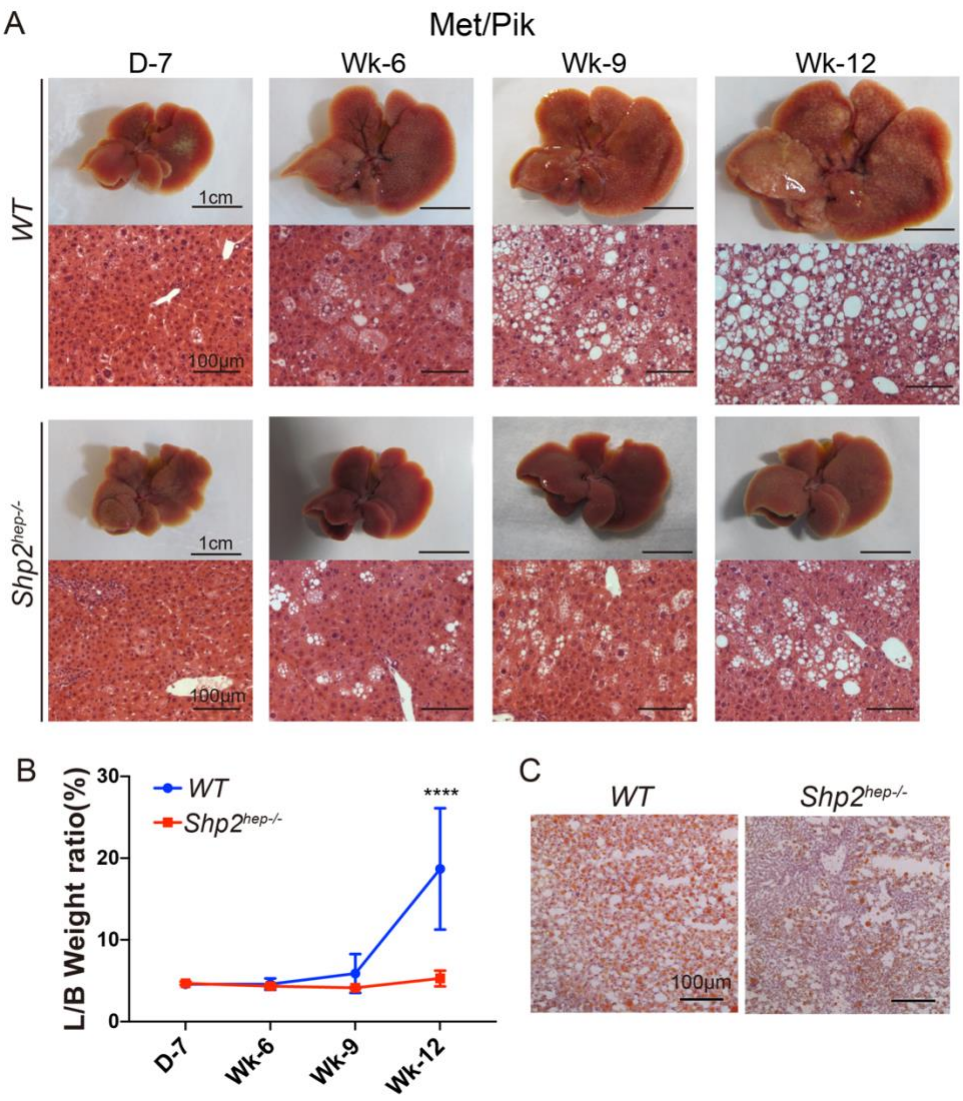

Figure 2. Shp2 loss inhibits Met/Pik-induced liver tumorigenesis

A. Representative macroscopic images and H&E staining of mouse liver sections at various time points post transfection of Met and PI3K p110α (Met/Pik). Scale bars: 1 cm (macroscopic), 100 μm (microscopic).

B. L/B weight ratios of MET/PIK-transfected mice were measure at various time points (n=3, D-7; n=4, Wk-6; n=4, Wk-9; n=7, Wk-12). Data are mean values ± SD and P values were calculated by unpaired two-tailed Student's T-test, ns or no annotation, not significant, ****P<0.0001.

C. Oil-Red-O staining of liver sections at week 12 post-injection of Met/Pik. Scale bars: 100 μm.

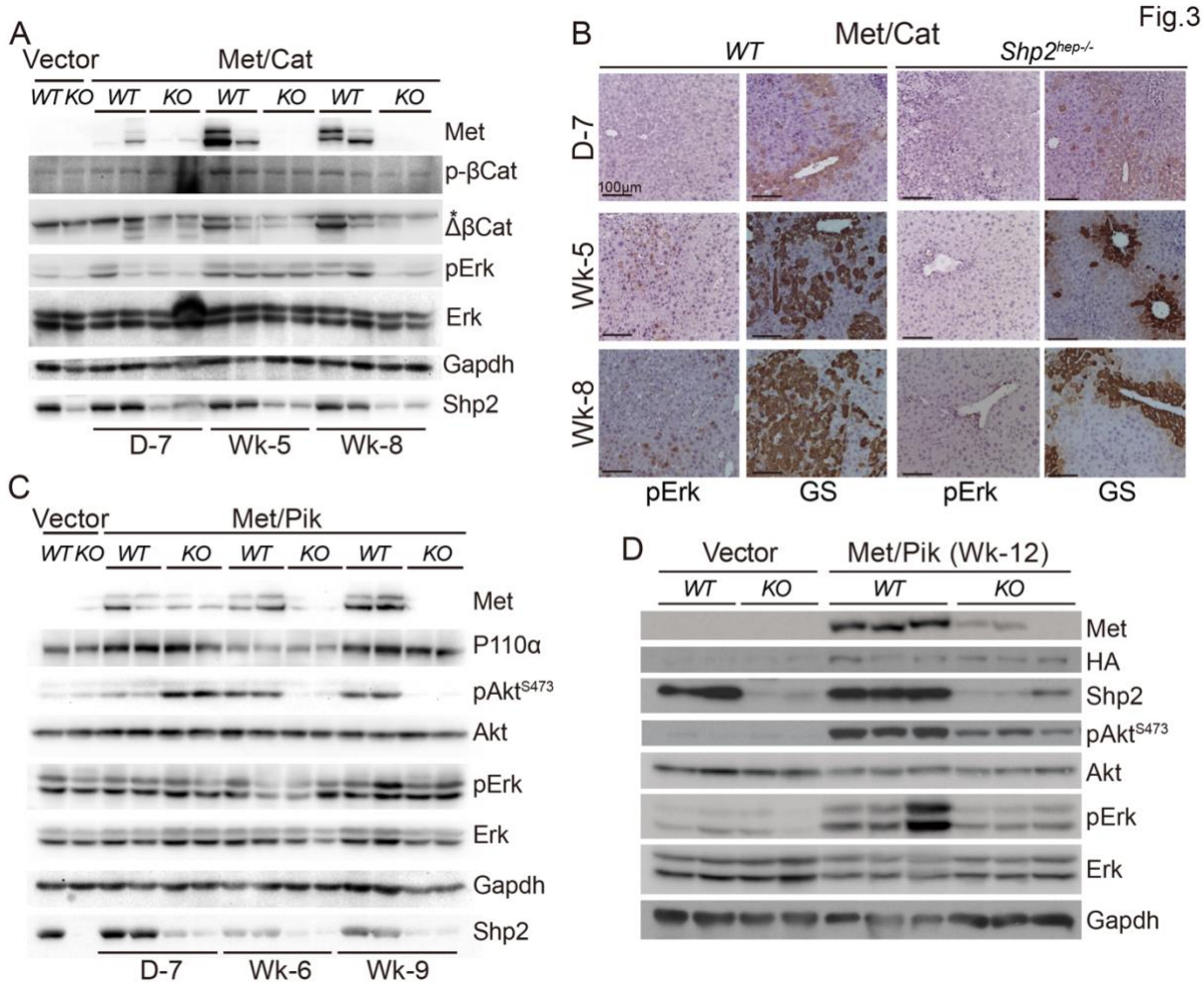

Figure 3. Shp2 loss suppresses critical proliferative signaling events induced by the injected oncogenes

A. Immunoblotting for indicated protein targets in Vector- or Met/Cat-transfected *WT* or *Shp2$^{hep-/-}$ (KO)* liver lysate at various time points after transfection. * Endogenous β-catenin.

B. Immunostaining of glutamine synthetase (GS) and phosphorylated Erk (pErk) on sections of *WT* or *Shp2$^{hep-/-}$* liver collected at day 7, week 5 and 8 post Met/Cat injection. Scale bars: 100 μm.

C. Immunoblotting for indicated protein targets in Vector- or Met/Pik-transfected *WT* or *Shp2$^{hep-/-}$(KO)* liver lysate at early or intermediate time points after transfection.

D. Immunoblotting for indicated protein targets in Vector- or Met/Pik-transfected *WT* or *Shp2$^{hep-/-}$(KO)* liver lysate at late time point (Week-12) after transfection.

Fig.4

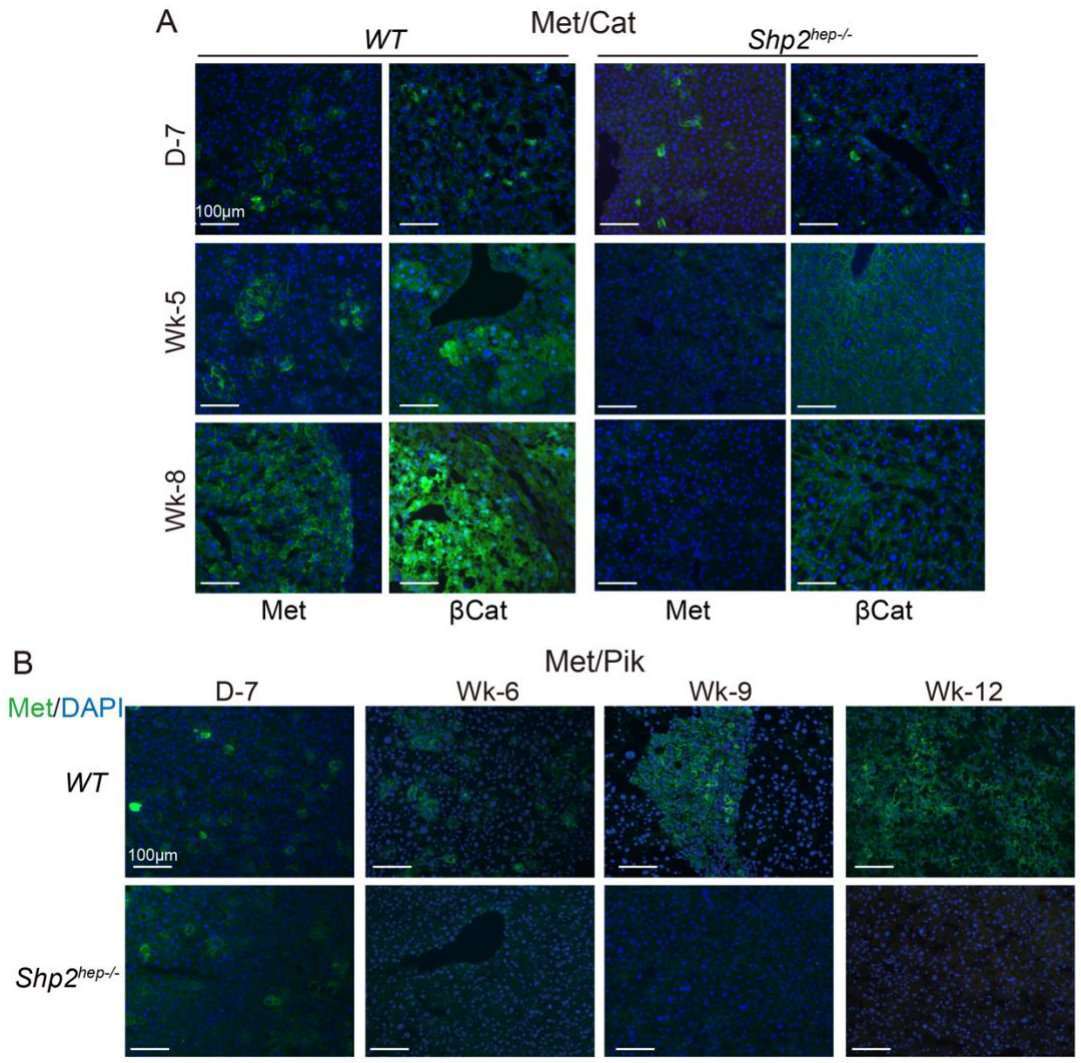

Figure 4. Shp2 loss downregulates expression of exogenous oncogenes

A. Immunostaining for exogenous Met and β-catenin on sections of *WT* or *Shp2*$^{hep-/-}$ liver collected at day 7, week 5 and 8 post injection of Met/Cat. Scale bars: 100 μm.

B. Immunostaining of *WT* and *Shp2*$^{hep-/-}$ liver sections for exogenous Met at day 7, week 6, 9 and 12 post Met/Pik injection. Scale bars: 100 μm.

2.4. *Shp2$^{hep-/-}$* liver is characterized by impaired proliferative capacity and increased oxidative and metabolic stresses

To explore the mechanism underlying the unique Shp2 function that mediated oncogene-induced liver tumor, we conducted bulk RNA-seq analysis to compare the transcriptomes in *WT* and *Shp2$^{hep-/-}$* livers, at day 0, 3 and 7 after delivery of Met/Cat or Met/Pik oncogenes. Overall, deleting Shp2 in hepatocytes caused dramatic changes in hepatic gene expression in comparison to its wildtype counterpart, both before and after transfection of the oncogenes (Figure 5A). We first analyzed the baseline transcriptomes in *WT* and *Shp2$^{hep-/-}$* livers without oncogene overexpression (Day-0). GSEA analysis showed that the gene cluster 1 highly expressed in *WT* livers was enriched for gene sets in mRNA processing (Figure 5A), including *SRSF7, HNRNPA2B1, TRA2B, FUS* and *RBMX*, with *SRSF7*, *TRA2B* and *HNRNPA2B1* identified as Myc targets (113). Relative to the *WT* control, the genes in cluster 2 highly expressed in *Shp2$^{hep-/-}$* livers featured increased oxidative stress and reprogramming of metabolic pathways. In particular, the highly expressed genes included *NSDHL*, *DHCR24*, *HSD17B7* and *CYP51A1* in cholesterol metabolism, *MGST1*, *GSTK1* and *GPX1* in response to oxidative stress, and the PPARα pathway that regulates lipid metabolism. Along this line, we also found that genes of nuclear receptor heterodimers PXR/RXR, LXR/RXR and FXR/RXR involved in modulation of metabolic processes were upregulated by Shp2 ablation (Figure 5D). Together, the RNA-seq data suggest that Shp2 deletion caused downregulation of hepatocyte proliferation potential, reprogramming of metabolic pathways and increased oxidative stress in the liver, before oncogene transfection. Moreover, the expression of *PIK3RI*, *JUN*, and *FOS*, genes downstream of the HGF/Met pathway, was downregulated in Shp2-deficient livers (Figure 5B). Shp2 ablation also caused changes in expression of genes in the Wnt/β-catenin

pathway, and most of the genes predicted to be upregulated by Wnt signaling expressed at higher levels in *WT* than *Shp2*$^{hep-/-}$ livers (Figure 5C). Together, these results suggested a negative impact of Shp2 loss on the basal levels of signaling through the HGF/Met and Wnt/β-catenin pathways in the liver, and also indicated the impact of Shp2 loss on hepatic environment by influencing oxidative stress status and reprogramming metabolic pathways.

2.5. Shp2 deletion disturbed multiple signaling events induced by Met/Cat or Met/Pik

Then we analyzed the transcriptomes of oncogene-transfected liver. Surprisingly, compared to baseline *WT* liver transcriptome, Met/Cat transfection did not lead to marked upregulations in cell growth and dividing related genes, but genes involved in complement and coagulation cascades, which may be a result of recovery process from hydrodynamic injection. Distinct from Met/Cat, Met/Pik-transfection led to high expression of genes in cluster 4, which were genes involved in DNA replication and G2/M transition pathways, such as *AURKB* and *PLK1* (Figure 5A).

We then used IPA to compare the transcriptomes in *WT* and *Shp2*$^{hep-/-}$ livers on day 3 post oncogene-transfection (Figure 6A,D). Met/Cat transfection triggered DNA damage response, coagulation, and fibrotic processes in both genotypes, noting the z-score of G2/M checkpoint regulation calculated by IPA was lower in the *WT* liver (*WT*: -2; *Shp2*$^{hep-/-}$: -1.667). Genes related to the checkpoint control and cell cycle progression, such as *PLK1, CDC25, TOP2A, CCNB1* and *CCNB2*, were more abundantly expressed in the *WT* than in mutant liver, while inhibitory checkpoint regulators including *P21* and *BRCA1* were upregulated in *Shp2*$^{hep-/-}$ livers. In addition to cell cycle progress, Shp2 ablation upregulated genes involved in severe inflammatory and immune responses such as IL-10 signaling and dendritic cell maturation upon

Met/Cat-transfection (Figure 6A). Consistently, the downstream targets in NFκB pathway were upregulated in *Shp2*$^{hep-/-}$ liver (Figure 6B), implying activation of NFκB pathway, which might account for the stimulation of inflammatory response genes. Of note, *Shp2*$^{hep-/-}$ liver was also characterized by downregulation of Myc targets (Figure 6C), suggesting impaired Myc signaling, which is likely one mechanism for inhibition of tumorigenesis in Met/Cat-transfected *Shp2*$^{hep-/-}$ liver. Consistent with Met/Cat, upon Met/Pik transfection, several cell cycle-related pathways were more upregulated in *WT* than in *Shp2*$^{hep-/-}$ livers (Figure 6D,E), consistent with the identification of cluster 4 (Figure 5A). In the contrast, p53 signaling and cell cycle inhibitors such as *GADD45G* and *P21*, were upregulated by Met/Pik in *Shp2*$^{hep-/-}$ livers (Figure 6D), suggesting relative cell cycle suppression by Shp2 loss.

We further analyzed the gene expression profiles 7 days after oncogenes' delivery. A GFP-encoding plasmid was also injected into *WT* and *Shp2*$^{hep-/-}$ livers as vector control, and the transcriptomes after the vector injection were very similar to the day-0 untreated livers in both genotypes (Figure 7A). The transcriptomes were very similar at day 3 and 7 in *WT* or *Shp2*$^{hep-/-}$ livers injected with the same oncogenes, but the differences in gene expression between the two genotypes remained very significant at day 7 after injection of the vector, Met/Cat or Met/Pik. Commonly enriched in untreated and vector-injected *Shp2*$^{hep-/-}$ livers were genes involved in redox reaction and metabolic pathways (Figure 7B). Genes downregulated in Met/Cat-injected *WT* livers at day 7 were enriched in RNA transcription related genes and genes transcriptionally targeted by NF1 (Neurofibromin 1), a negative regulator of Ras (Figure 7C). Enriched in Met/Cat-injected *Shp2*$^{hep-/-}$ livers were genes in immune response pathways and targets of GABPA (GA binding protein transcription factor, alpha subunit) (Figure 7C). Met/Pik transfection induced cell cycle progression related pathways in *WT* liver, while *Shp2*$^{hep-/-}$ liver

was featured by elevated immune response (Figure 7D). The target genes of Myc and SP1 were downregulated in Met/Pik-injected *Shp2*$^{hep-/-}$ livers (Figure 7D), suggesting impaired cell proliferation in the mutant liver.

Together these transcriptome changes suggested that Shp2 deletion affected hepatic cell checkpoint progression and M phase entry (114-116) in both Met/Cat- and Met/Pik-induced liver, by both downregulating cell cycle progression related gene expression and upregulating cell cycle suppressive regulator gene expression. The transcriptomic analysis indicated that the inhibitory effect of Shp2 loss on the oncogenes-driven tumorigenesis is likely attributed to suppression of cell-intrinsic oncogenic signaling. In addition, Shp2 loss led to hepatic environmental changes including increased oxidative stress and inflammation, and metabolism reprogramming, suggesting that Shp2 loss in hepatocytes was associated with formation of a tumor-promoting hepatic microenvironment, which is along the same line with the physiological changes in Shp2 depleted liver in our previous study (63).

Fig.5

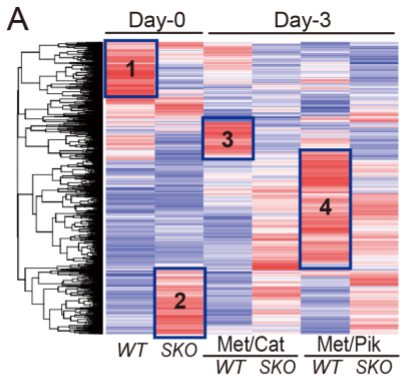

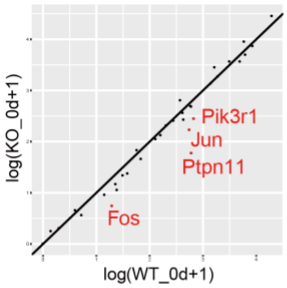

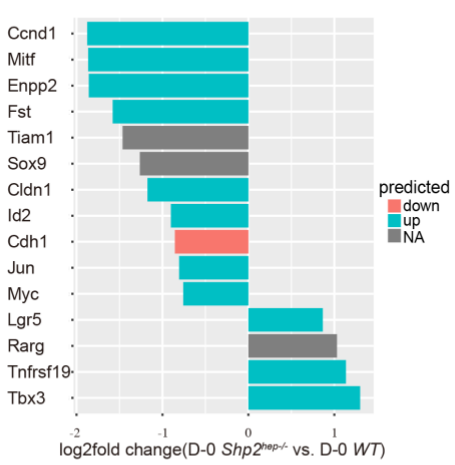

Highly enriched gene sets in cluster by GSEA	*P* value
Cluster 1: D-0 *WT* liver	
REACTOME: mRNA splicing	1.61E-07
KEGG: Spliceosome	3.28E-07
REACTOME: Processing of capped intron-containing pre-mRNA	5.12E-07
Cluster 2: D-0 *Shp2*$^{hep-/-}$ liver	
REACTOME: Metabolism of lipids and lipoproteins	6.52E-18
REACTOME: Cholesterol biosynthesis	5.65E-10
KEGG: Steroid biosynthesis	6.63E-09
REACTOME: PPARa activates gene expression	2.70E-07
KEGG: PPAR signaling pathway	4.32E-07
Cluster 3: Met/Cat D-3 *WT* liver	
KEGG: Complement and coagulation cascades	1.28E-07
Cluster 4: Met/Pik D-3 *WT* liver	
REACTOME: Cell cycle	1.17E-21
PID: Aurora B pathway	7.94E-18
PID: PLK1 pathway	7.60E-11
REACTOME: DNA replication	3.11E-16
KEGG: ECM receptor interaction	5.89E-15
REACTOME: Immune system	1.33E-12
REACTOME: Cyclin A/B1 associated events during G2/M transition	1.92E-12

D

Pathways positively regulated by Shp2 deletion by IPA	*P* value
Glutathione-mediated Detoxification	1.26E-12
NRF2-mediated Oxidative Stress Response	2.57E-08
Superpathway of Cholesterol Biosynthesis	1.00E-06
Superpathway of Geranylgeranyldiphosphate Biosynthesis I (via Mevalonate)	1.00E-05
PXR/RXR Activation	5.89E-05
FXR/RXR Activation	1.10E-03
LXR/RXR Activation	0.011482

Figure 5. Comparative analysis of transcriptomes in *WT* and *Shp2*$^{hep-/-}$ livers

A. Upper: Heatmap visualizing the FPKM values for differentially expressed genes across all 6 groups (n=3): *WT* and *Shp2*$^{hep-/-}$ livers before (Day-0) or after (Day-3) transfection of Met/Cat or Met/Pik, with red and blue indicating high and low gene expression, respectively. Highly expressed gene clusters are highlighted and numbered.

Lower: GSEA analysis showing the most enriched gene sets in each highly expressed gene cluster.

B. Comparison of baseline transcripts of HGF/Met targets between *WT* and *Shp2*$^{hep-/-}$ livers on Day 0. For each target gene, x- and y-axis values are its FPKM values in *WT* liver and *Shp2*$^{hep-/-}$ livers, respectively. Genes expressed at significantly lower levels in *Shp2*$^{hep-/-}$ than *WT* livers are annotated.

C. Comparison of transcript levels of Wnt target genes between *Shp2*$^{hep-/-}$ and *WT* livers on Day 0. Red, blue and grey colors indicate the genes down-regulated, up-regulated or not affected by the Wnt pathway.

Fig.6

A

Pathways positively regulated by Met/Cat on D-3 by IPA	*P* value
WT liver	
Hepatic Fibrosis / Hepatic Stellate Cell Activation	9.12E-06
Ubiquinol-10 biosynthesis	0.001696
DNA damage-induced 14-3-3σ Signaling	0.003467
Cell Cycle: G2/M DNA Damage Checkpoint Regulation	0.009550
Shp2$^{hep-/-}$ liver	
Agranulocyte Adhesion and Diapedesis	6.31E-12
Hepatic Fibrosis / Hepatic Stellate Cell Activation	1.23E-10
IL-10 Signaling	1.74E-05
Dendritic Cell Maturation	5.89E-05
GADD45 signaling	7.41E-05
p53 signaling	4.68E-04
Cell Cycle: G2/M DNA Damage Checkpoint Regulation	0.001995

D

Pathways positively regulated by Met/Pik on D-3 by IPA	*P* value
WT liver	
Agranulocyte Adhesion and Diapedesis	3.16E-13
Granulocyte Adhesion and Diapedesis	5.01E-13
Hepatic Fibrosis / Hepatic Stellate Cell Activation	1.00E-11
Atherosclerosis Signaling	1.74E-08
Th1 and Th2 Activation Pathway	1.86E-07
Shp2$^{hep-/-}$ liver	
Hepatic Fibrosis / Hepatic Stellate Cell Activation	4.47E-10
Agranulocyte Adhesion and Diapedesis	9.77E-07
Mitotic Roles of Polo-Like Kinase	2.14E-06
GADD45 Signaling	4.17E-06
Cell Cycle: G2/M DNA Damage Checkpoint Regulation	7.94E-05
p53 Signaling	1.82E-04

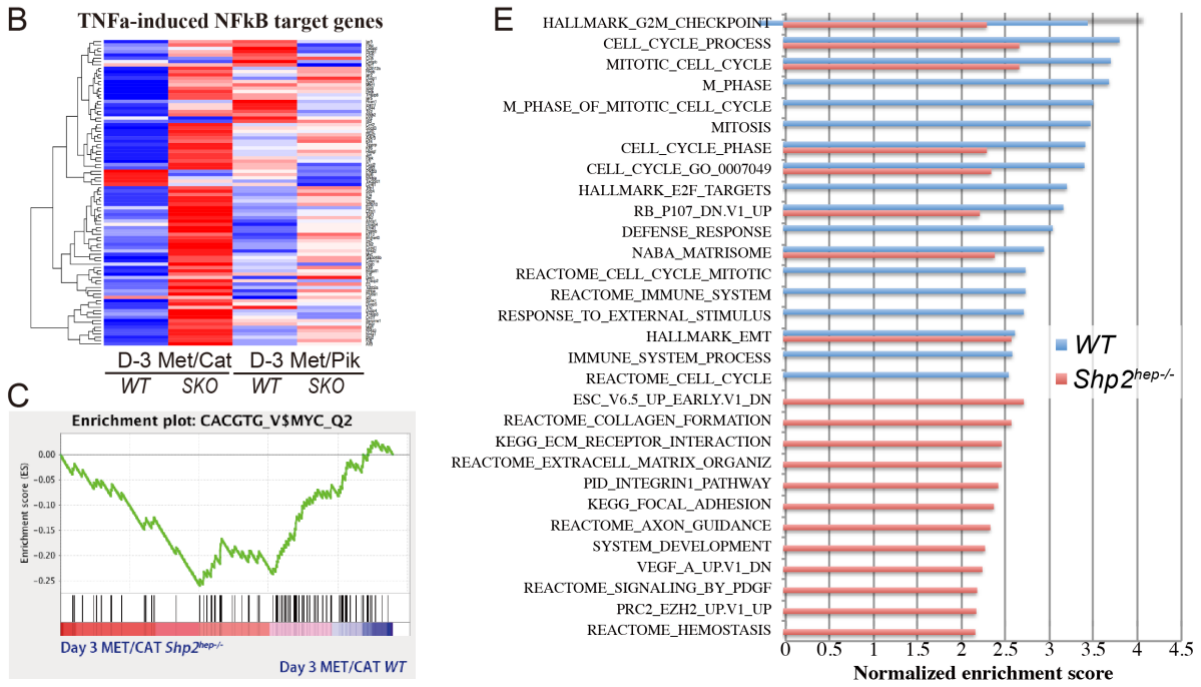

Figure 6. Transcriptomic analysis of Met/Cat- or Met/Pik-transfected *WT* and *Shp2*$^{hep-/-}$ livers

A. IPA of Day-3 Met/Cat-transfected *WT* or *Shp2*$^{hep-/-}$ livers versus Day-0 non-transfected genotype-matched livers.

B. Heatmap representation of TNFα-induced NFκB target genes. Gene expression variations are presented by fold change of expression with red and blue indicating increase and decrease respectively, compared to genotype-matched Day-0 controls.

C. Enrichment plots of gene set containing Myc target genes comparing Day-3 Met/Cat-transfected *Shp2*$^{hep-/-}$ and *WT* livers.

D. IPA of Day-3 Met/Pik-transfected *WT* or *Shp2*$^{hep-/-}$ livers versus Day-0 non-transfected genotype-matched livers.

E. Top-ranked up-regulated gene sets in Day-3 Met/Pik-transfected *WT* or *Shp2*$^{hep-/-}$ livers versus Day-0 non-transfected genotype-matched livers.

Fig.7

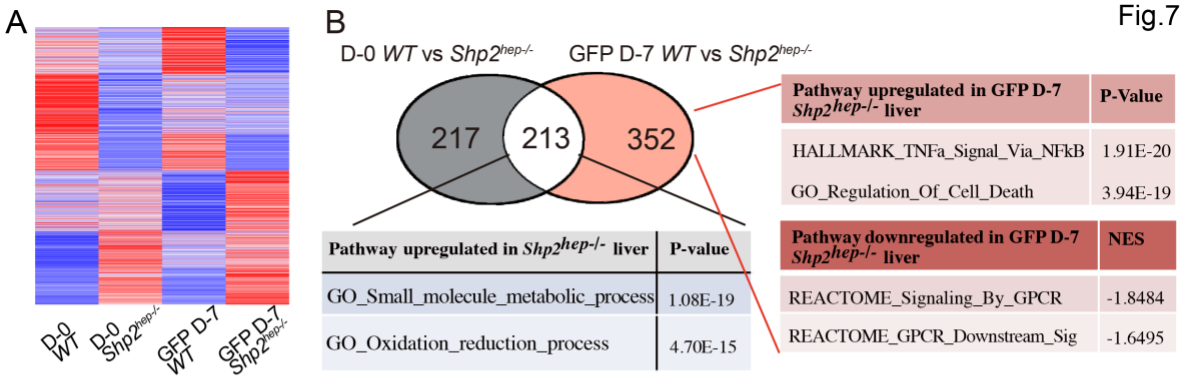

Pathway upregulated in *Shp2*$^{hep-/-}$ liver	P-value
GO_Small_molecule_metabolic_process	1.08E-19
GO_Oxidation_reduction_process	4.70E-15

Pathway upregulated in GFP D-7 *Shp2*$^{hep-/-}$ liver	P-Value
HALLMARK_TNFa_Signal_Via_NFkB	1.91E-20
GO_Regulation_Of_Cell_Death	3.94E-19

Pathway downregulated in GFP D-7 *Shp2*$^{hep-/-}$ liver	NES
REACTOME_Signaling_By_GPCR	-1.8484
REACTOME_GPCR_Downstream_Sig	-1.6495

C

Pathway upregulated in Met/Cat D-7 *Shp2*$^{hep-/-}$ liver	NES
Defense_Response	2.84639
REACTOME_Adaptive_Immune_System	1.92227
GGAAGTG_V$GABP_B	1.83922

Pathway downregulated in Met/Cat D-7 *WT* liver	NES
Regulation_of_RNA_Metabolic_Process	-2.00097
Regulation_of_Transcription_DNA_Dependent	-1.99496
TGCCAAR_V$NF1_Q6	-1.98075

D

Pathway upregulated in Met/Pik D-7 *WT* liver	NES
HALLMARK_G2M_Checkpoint	2.78143
M_PHASE	2.51424

Pathway upregulated in Met/Pik D-7 *Shp2*$^{hep-/-}$ liver	NES
REACTOME_Immune_System	1.80404
HALLMARK_Interferon_Gamma_Respons	1.60970

Pathway downregulated in Met/Pik D-7 *Shp2*$^{hep-/-}$ liver	NES
CACGTG_V$MYC_Q2	-2.50827
GGGCGGR_V$SP1_Q6	-2.01403

Figure 7. Comparative analysis of transcriptomes between non-transfected and GFP-transfected liver

A. Overview heatmap of transcriptomes from Day-0 and GFP-transfected Day-7 *WT* and *Shp2*$^{hep-/-}$ livers. Red and blue represent high and low absolute expression level respectively.

B. Overlap of differentially expressed genes (DEGs) in both Day-0 *WT* vs. *Shp2*$^{hep-/-}$ livers, and GFP Day-7 *WT* vs. *Shp2*$^{hep-/-}$ livers. The numbers indicate DEGs identified in both or only one comparison. Pathway analysis was performed on the DEGs from indicated groups.

C. GSEA analysis of DEGs between Met/Cat-transfected *Shp2*$^{hep-/-}$ and *WT* livers on Day-7 post transfection.

D. GSEA analysis of DEGs identified by comparing Met/Pik-*WT* livers versus GFP-*WT* liver on day-7, or Met/Pik-*Shp2*$^{hep-/-}$ livers versus GFP-*Shp2*$^{hep-/-}$ livers on day-7.

2.6. Shp2 removal promotes cell senescence induced by oncoproteins

We explored whether Shp2 deficiency in hepatocytes promoted cell senescence in response to transfection of the oncogenes, given the upregulation of p53 signaling and cell cycle progression inhibitors induced in oncogene-overexpressing *Shp2*$^{hep-/-}$ liver (Figure 6A,D). Staining of liver sections demonstrated significantly increased signals for the primary senescence marker SA-β-galactosidase (SA-β-gal) in *Shp2*$^{hep-/-}$ livers, compared to *WT* livers, on day-12 after transfection of Met/Cat or Met/Pik (Figure 8A). Consistently, qRT-PCR analysis detected higher expression of cell cycle inhibitors p16 and p19, and senescence-associated genes mcp1, il-15 and csf1 in *Shp2*$^{hep-/-}$ than *WT* liver lysates, in response to expression of the oncogenes (Figure 8B). Meanwhile, proliferative hepatocyte numbers were decreased in *Shp2*$^{hep-/-}$ livers compared to *WT* livers, as assessed by proliferative marker Ki67 and hepatocyte marker HNF4α staining (Figure 8C). SA-β-gal signals diminished in *Shp2*$^{hep-/-}$ liver at week-3, and were barely detectable at week-5 post-injection (Figure 8A), suggesting clearance of senescent cells. Together, these results suggest that deleting Shp2 in hepatocytes not only inhibited proliferative signaling but also induced cell senescence, collectively contributing to the suppression of hepato-oncogenesis induced by Met/Cat or Met/Pik.

2.7. Shp2 modulates mitogenic signaling elicited by HGF and Wnt3a in the liver

We further investigated the impact of Shp2 deficiency on acute HGF/Met and Wnt signaling following portal vein administration of the ligands into the liver. Injection of HGF potently stimulated *in vivo* pMet, pErk and pAkt signals, but these signals were abolished or diminished in *Shp2*$^{hep-/-}$ livers (Figure 9A), confirming the requirement of Shp2 in HGF/Met/MAPK axis signaling. On the other hand, intraportal administration of Wnt3a plus

R-spondin1 did not stimulate changes in Wnt/β-catenin pathway direct indicator, such as Ser33/Ser37/Thr41 phosphorylation of β-catenin or its nuclear translocation, in *WT* or *Shp2*$^{hep-/-}$ livers (Figure 10), whereas transcription of some Wnt targets were activated in *WT* rather than in mutant liver (Figure 9C). Surprisingly, Wnt ligands induced modest elevation of pErk in *WT* liver, which might be caused by the crosstalk between Wnt/β-catenin and Ras/Erk pathway. It has been reported that Wnt3a could induce Raf1-Mek-Erk axis activation, probably through Wnt-regulated Ras stabilization (117). Wnt3a-induced Erk phosphorylation was abolished by hepatic Shp2 loss (Figure 9A), probably owing to impaired Ras activity in absence of Shp2, which acted in parallel with Ras stability regulation. Consistently, *in vitro* HGF or Wnt3a stimulation induced higher pErk signal in *WT* than in Shp2-deficient isolated primary hepatocytes (Figure 9B).

The impaired stimulation of Met/MAPK pathway in Shp2 depleted liver by either Met overexpression and HGF ligand stimulation supported a critical role of Shp2 in mediating Met/MAPK pathway. However, the activation result of Wnt/β-catenin pathway in Shp2 depleted liver varied dependent on approaches of stimulation. Furthermore, the possible crosstalk between Met/MAPK and Wnt/β-catenin pathway made it even harder to segregate Shp2 function on Wnt/β-catenin pathway.

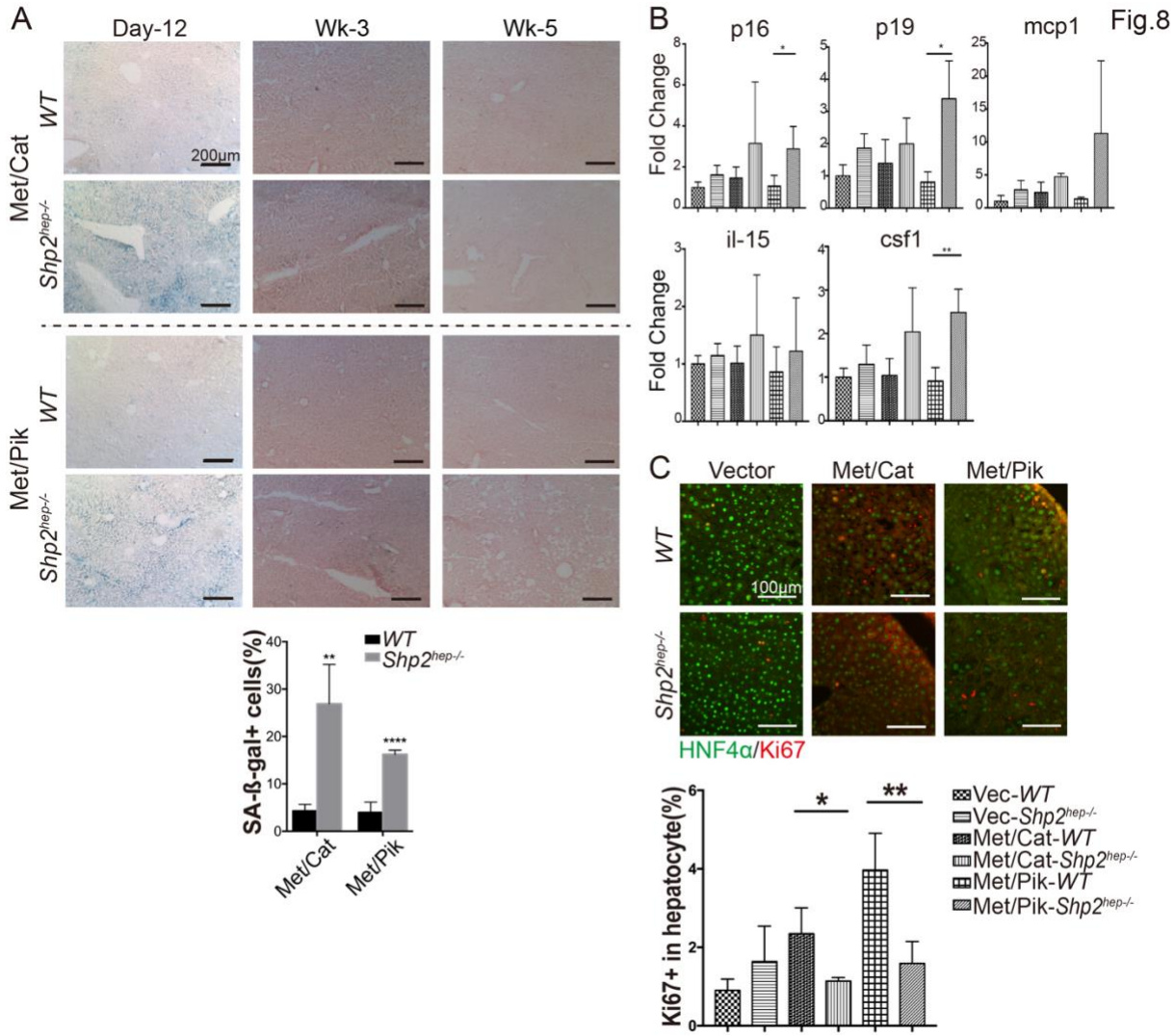

Figure 8. Shp2 deficiency promotes oncogene-induced cell senescence

A. Representative SA-β-galactosidase staining of *WT* and *Shp2*$^{hep-/-}$ liver sections on day-12 post Met/Cat or Met/Pik transfection. Quantification was based on more than four randomly selected microscopic fields of view of each biological sample, n=3.

B. Transcript level of senescence-associated genes in whole liver lysate, n=3-4.

C. Representative images of co-staining of HNF4α and Ki67 of liver sections on day 12 post injection. Quantification was based on more than four randomly selected microscopic fields of view of each biological sample, n=3-4.

Data are mean values ± SD and P values were calculated by unpaired two-tailed Student's T-test. ns or no annotation, not significant, *P<0.05, **P < 0.01, ****P<0.0001.

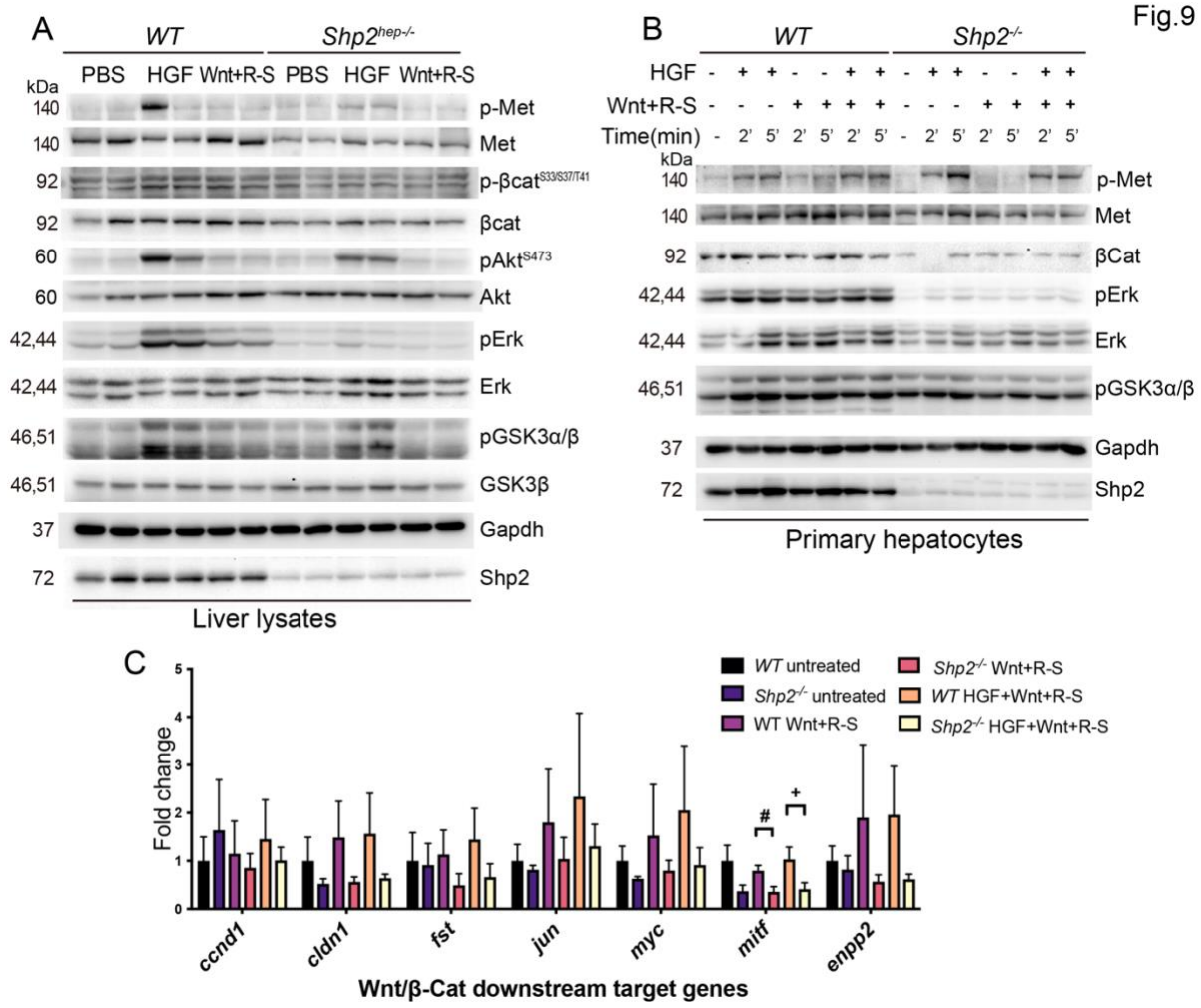

Figure 9. Shp2 deficiency affects HGF and Wnt3a signaling *in vivo* and *in vitro*

A. Immunoblotting for indicated proteins in lysates of PBS-, HGF- or Wnt+R-S-treated *WT* or *Shp2*$^{hep-/-}$ livers.

B. Immunoblotting for indicated proteins in lysates of control-, HGF- or Wnt+R-S-treated *WT* or *Shp2*$^{-/-}$ primary hepatocytes.

C. Transcript expressions of Wnt/β-Cat downstream target genes in control or ligand-treated *WT* or *Shp2*$^{hep-/-}$ livers. Data are mean values ± SD and P values were calculated by unpaired two-tailed Student's T-test. ns or no annotation, not significant, $^{\#,+}P<0.05$.

Fig.10

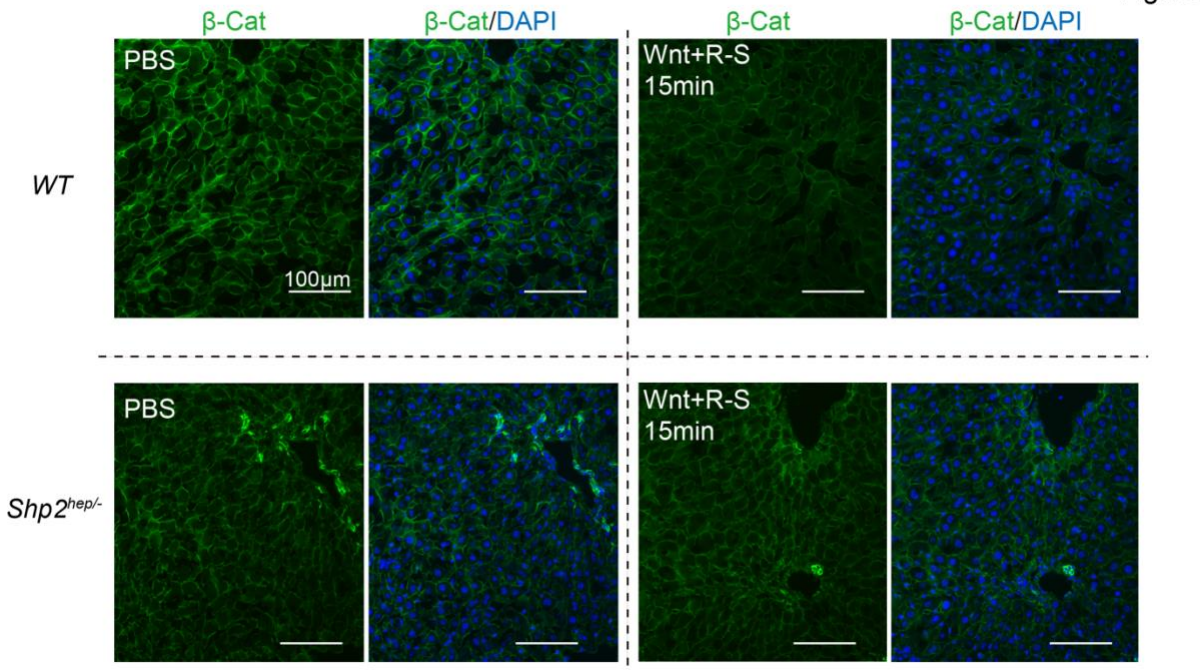

Figure 10. Cellular localization of β-Catenin after Wnt/R-spondin stimulation in vivo
β-Catenin immunofluorescence staining of sections of *WT* and *Shp2*$^{hep-/-}$ livers that were stimulated *in vivo* with Wnt3a+R-spondin1 for 15 minutes.

2.8. Shp2 is stringently required for hepatocarcinogenesis driven by RTK signaling

Based on the data obtained, we hypothesized that whether Shp2 is critical for mediating c-Met signaling, but rather dispensable in β-Catenin and PI3K signaling. To examine this hypothesis, we tested whether Shp2 loss has an impact on oncogenic β-Catenin and PI3K p110α (Cat/Pik)-induced hepatic tumorigenesis independent of Met. By evaluating liver/body weight ratios, tumor numbers and sizes 15 weeks later, we detected similar tumor burdens in *Shp2*$^{hep-/-}$ and *WT* livers (Figure 11A). Consistently, comparable levels of glutamine synthetase, phosphorylated Akt and Erk (pAkt and pErk) were detected in mutant and WT liver sections or lysates (Figure 11B,C). Lipid droplet accumulations, driven by overactivation of the PI3K pathway, were also similar in transfected WT and mutant livers (Figure 11D). Taken together, these results suggest that Shp2 is indeed necessary for relay of oncogenic signals from Met but is dispensable for hepato-oncogenesis driven by β-catenin and PI3K mutants.

We also examined the impact of Shp2 deficiency on HCC induced by another pair of oncogenes, Nras^{G12V} and Δβ-catenin (Ras/Cat). Notably, Shp2 deletion in hepatocytes did not impair but even aggravated Ras/Cat-induced tumors (Figure 12A,B), consistent with previous data showing a more severe tumor phenotype driven by DEN in *Shp2*$^{hep-/-}$ mice (63). Likewise, co-transfection of Nras^{G12V} and a nuclear oncogene Myc (Ras/Myc) induced heavier tumor loads in *Shp2*$^{hep-/-}$ than *WT* livers (Figure 13A). Augmented cell proliferation and hence more aggressive tumor progression were detected, as evaluated by elevated proliferative marker Ki67 and stemness marker CD133 levels in *Shp2*$^{hep-/-}$ compared to *WT* livers following Ras/Myc transfection (Figure 13B,C).

To extend these observations, we evaluated growth of liver metastasized tumors following intrasplenic injection of MC38 colorectal cancer cells. Indeed, more aggressive tumor

metastasis was observed in *Shp2*$^{hep-/-}$ than *WT* livers (Figure 13D). In aggregate, these experiments, while disclosing a cell-intrinsic role of Shp2 in RTK-driven hepatocarcinogenesis, also revealed that genetic deletion of Shp2 in hepatocytes induced a hepatic microenvironment conducive for growth of both primary and metastasized liver tumors.

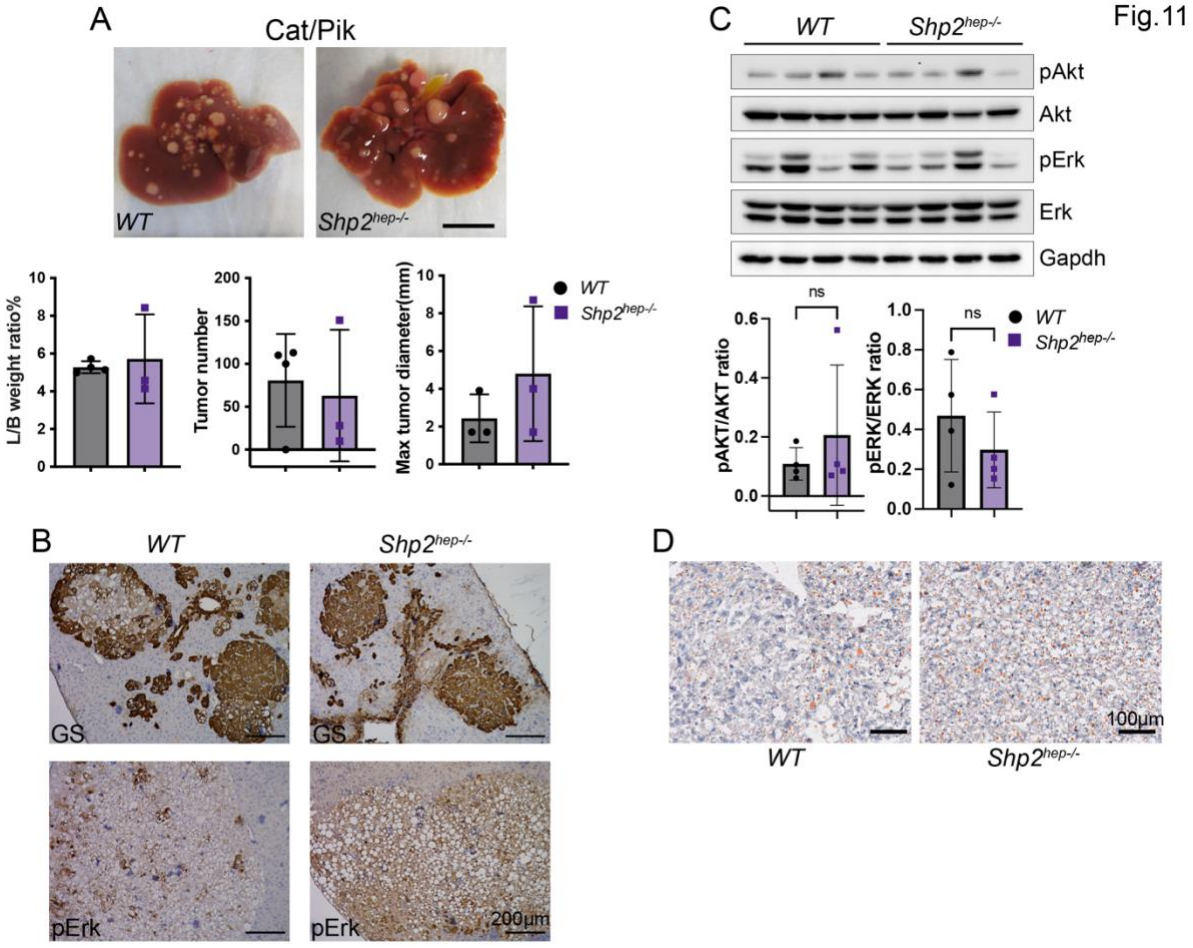

Figure 11. Hepatocyte Shp2 is dispensable for Cat/Pik-induced liver tumorigenesis

A. Representative macroscopic liver images, and liver/body (L/B) weight ratios, numbers and maximal diameters of liver tumors induced by Cat/Pik in *WT* and *Shp2*$^{hep-/-}$ mice at week-15 post transfection. n=4(*WT*), 3(*Shp2*$^{hep-/-}$). Scale bar: 1 cm.

B. Immunostaining of glutamine synthetase (GS) and phosphorylated Erk (pErk) on Cat/Pik-transfected liver sections at 15 weeks post transfection.

C. Immunoblotting of indicated proteins in whole liver lysate of Cat/Pik-transfected liver at week-15 with quantification of band intensity ratios. Western blot quantification was performed on four biological replicates and two technical replicates.

D. Oil red O staining of Cat/Pik-transfected *WT* and *Shp2*$^{hep-/-}$ livers.

Fig.12

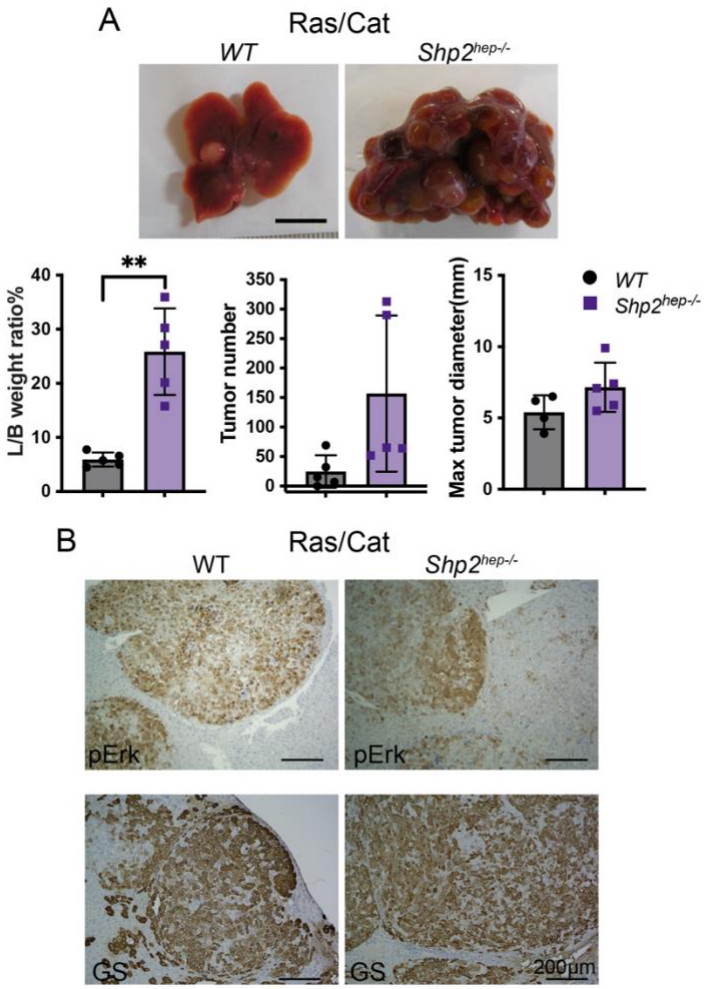

Figure 12. Genetic deletion of Shp2 in hepatocyte aggravates Ras/Cat-induced liver tumorigenesis

A. Representative macroscopic liver images, L/B weight ratios, numbers and maximal diameters of Ras/Cat-induced tumors in *WT* and *Shp2*$^{hep-/-}$ mice at week-8 post transfection. n=5. Scale bar: 1 cm.

B. Immunostaining of pErk and GS on Ras/Cat-transfected liver sections.

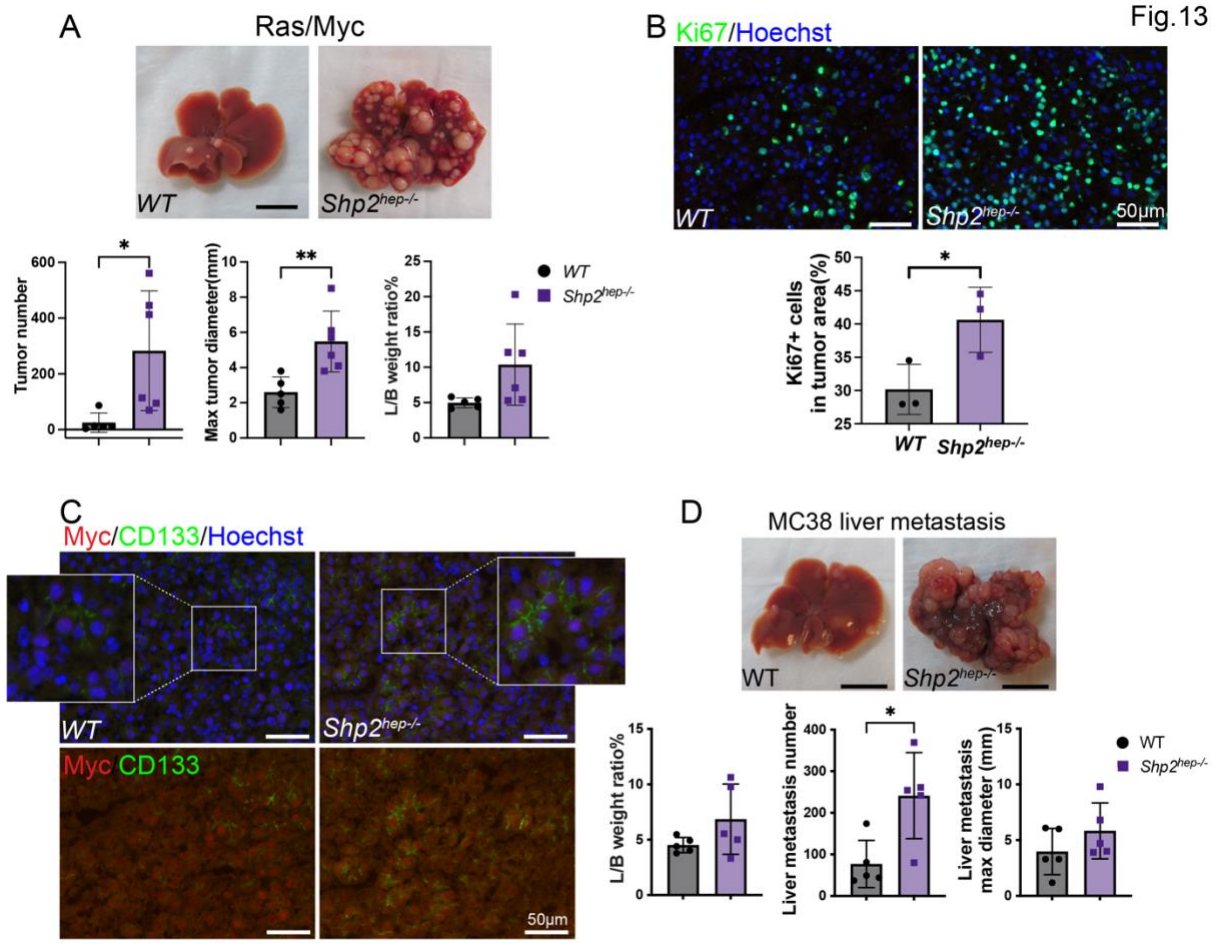

Figure 13. Genetic deletion of Shp2 in hepatocyte aggravates Ras/Myc-induced autochthonous liver tumor and metastasized liver tumor

A. Representative macroscopic images and physiological parameters of Ras/Myc-transfected (week-5) *WT* and *Shp2*$^{hep-/-}$ livers. Scale bar: 1cm.

B. Immunofluorescence staining of Myc and Ki67 on Ras/Myc-induced tumor areas in *WT* liver following DMSO or SHP099, with quantification of Ki67^{+} cell percentage in Myc^{+} tumor areas. Six randomly selected microscopic fields of view were quantified for each biological sample. n=5(DMSO), 4(SHP099).

C. Immunostaining of Myc and CD133 in Ras/Myc-transfected liver.

D. Representative macroscopic images and liver metastasis measurements of DMSO- and SHP099-pretreated *WT* liver on day-15 post injection of MC38 cells (20,000 cells per mouse). n=4. Scale bar: 1 cm.

In A,D, Data are mean values ± SD and P values were calculated by unpaired two-tailed Student's T-test. ns, not significant, *P < 0.05, **P < 0.01.

2.9. The catalytic activity is essential for Shp2 relay of oncogenic signal from RTK

To dissect the biochemical mechanism underlying a pivotal role of Shp2 in RTK-dependent tumorigenesis, we performed co-transfection of WT, $Shp2^{C463S}$ (catalytically inactive) or $Shp2^{D61A}$ (constitutively active) mutant with Met/Cat or Met/Pik oncogenes. Co-delivery of WT or $Shp2^{D61A}$ mutant rescued the tumor phenotype in *Shp2*$^{hep-/-}$ mice by Met/Cat or Met/Pik, but $Shp2^{C463S}$ mutant failed to do so (Fig.14A-C). Further, co-transfection of the $Shp2^{C463S}$ mutant even suppressed Met/Cat-induced tumors in *WT* mice (Figure 14A). Together, these results indicate a stringent dependence of Shp2 on its catalytic activity in Met-driven oncogenic signaling in hepatocytes. Consistent with the rescued tumor phenotype, re-expressing wild-type Shp2 in Shp2-deficient hepatocytes restored Met- and β-catenin-mediated signaling events and restored ectopic Met expression, which was not stably expressed in Shp2-deficient hepatocytes (Figure 15A,B). Also, expressing the $Shp2^{C463S}$ mutant induced hepatocyte senescence, contributing to tumor suppression in *WT* liver (Figure 15C).

As Suppressor of cytokine signaling 1 (Socs1) was shown to inhibit Met expression and signaling (106), we explored a possible role of Socs1 in mediating Shp2 modulation of Met activity. Expressing a dominant negative mutant of Socs1 ($Socs1^{F59D}$) partially restored Met/Cat-induced tumor phenotype in *Shp2*$^{hep-/-}$ liver (Figure 16A). Meanwhile, expressing a dominant negative mutant ($Socs3^{F25A}$) of Socs3, another member of the family, drove a more severe tumor phenotype (Figure 16A). However, co-transfection of $Socs3^{F25A}$ mutant with Δβ-catenin, without including Met, did not rescue the tumor phenotype in *Shp2*$^{hep-/-}$ liver, suggesting that abrogating Socs1 or Socs3 functions played a permissive role in Met signaling but was not sufficient to drive HCC (Figure 16C). Met expression was fully rescued by co-transfection with $Socs3^{F25A}$ mutant (Figure 16B,D), and a similar rescuing effect of the tumor

phenotype was observed by expressing an undegradable mutant Met^{Y1003F} (Met^{YF}) (Figure 17A,B), which induced abundant Met expression on cell surface and more aggressive tumor progression as revealed by CD133 expression (Figure 17C). Together, these data suggest that Shp2 transduced oncogenic signals at least in part by overcoming Socs3-mediated downregulation of Met expression and activity.

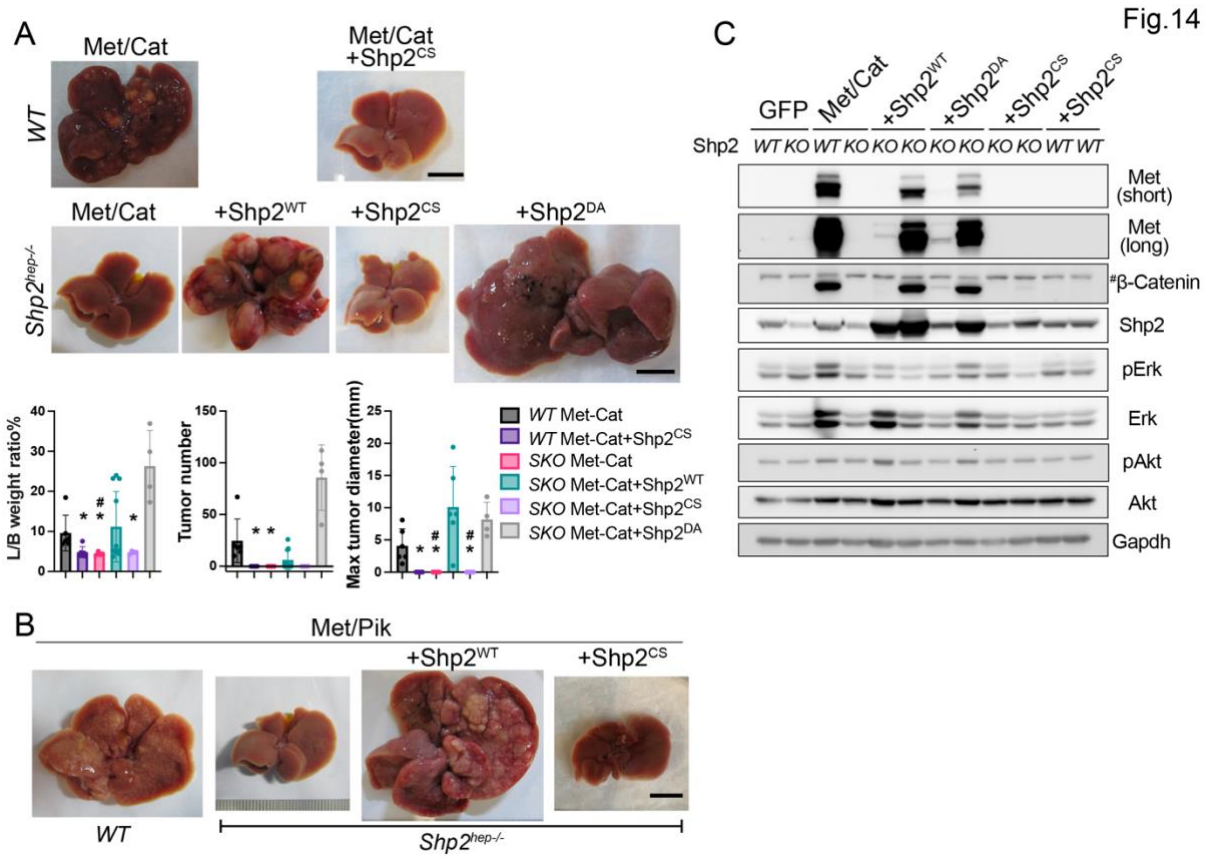

Figure 14. Rescuing effect of Shp2 expression on liver tumors induced by various oncogenes

A. Representative macroscopic liver images, L/B weight ratios, numbers and maximal tumor diameters in *WT* or *Shp2*$^{hep-/-}$*(SKO)* livers following co-transfection of Met/Cat with Shp2^{WT}, Shp2^{CS} or Shp2^{DA}. n=6(*WT* Met/Cat),6(*WT* Met/Cat+Shp2^{CS}),4(*SKO* Met/Cat),11(*SKO* Met/Cat+Shp2^{WT}),4(*SKO* Met/Cat+Shp2^{CS}), 4(*SKO* Met/Cat+Shp2^{DA}). Scale bar: 1 cm. *,# indicate a significant difference between the annotated group versus *WT* Met/Cat group or versus *SKO* Met/Cat+Shp2^{WT} group, respectively.

B. Representative macroscopic images of *WT* and *Shp2*$^{hep-/-}$ livers transfected with Met/Pik in combination with wild-type or mutant Shp2 at week-12 post transfection. Scale bar:1 cm.

C. Immunoblotting of indicated proteins in whole liver lysates of Met/Cat+Shp2-transfected liver. *no specific band can be detected with Socs1 antibody. #Upper and lower β-Catenin bands detect endogenous and exogenous (truncated) β-Catenin, respectively.

Fig.15

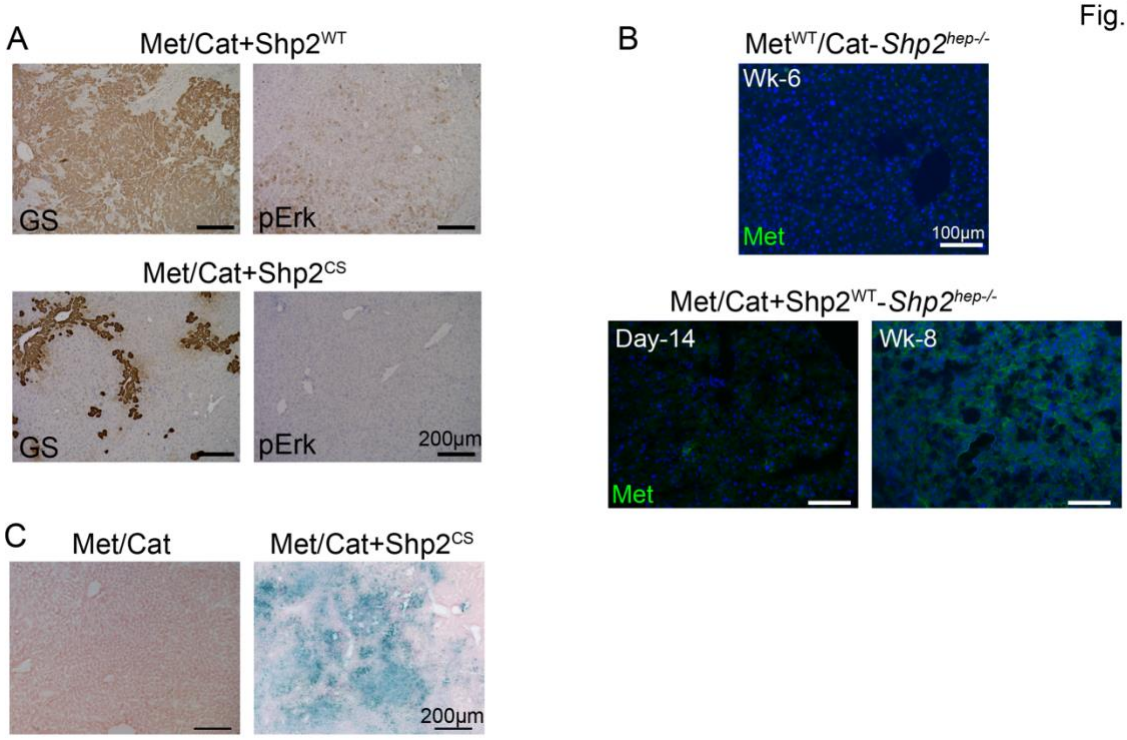

Figure 15. Effects of modulating hepatic Shp2 catalytic activity on oncogene-induced liver tumor

A. Immunostaining of GS and pErk on sections of *Shp2*$^{hep-/-}$ liver transfected with Met/Cat plus wild-type or mutant Shp2.

B. Immunofluorescence staining of Met in *Shp2*$^{hep-/-}$ liver transfected with Met^{WT}/Cat or Met^{YF}/Cat, with or without re-expression of Shp2^{WT}.

C. Detection of cell senescence by β-galactosidase staining of *WT* liver sections transfected by Met/Cat, with or without Shp2^{CS} mutant.

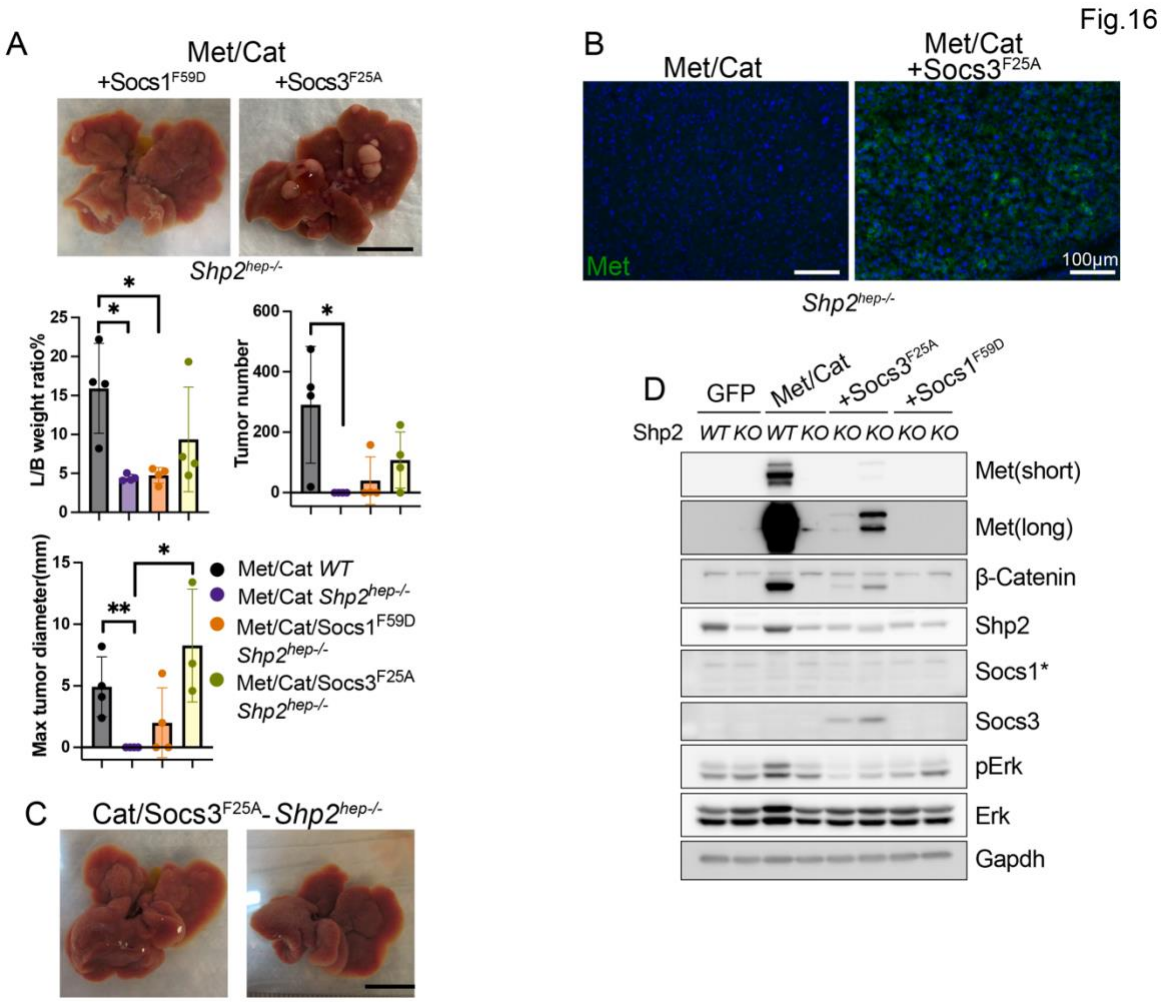

Figure 16. Rescuing effect of Socs1/3 function abrogation on liver tumors induced by various oncogenes

A. Representative macroscopic images and physiological parameters of *Shp2*$^{hep-/-}$ livers transfected with Met/Cat+Socs1^{F59D} or Met/Cat+Socs3^{F25A} at week-10 post transfection (tumorigenesis penetration ratio: 2/4 versus 3/4). n=4. Scale bar: 1cm.

B. Immunofluorescence staining of Met on Met/Cat or Met/Cat+Socs3^{F25A} transfected *Shp2*$^{hep-/-}$ livers at week-8 post transfection.

C. Representative macroscopic images of *Shp2*$^{hep-/-}$ liver transfected with Cat/Socs3^{F25A}. Scale bar: 1cm.

D. Immunoblotting of indicated proteins in whole liver lysates of (I)Met/Cat+Shp2-transfected liver or (J)Met/Cat+Socs1/Socs3-transfected liver. *no specific band can be detected with Socs1 antibody. #Upper and lower β-Catenin bands detect endogenous and exogenous (truncated) β-Catenin, respectively.

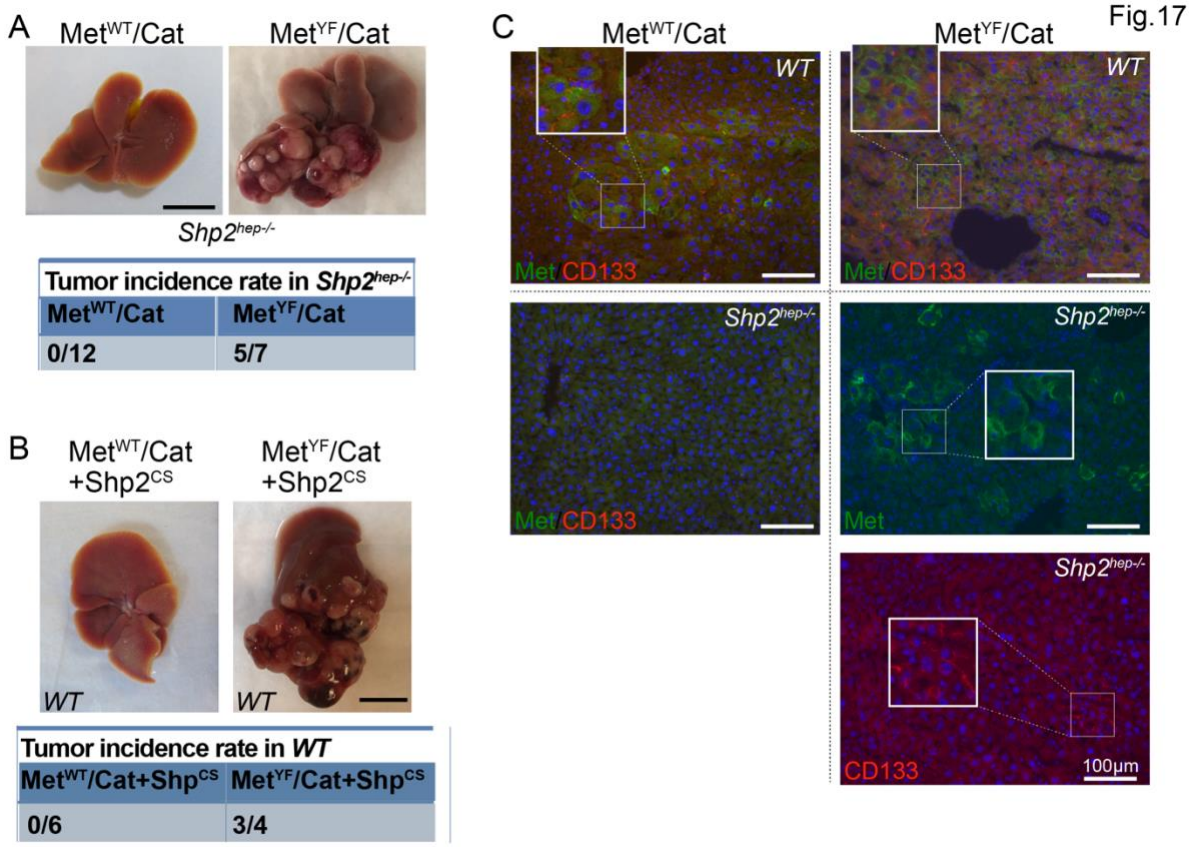

Figure 17. Rescuing effect of Shp2 or Met mutant expression on liver tumors induced by various oncogenes

A. Representative macroscopic liver images and tumor incidence rates of *Shp2*$^{hep-/-}$ livers transfected with Met^{WT}/Cat or Met^{YF}/Cat. Scale bar: 1cm.

B. Representative macroscopic liver images and tumor incidence rates of *WT* livers transfected with Met^{WT}/Cat or Met^{YF}/Cat together with Shp2^{CS}. Scale bar: 1cm.

C. Immunofluorescence staining of Met and CD133 in *WT* and *Shp2*$^{hep-/-}$ liver transfected with Met^{WT} or Met^{YF} together with Cat.

2.10. Pharmaceutical inhibition of Shp2 robustly suppresses primary liver cancer

Given a critical role of Shp2's catalytic activity in mediating Met-induced oncogenesis, but also an opposite tumor-promoting environmental effect generated in *Shp2*$^{hep-/-}$ liver, we wanted to determine how a Shp2 inhibitor might influence HCC progression in mice. We first examined the effect of an allosteric Shp2 inhibitor (SHP099) in cultured HEK293T cells *in vitro*. As expected, treatment with this compound inhibited pErk signal stimulated by Met overexpression and HGF, the Met ligand (Figure 18A), but SHP099 failed to inhibit Ras-induced pErk signal in Ras/Myc-transfected cells (Figure 18B). Next, we tested its therapeutic effect in mouse HCC induced by Met/Cat. When tumor nodules reached 2-3 mm, around 3 weeks after oncogene transfection, the mice were injected intraperitoneally (i.p.) every day for three weeks (Figure 19A). SHP099 treatment effectively decreased tumor sizes and numbers, compared to the vehicle control (Figure 19B). Shp2 inhibition impaired pErk signal and reduced proliferation of Met^{+} tumor cells (Figure 19C,D). These results demonstrate a therapeutic effect of SHP099 in an autochthonous HCC model, although this treatment did not lead to a complete tumor remission in these mice.

We further tested the therapeutic effect of SHP099 in liver tumors driven by Ras/Myc. The Shp2 inhibitor exhibited no significant suppression on tumor progression, tumor cell proliferation and pErk signals (Figure 20A-C). Meanwhile, treatment with Trametinib (Tram), a Mek inhibitor, showed a robust suppression of Ras/Myc-driven tumor progression (Figure 20A). The poor efficacy of SHP099 on Ras/Myc-induced tumors was expected, as Shp2 was dispensable for Ras/Myc-driven HCC (Figure 13A).

Fig.18

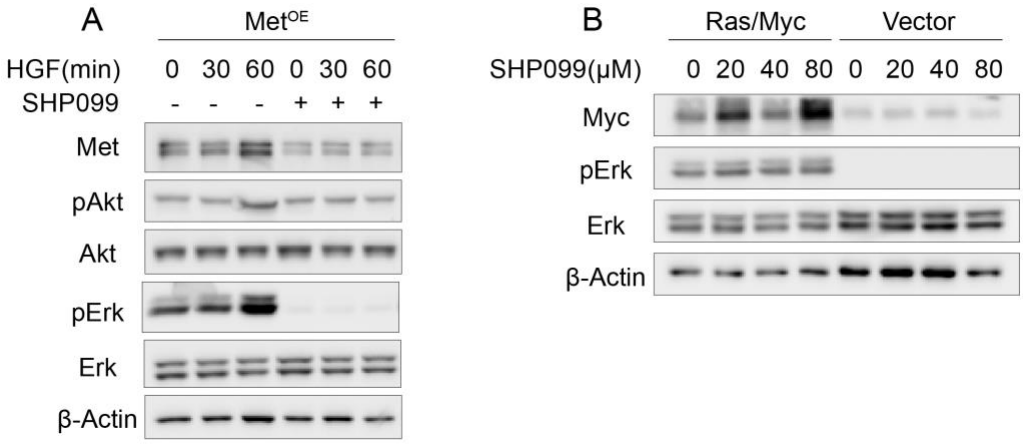

Figure 18. Effect of SHP099 on HGF/Met-elicited signals

A. Immunoblotting of signaling proteins in whole cell lysate of HEK293T cells overexpressing Met upon treatment of SHP099 (80μM) for 6hr with HGF (20ng/ml) short-term stimulation.
B. Immunoblotting of signaling proteins in whole cell lysate of HEK293T cells overexpressing vector or Ras/Myc upon 6-hour SHP099 treatment.

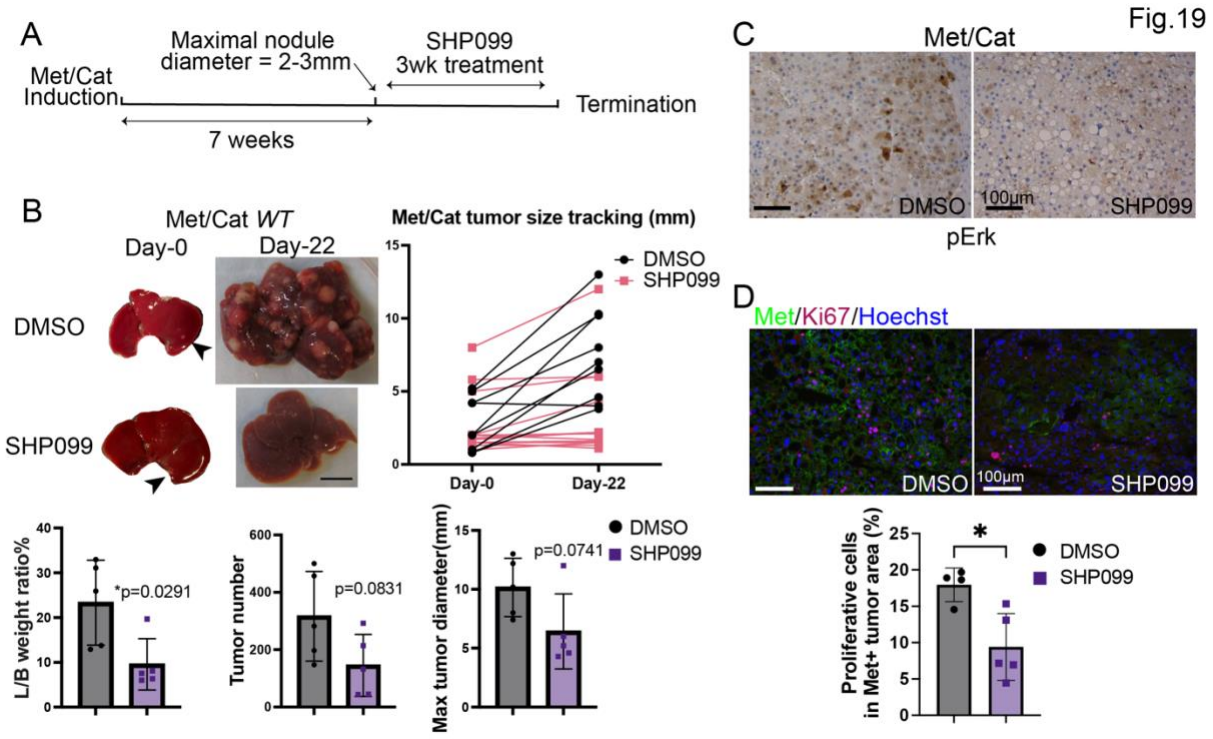

Figure 19. Autochthonous liver tumor-inhibitory effects of SHP099

A. Scheme of SHP099 treatment on Met/Cat-autochthonous liver tumor.

B. Upper left: representative macroscopic liver images before and after 3-week treatment of SHP099 or DMSO. Arrows point at established tumor nodules. Scale bar: 1 cm. Upper right: size tracking of trackable tumor nodules. Lower: quantitative analysis of L/B weight ratios, tumor numbers and sizes post treatment. n=5.

C. Immunostaining of pErk on Met/Cat-tumor areas following DMSO or SHP099 treatment.

D. Immunofluorescence staining of Met and Ki67 on Met/Cat-tumor areas following DMSO or SHP099 treatment, with quantification of $Ki67^{+}$ cell percentage in Met^{+} tumor areas. Six randomly selected microscopic fields of view were quantified for each biological sample. n=4(DMSO), 5(SHP099).

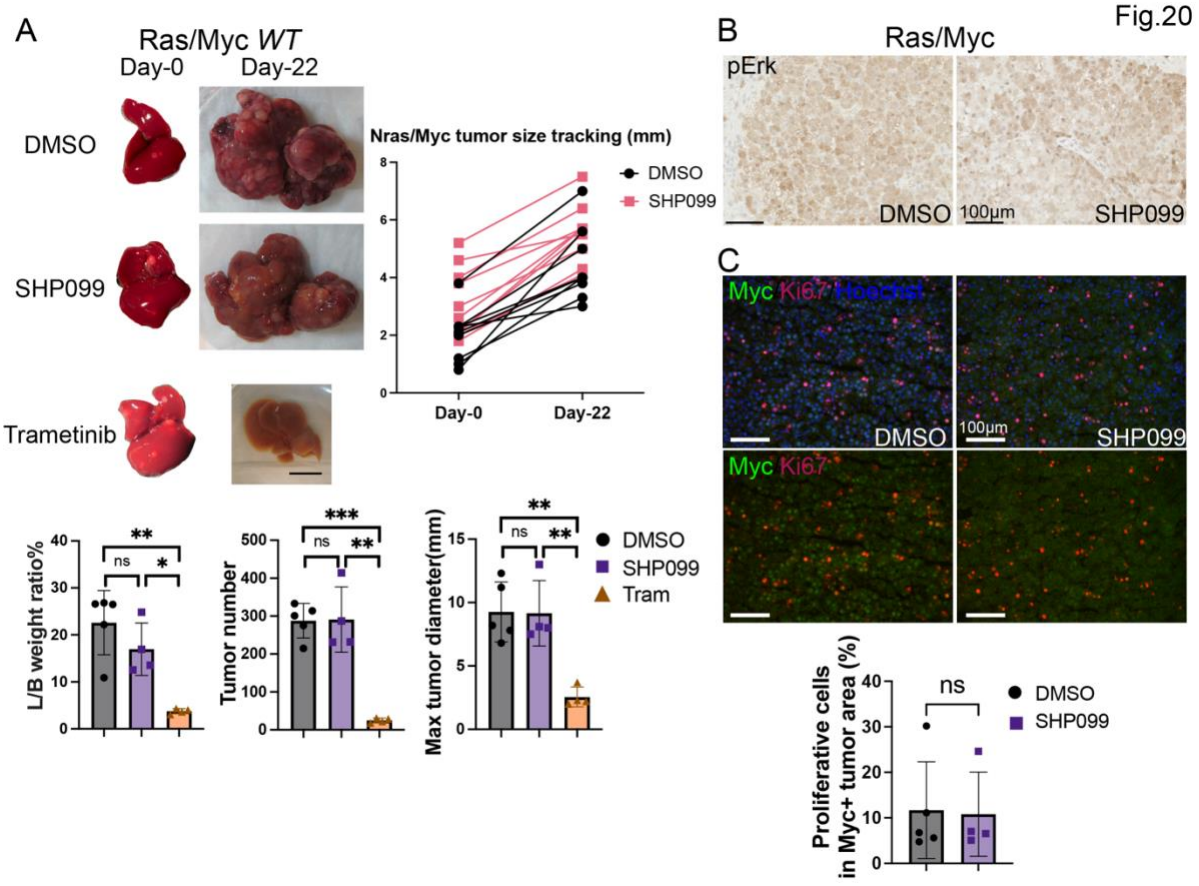

Figure 20. Effect of SHP099 of Ras/Myc-autochthonous liver tumor

A. Upper left: representative macroscopic liver images of Ras/Myc-transfected *WT* mice before and after 3-week treatment of DMSO, SHP099 or Trametinib (Tram), which started when tumor sizes reached 2-3 mm. Upper right: size tracking of trackable tumor nodules. Lower: L/B weight ratio, tumor numbers and sizes. n=5(DMSO), 4(SHP099), 4(Trametinib). Scale bar: 1cm.

B. Immunostaining of pErk on Ras/Myc-induced tumor areas following DMSO or SHP099 treatment in *WT* liver.

C. Immunofluorescence staining of Myc and Ki67 on Ras/Myc-induced tumor areas in *WT* liver following DMSO or SHP099, with quantification of $Ki67^+$ cell percentage in Myc^+ tumor areas. Six randomly selected microscopic fields of view were quantified for each biological sample. n=5(DMSO), 4(SHP099).

2.11. Pharmaceutical inhibition of Shp2 prevents metastasized tumor growth in the liver

Given the more aggressive growth of metastasized tumors in *Shp2*$^{hep-/-}$ liver (Figure 13D), we wondered if a Shp2 inhibitor had a similar effect of inducing a pro-tumorigenic niche in the liver as genetic removal of Shp2 in hepatocytes. To address this issue, we pre-treated *WT* mice with SHP099 before splenic injection of MC38 cells (Figure 21A). In contrast to genetic ablation of Shp2, we found that pre-treatment with SHP099 suppressed metastasized tumors in the liver, by evaluating tumor sizes and numbers (Figure 21B). The tumor-inhibitory effect of SHP099 pre-treatment was gradually diminished, as revealed by implanting tumor cells at day 3 or 10 following the last injection of the compound (Figure 21C). However, pretreatment with Trametinib did not exhibit a similar inhibitory effect on metastasized tumor growth (Figure 21D), suggesting a unique hepatoprotective effect of pharmaceutical Shp2 inhibition. We investigated how SHP099 pre-treatment remodeled the liver microenvironment. Hepatic inflammation was induced in *Shp2*$^{hep-/-}$ mice (63), featured by inflammatory and immune cell accumulation near portal triads and ballooning hepatocytes (Figure 22A). However, SHP099-treated livers exhibited normal and healthy histology (Figure 22A). Liver fibrosis and enlarged gallbladder induced in *Shp2*$^{hep-/-}$ mice were not observed in SHP099-treated liver (Figure 22B,C).

We compared the effects of gene deletion and chemical inhibition on hepatic immune cell profiles in mice at 2-3 months of age. Flow cytometry showed that neither Shp2 deletion nor SHP099 treatment marked altered the percentages of major lymphoid or myeloid cell subsets in the CD45^{+} cell population (Figure 23A,B; 24A-C), whereas LSEC subpopulation percentage was drastically changed by Shp2 deletion (Figure 24D). However, the absolute numbers of most immune cell subsets increased significantly in *Shp2*$^{hep-/-}$ livers, which were

compromised by SHP099 treatment (Figure 25A-C). The numbers of proliferative ($Ki67^+$) and activated (Granzyme B^+, or $CD69^+$) T cells and NK cells increased in *Shp2*$^{hep-/-}$ liver (Figure 25D-E), and PD-L1 expression on macrophages and liver specific endothelial cells (LSEC) were upregulated (Figure 26A). Moreover, Shp2 deletion altered polarization of macrophages, favoring M1 polarization, another sign of enhanced inflammatory response in *Shp2*$^{hep-/-}$ liver (Figure 24E). In comparison to genetic deletion, pharmaceutical inhibition of Shp2 induced only modest alterations in immune cell profiles in *WT* mice (Figure 23; 24), and attenuated some drastic changes in cell composition in *Shp2*$^{hep-/-}$ livers (Figure 24D,E; 25).

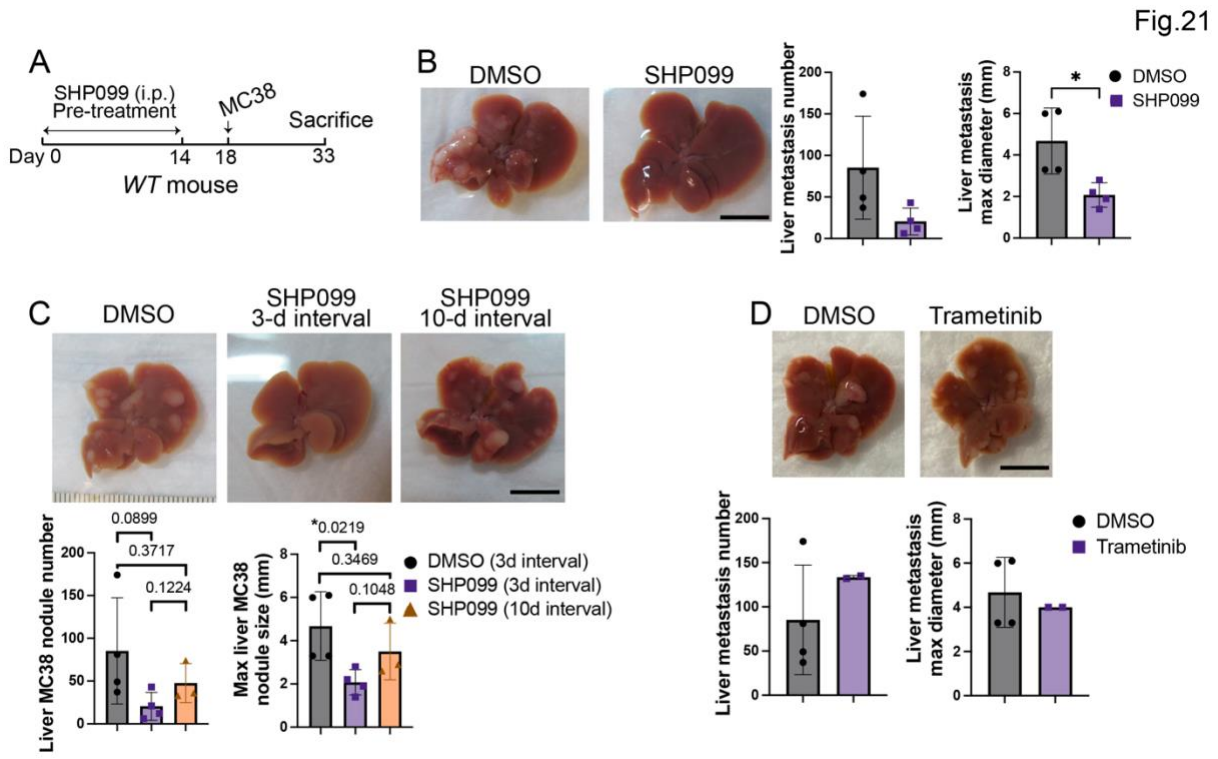

Figure 21. Hepatoprotective effect by SHP099 pretreatment

A. Scheme of SHP099 pretreatment on healthy *WT* liver.

B. Representative macroscopic images and liver metastasis measurements of DMSO- and SHP099-pretreated *WT* liver on day-15 post injection of MC38 cells (20,000 cells per mouse). n=4. Scale bar: 1 cm.

C. Representative macroscopic images and liver metastasis parameters of *WT* livers pre-treated with SHP099 followed by a 3-day or 10-day interval before MC38 intrasplenic transplantation (20000 cells per mouse). n=4(DMSO, SHP099 3d), 3(SHP099 10d). Scale bar: 1cm.

D. Representative macroscopic images and liver metastasis parameters of *WT* liver pre-treated with DMSO or Trametinib (Tram), followed by intrasplenic transplantation of MC38 (20000 cells per mouse). n=4(DMSO), 2(Tram). Scale bar: 1cm.

Fig.22

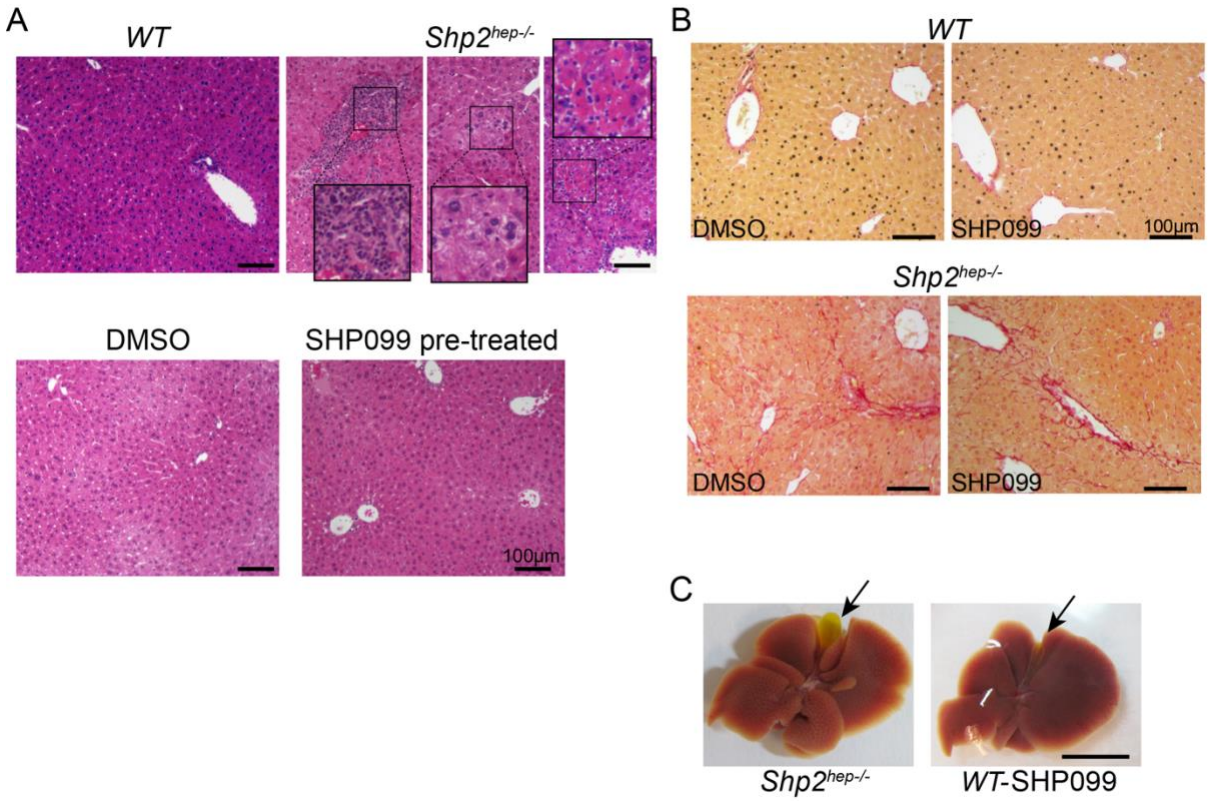

Figure 22. Effects by genetic and pharmaceutical inhibition of Shp2 on liver histology

A. H&E staining of untreated *WT* versus *Shp2*$^{hep-/-}$ liver, and DMSO- versus SHP099-pretreated *WT* livers. Areas displaying infiltration of small-nucleus cells, ballooning hepatocytes and necrotic tissue are highlighted and enlarged to show details.

B. Picrosirius red staining of DMSO/SHP099-pretreated *Shp2*$^{hep-/-}$ and *WT* liver.

C. Observation of enlarged gall bladder in *Shp2*$^{hep-/-}$ liver indicating defective bile acid clearance caused by cholestasis. Scale bar: 1cm.

Fig.23

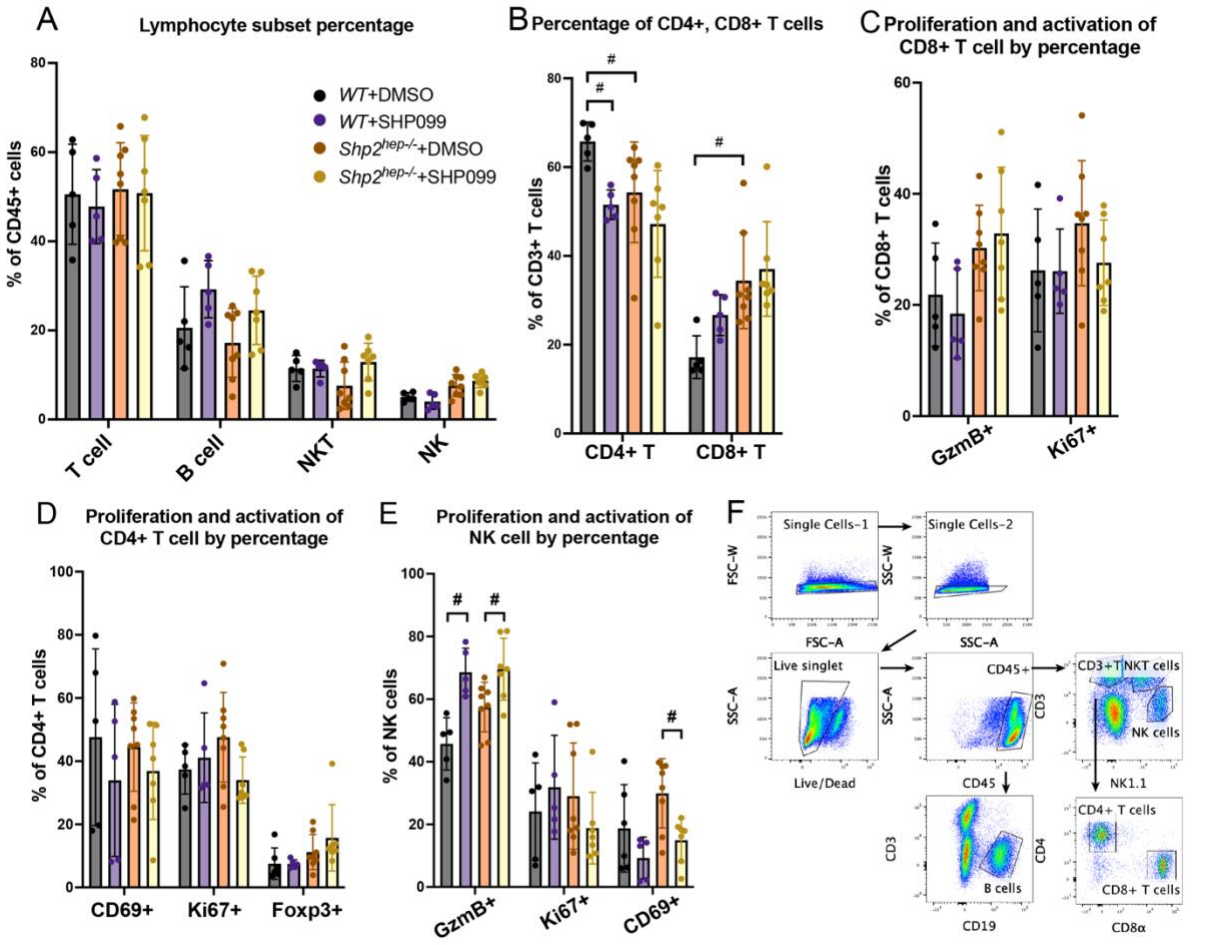

Figure 23. Effects by genetic and pharmaceutical inhibition of Shp2 on hepatic lymphoid immune profiles

A-B. Percentage of major immune cell subsets ($CD3^+$ T cell (T cell), $CD4^+$ T cell, $CD8^+$ T cell, B cell, NKT cell, NK cell) in the lymphoid compartment.

C-E. Percentages of proliferative and activated $CD4^+$ T, $CD8^+$ T and NK cells. Abbreviations used in A-E include: Regulatory T cell(T reg), Granzyme B(GzmB).

F. Representative flow cytometric pseudocolor plots showing the gating strategy for identification of lymphoid cell subsets.

Fig.24

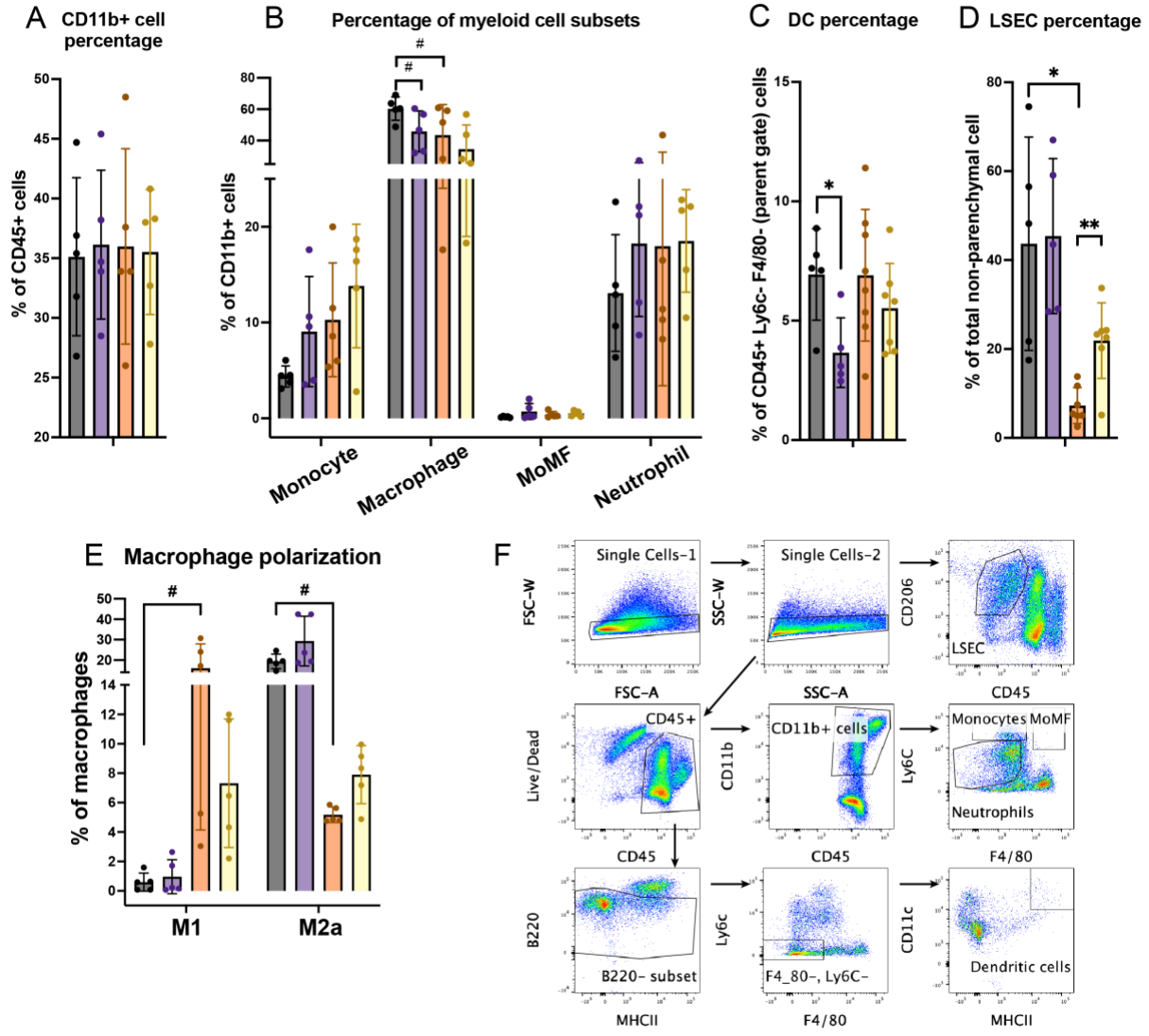

Figure 24. Effects by genetic and pharmaceutical inhibition of Shp2 on hepatic myeloid immune profiles

A-D. Percentage of (A-C) major immune cell subsets in the myeloid compartment or (D)liver specific endothelial cells(LSECs). Abbreviation used: MoMF, monocyte-derived macrophage.
E. Percentages of polarized macrophages M1 ($CD11c^+$ $CD206^-$ $F4/80^+$) and M2a ($CD11c^-$ $CD206^+$ $F4/80^+$) of total macrophages in whole liver.
F. Representative flow cytometric pseudocolor plots showing the gating strategy for identification of lymphoid, myeloid cell subsets and LSEC.

Fig.25

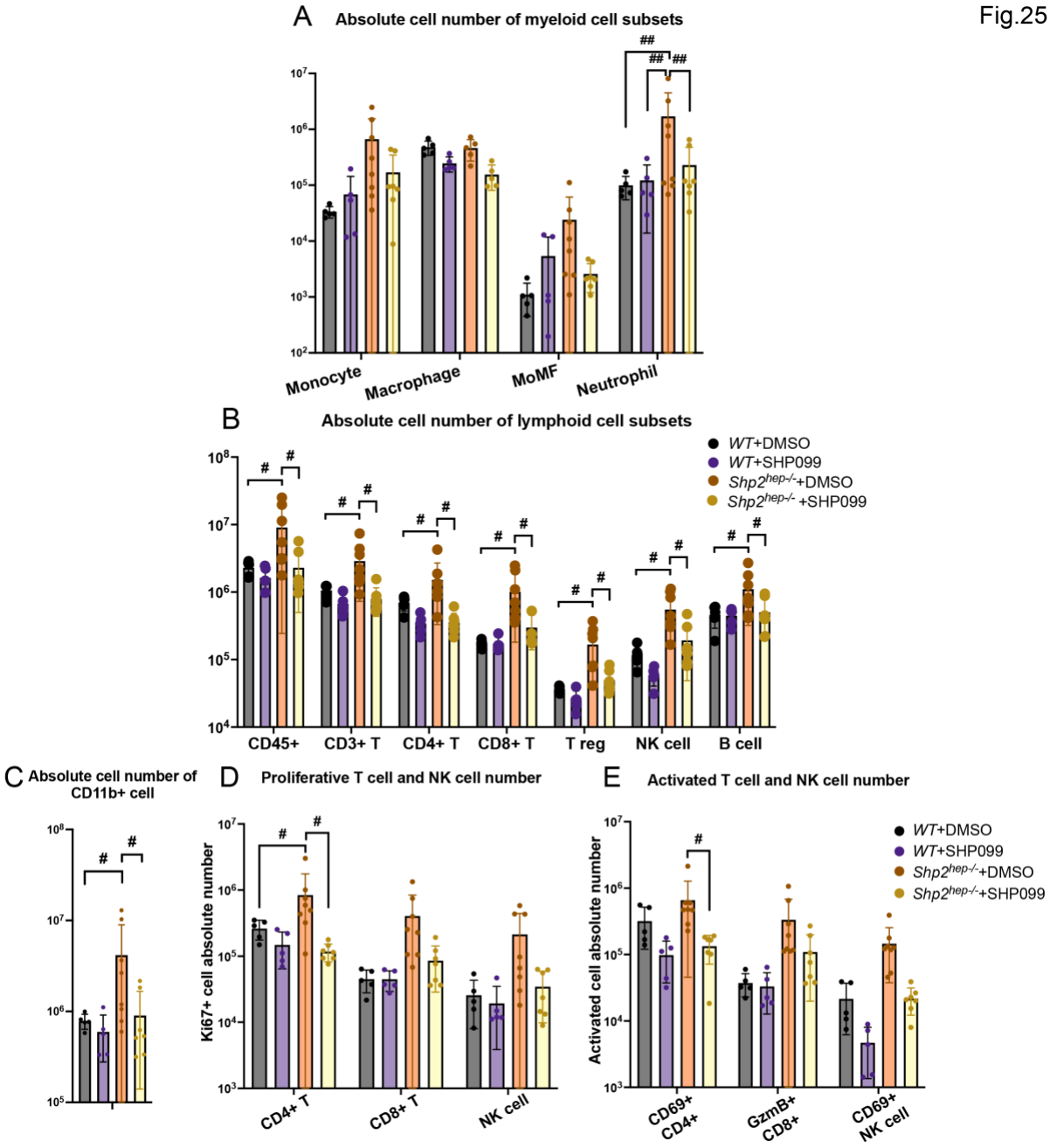

Figure 25. Effects by genetic and pharmaceutical inhibition of Shp2 on hepatic immune cell absolute number

A-C. Absolute cell numbers of annotated immune subsets in whole liver. Abbreviation used: MoMF, monocyte-derived macrophage; T reg, Regulatory T cell.

D-E. Absolute cell numbers of (D)proliferative or (E)activated T and NK cells in whole liver. Abbreviation used: GzmB, Granzyme B.

Data are mean values ± SD and statistical analysis was performed by 2way ANOVA together with multiple comparisons by Two-stage linear step-up procedure of Benjamini, Krieger and Yekutieli. # indicates false discovery rate $q<0.05$ and $^{\#}P<0.05$.

2.12. Shp2 inactivation has multiple effects on the tumor immune environment

As the analysis above suggested a potential effect of SHP099 in improving the hepatic immune environment, we further examined how SHP099 pretreatment influenced hepatic immune cells in tumor-bearing liver over the course of metastasized tumor progression, at day 5, 7, 9 and 15 after tumor cell injection. The Shp2 inhibitor downregulated $CD3^+$ T cell percentages in $CD45^+$ cells, without changing the $CD4^+$, $CD8^+$ T cell frequency, relative $CD4^+/CD8^+$ ratio or T cell numbers (Figure 27A-C). The percentages of proliferative $CD4^+$, $CD8^+$ T cell and NK cells were upregulated by SHP099 pre-treatment, especially at early stages of tumor metastasis (Figure 28A,B,F), with similar ratios of $GzmB^+$ and $CD69^+$ cells (activated cells) in these subsets (Figure 28D-F). The Treg cell percentages were gradually increased during tumor progression (Figure 28C). However, $CD8^+/CD4^+$ T cell and $CD8^+$ T/Treg ratios were not significantly altered by SHP099 pretreatment (Figure 27D,E), suggesting that SHP099 only had modest impact on immunosuppression despite modulating Treg frequency.

In the hepatic myeloid compartment of tumor-bearing mice, SHP099 pretreatment upregulated the percentages of $CD11b^+$ cells and dendritic cells (DC) but downregulated macrophage percentages, without significant impact on the percentages of other myeloid cells and LSECs (Figure 29A-D). Conventional macrophage polarization was marginally affected by SHP099 (Figure 29E). Interestingly, polarized M1 and M2a macrophages comprised low percentages of total macrophages in the liver, with the majority being $CD11c^-CD206^-$ macrophages. M2b macrophages ($F4/80^+$ $CD11c^-$ $MHCII^+$) comprised the majority of hepatic macrophages (Figure 29E), which is an alternatively polarized macrophage group with proinflammatory and tumor-promoting activities (118).

We measured expression of proinflammatory factors in non-parenchymal cells of control and SHP099-pretreated tumor-bearing livers. On day 7 and 9 post tumor cell challenge, SHP099 pretreatment led to impaired expression of IL-1β, IL-6 and TNFα (Figure 30A), as well as M2b macrophage polarization marker LIGHT (Figure 30B), suggesting that SHP099 downregulated inflammatory responses to metastasized tumor invasion. By measuring a full panel of CCL and CXCL chemokines, we detected a significant drop in CCL4 and CCL5 expression in SHP099-pretreated livers (Figure 30C; 31; 32). Consistently, the expression of their corresponding receptors CCR2 and CCR5 were also downregulated by Shp2 inhibitor, accompanied by lower expression of IRF5, a master regulator for inflammatory response and CCL5 expression (Figure 30C). As CCL4/5-CCR2/5 axis and IRF5 are known to promote inflammation (119, 120), their reduced expression suggests that SHP099 ameliorated hepatic inflammatory response to tumor cell metastasis, leading to less severe tumor development. In contrast to SHP099 treatment, CCL5/CCR5 axis-related genes were upregulated in *Shp2*$^{hep-/-}$ livers (Figure 30D), revealing an association of the CCL5/CCR5 axis, inflammation and tumor progression. Together, these results revealed opposite environmental impacts, especially the bi-directional regulation of CCL5/CCR5 signaling, induced by genetic deletion of Shp2 in hepatocytes and chemical inhibition of Shp2, leading to the pro- and anti-tumorigenic effects.

Fig.26

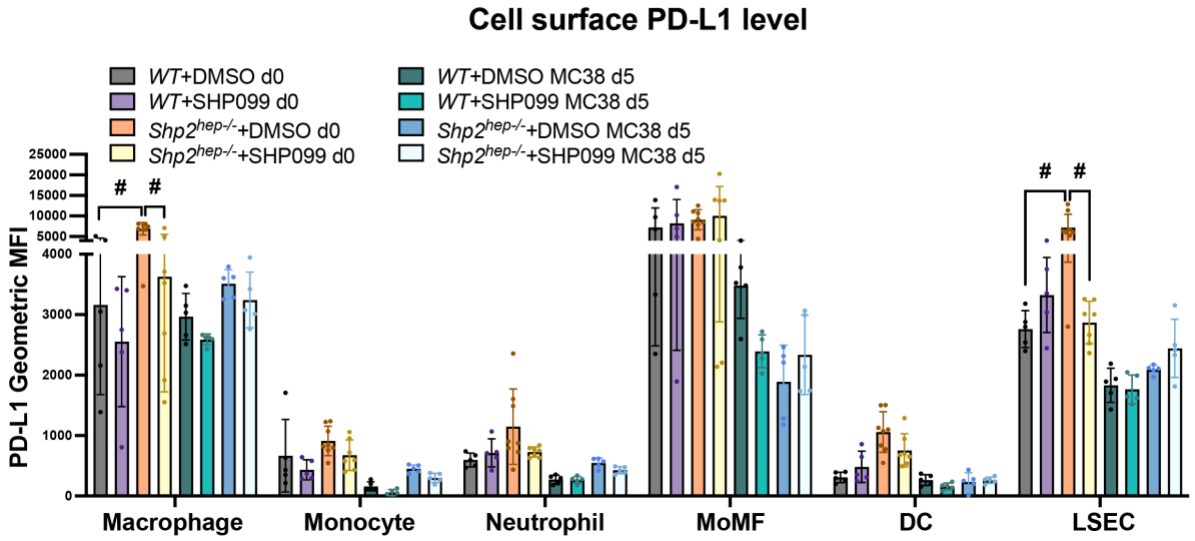

Figure 26. Effect by genetic and pharmaceutical inhibition of Shp2 on cell surface PD-L1 expression on myeloid subsets and LSEC

Data are mean values ± SD and statistical analysis was performed by 2way ANOVA together with multiple comparisons by Two-stage linear step-up procedure of Benjamini, Krieger and Yekutieli. # indicates false discovery rate $q<0.05$ and $^{\#}P<0.05$.

Fig.27

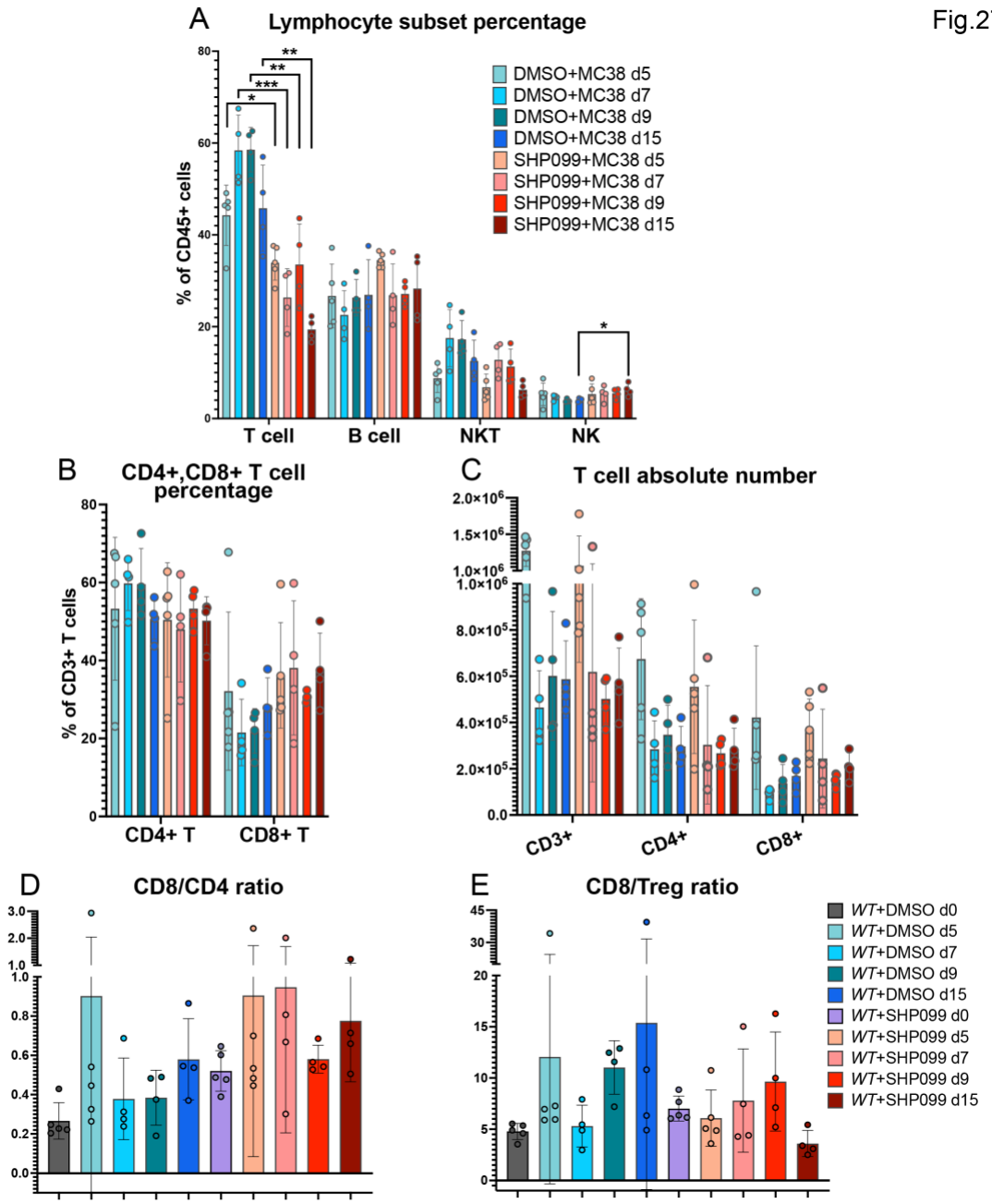

Figure 27. Effects of SHP099 on hepatic immune profiles under metastatic liver tumor stress

A-C. (A)Percentage of lymphocyte subsets, (B)percentages of $CD4^+$ and $CD8^+$ T cells and (C)absolute cell numbers of $CD3^+$ T, $CD4^+$ T, $CD8^+$ T cells comparing DMSO and SHP099 pre-treated *WT* liver under MC38 metastasis stress.

D-E. (D)Hepatic $CD8^+/CD4^+$ T cell ratio and (E)$CD8^+$ T/Treg ratio measured in annotated groups.

Data are mean values ± SD and statistical analysis was performed by unpaired two-tailed Student's T-test. No annotation, not significant; *P < 0.05, **P < 0.01, ***P < 0.001.

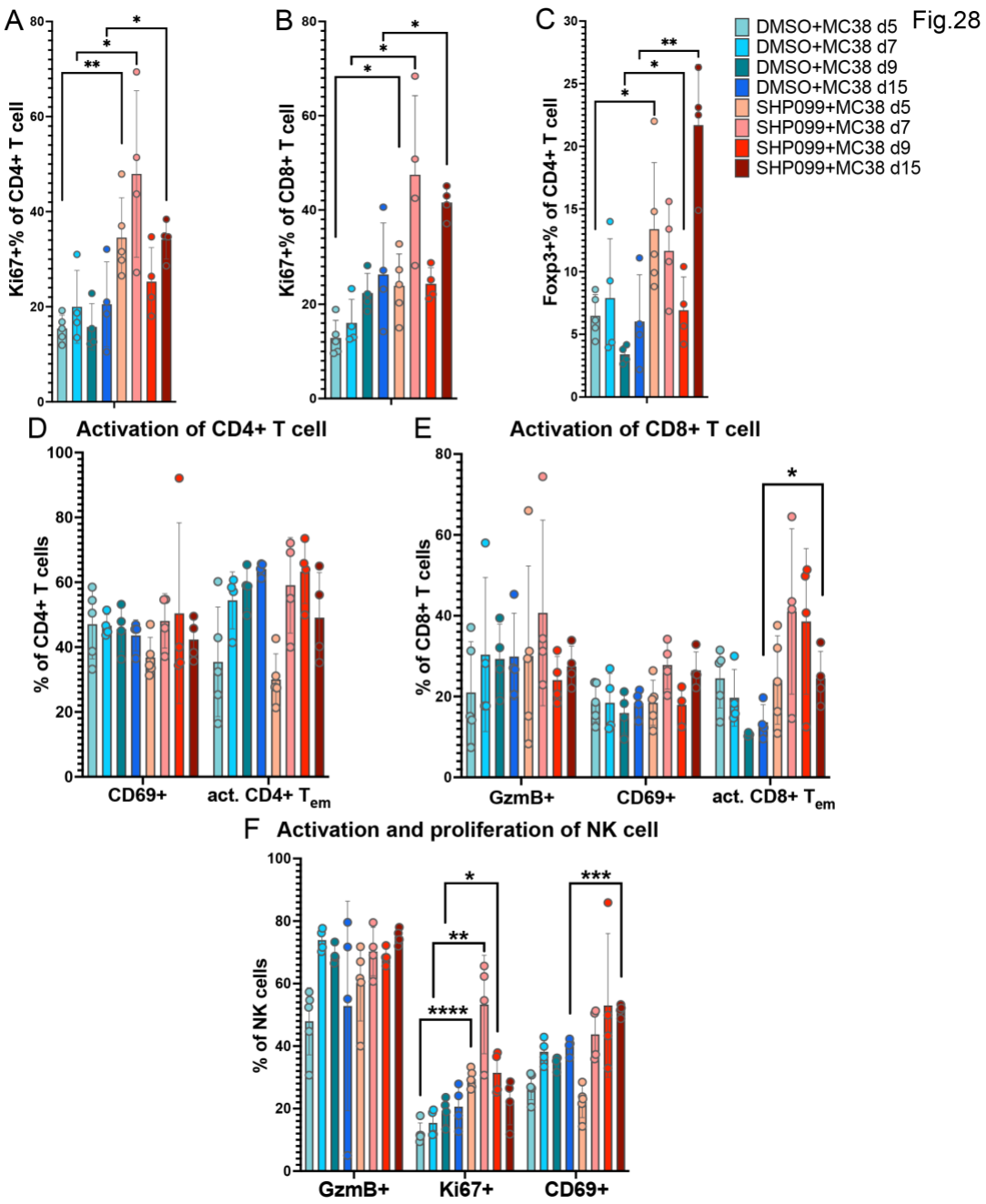

Figure 28. Effects of SHP099 on hepatic T cell activity under metastatic liver tumor stress

A-**B**. Percentages of Ki67$^+$ proliferative cells of (A)CD4$^+$ and (B)CD8$^+$ T cells in whole *WT* liver.

C. Percentages of Treg cells (Foxp3$^+$ CD4$^+$) in total CD4$^+$ T cells in whole *WT* liver.

D-**F**. Percentage of stimulated (D)CD4$^+$, (E)CD8$^+$ T and (F)NKcells in whole *WT* liver. Abbreviation used: act. CD4+ T_{em}, activated CD4+ effector memory T cell; CD8+ T_{em}, activated CD8+ effector memory T cell. Data are mean values ± SD and statistical analysis was performed by unpaired two-tailed Student's T-test. No annotation, not significant; *P < 0.05, **P < 0.01, ***P < 0.001, ****P < 0.0001.

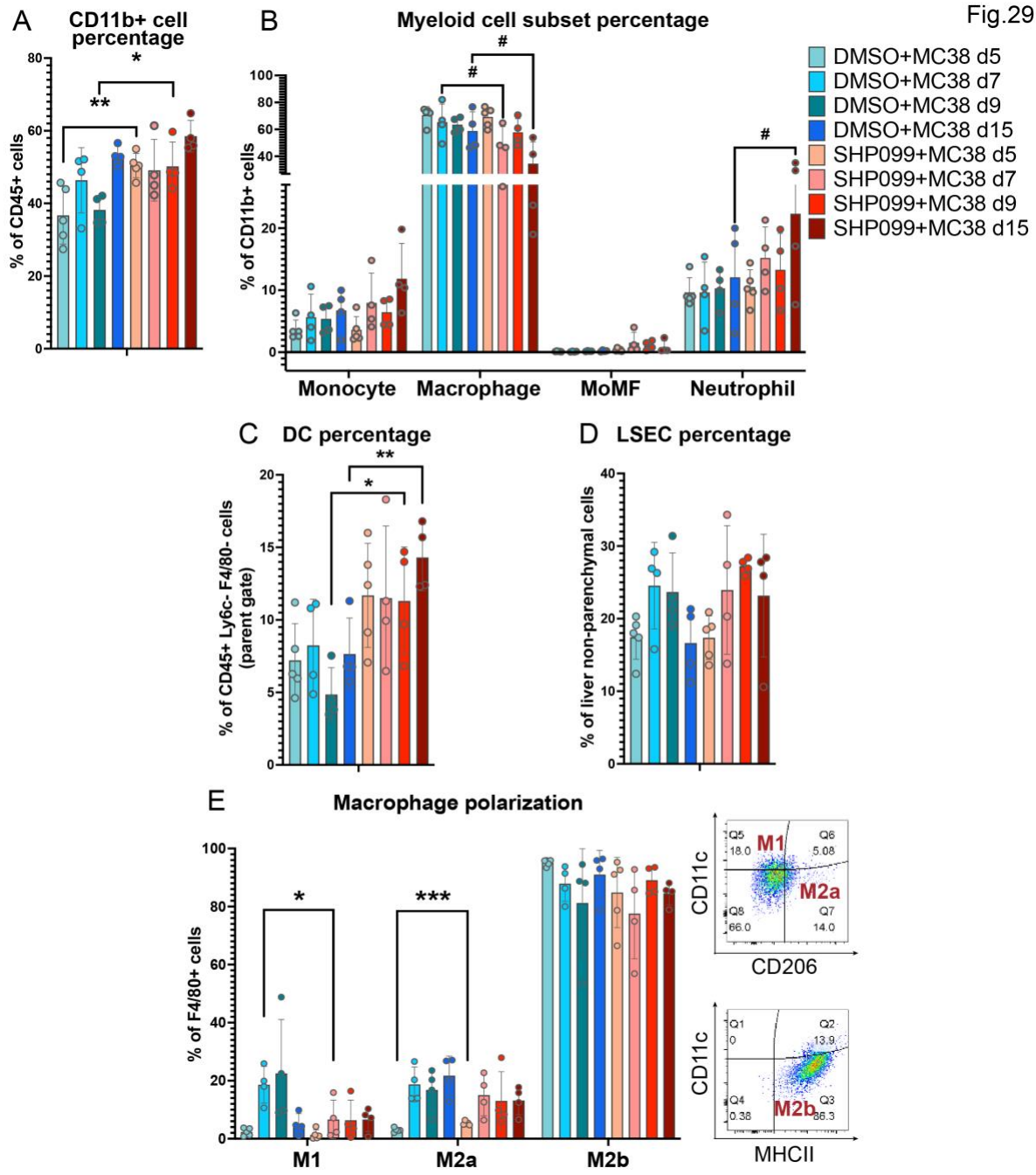

Figure 29. Effects of SHP099 on hepatic myeloid cell profiles under metastatic liver tumor stress

A-D. Percentage of (A-C)major myeloid cell populations or (D)LSEC in whole *WT* liver.

E. Left: Percentages of polarized macrophages M1 ($CD11c^+$ $CD206^-$ $F4/80^+$), M2a ($CD11c^-$ $CD206^+$ $F4/80^+$) and M2b ($CD11c^-$ $MHCII^+$ $F4/80^+$) in total macrophages in whole *WT* liver. Right: Representative FACS plots gated on macrophages showing separation of three polarized subsets.

Fig.30

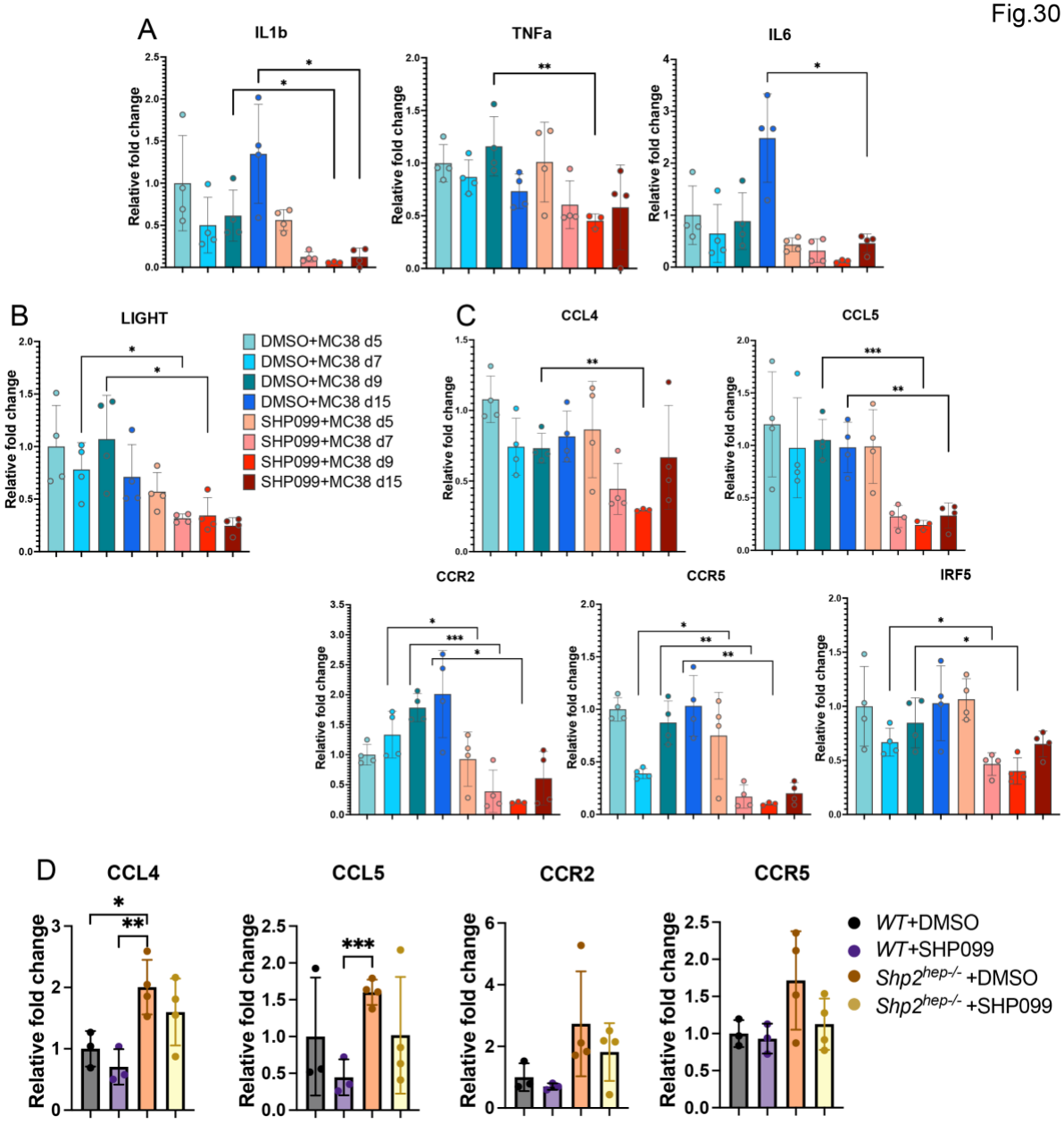

Figure 30. Effects by genetic deletion or pharmaceutical inhibition of Shp2 on CCL5/CCR5 axis

A-C. Transcript levels of (A)pro-inflammatory factors; (B)LIGHT; (C)CCL5/CCR5 axis-related genes in isolated NPCs from pretreated whole *WT* liver.

D. Transcript levels of CCL5/CCR5 axis-related genes in NPCs from whole liver.

Data are mean values ± SD and P values were calculated by unpaired two-tailed Student's T-test. No annotation, not significant, *P < 0.05, **P < 0.01, ***P < 0.001.

Fig.31

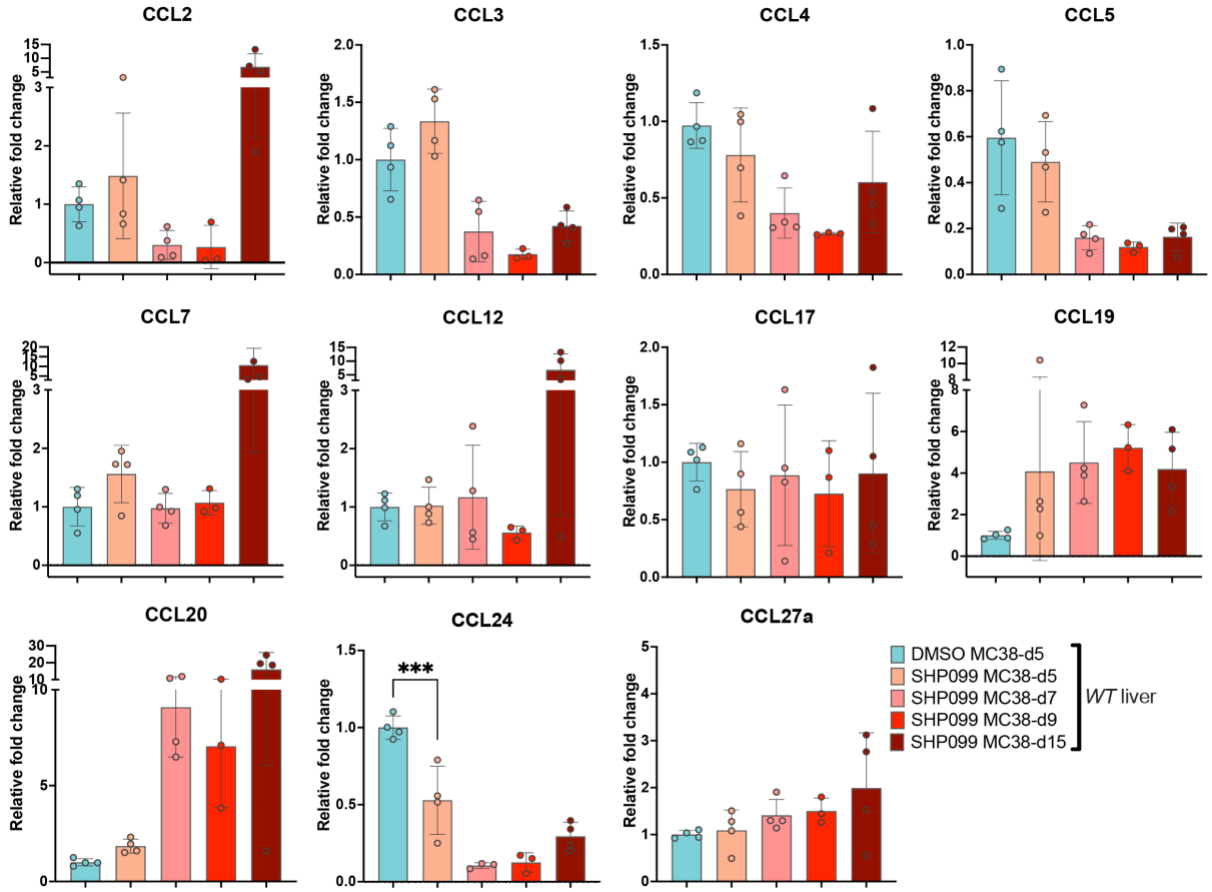

Figure 31. Effects of SHP099 on CC chemokine transcript expression in liver NPCs

Data are mean values ± SD. Statistical analysis was performed by unpaired two-tailed Student's T-test. No annotation, not significant, ***P < 0.001.

Fig.32

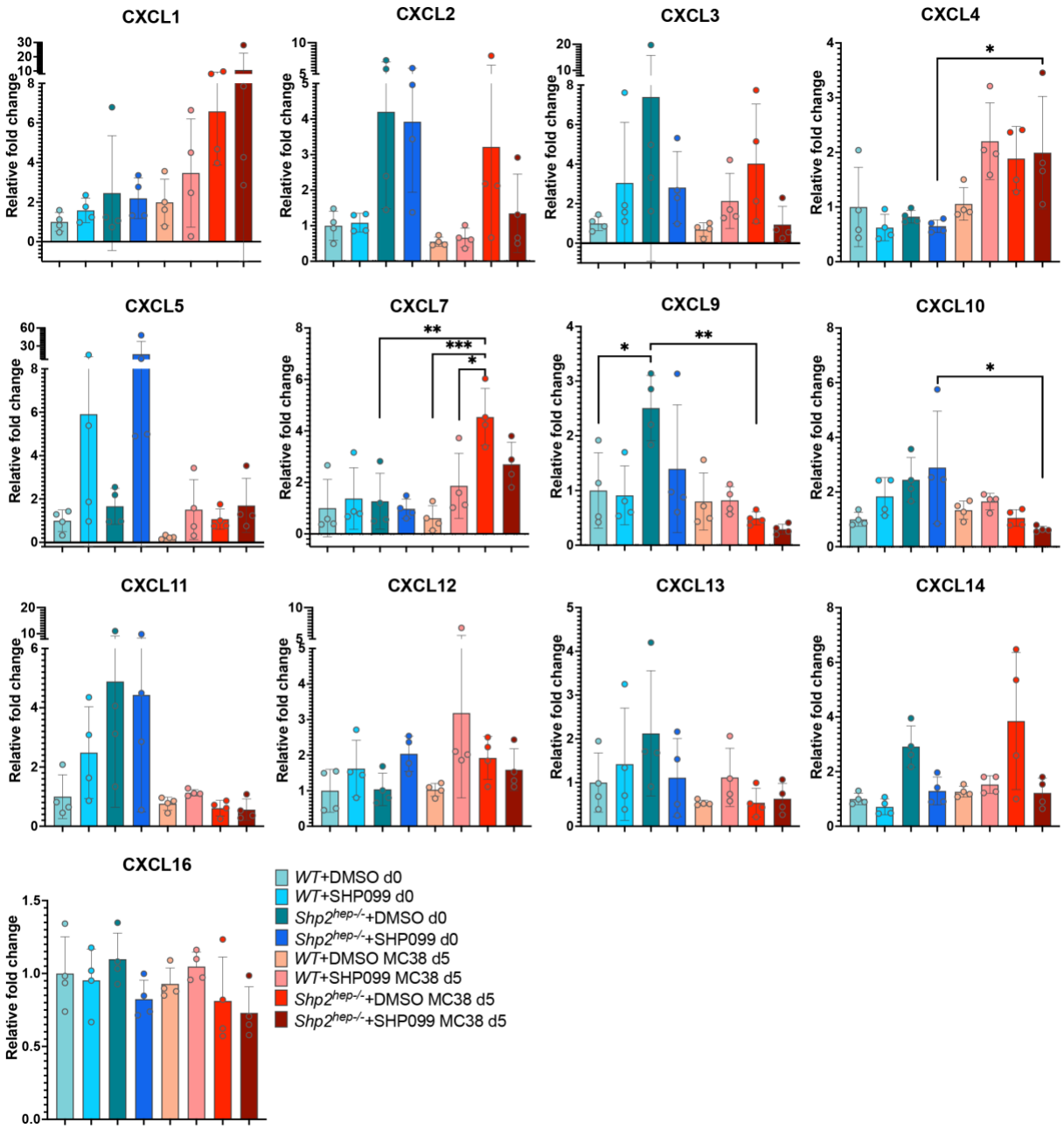

Figure 32. Effects of SHP099 on CXC chemokine transcript expressions in liver NPCs
Data are mean values ± SD. Statistical analysis was performed by unpaired two-tailed Student's T-test. No annotation, not significant, *P < 0.05, **P < 0.01, ***P < 0.001.

2.13. Shp2 inhibition enhances IFNβ secretion from liver macrophages

CCR5 was most abundantly expressed in liver macrophages as measured by flow cytometry, with nearly 43% of the cell population being CCR5-positive. The second group was LSEC cells at 23% followed by $CD8^+$ T cells at 16.8%, among all non-parenchymal cell types examined (Figure 33A). Largely overlapping cell surface expression of F4/80 and CCR5 supported the abundant CCR5 expression on liver macrophages (Figure 33B). These data suggest a critical role of CCL5/CCR5 signaling in modulating macrophage functions, consistent with previous observations that the pro-tumor effect of tumor-associated macrophages (TAMs) was augmented by CCL5 in tumor microenvironment, which was abrogated by CCR5 inhibition and induced IFN production in macrophages (121). We examined if SHP099 treatment led to type I IFN induction. Drastically increased expression of IFNα1, IFNα2 and IFNβ1, as well as the expression and phosphorylation of IRF3, a transcription factor for type I IFNs, were detected in SHP099-pretreated liver (Figure 34A,B). Consistently, we detected significantly increased IFNβ secretion from isolated liver macrophages following SHP099 treatment *in vitro* (Figure 34C), but not from isolated dendritic cells (Figure 34D), identifying macrophages as the main source of IFNβ. These results suggest that Shp2 inhibition enhanced IFNβ secretion from macrophages and also ameliorated inflammation through suppressing CCR5 signaling, generating an anti-tumor niche in the liver. Treatment with a CCR5 antagonist Maraviroc also promoted IFNα and IFNβ expression (Figure 35A), but did not stimulate IFNβ secretion from isolated macrophages (Figure 34C) or induce phosphorylation of IRF3 *in vivo* (Figure 35C), suggesting that suppressed CCR5 signaling and augmented IFNβ secretion from macrophages are two separate events induced by SHP099 pretreatment.

Maraviroc treatment did not significantly inhibit metastasized tumor growth in the liver (Figure 36A), which might be due to its failure to alleviate severe inflammation in tumor microenvironment and to cap the complementary upregulation of CCL5/CCR5 axis gene expression (Figure 36B,C). SHP099 pretreatment reduced surface CCR5 level and further restricted CCR5 expression to intracellular discrete puncta in macrophages, whereas in control and Maraviroc-treated liver, CCR5 was mostly dispersed in the cytoplasm, indicating that Shp2 inhibition retained at least part of CCR5 in intracellular puncta of macrophages to hinder their recycling back to cell membrane (Figure 33B; 35B,D). We also demonstrated that following splenic injection of MC38 cells, SHP099 treatment suppressed significantly metastasized tumor progression in the liver (Figure 37). This result further suggests a therapeutic effect of SHP099, through acting on both tumor cells and hepatic niche cells. Mechanistically, SHP099 attenuated oncogenic MAPK pathway in malignant cells and also enhanced IFNβ secretion from hepatic macrophages, consistent with our previous data on the liver tumor-suppressing effect of polyIC, an IFN inducer (122-124).

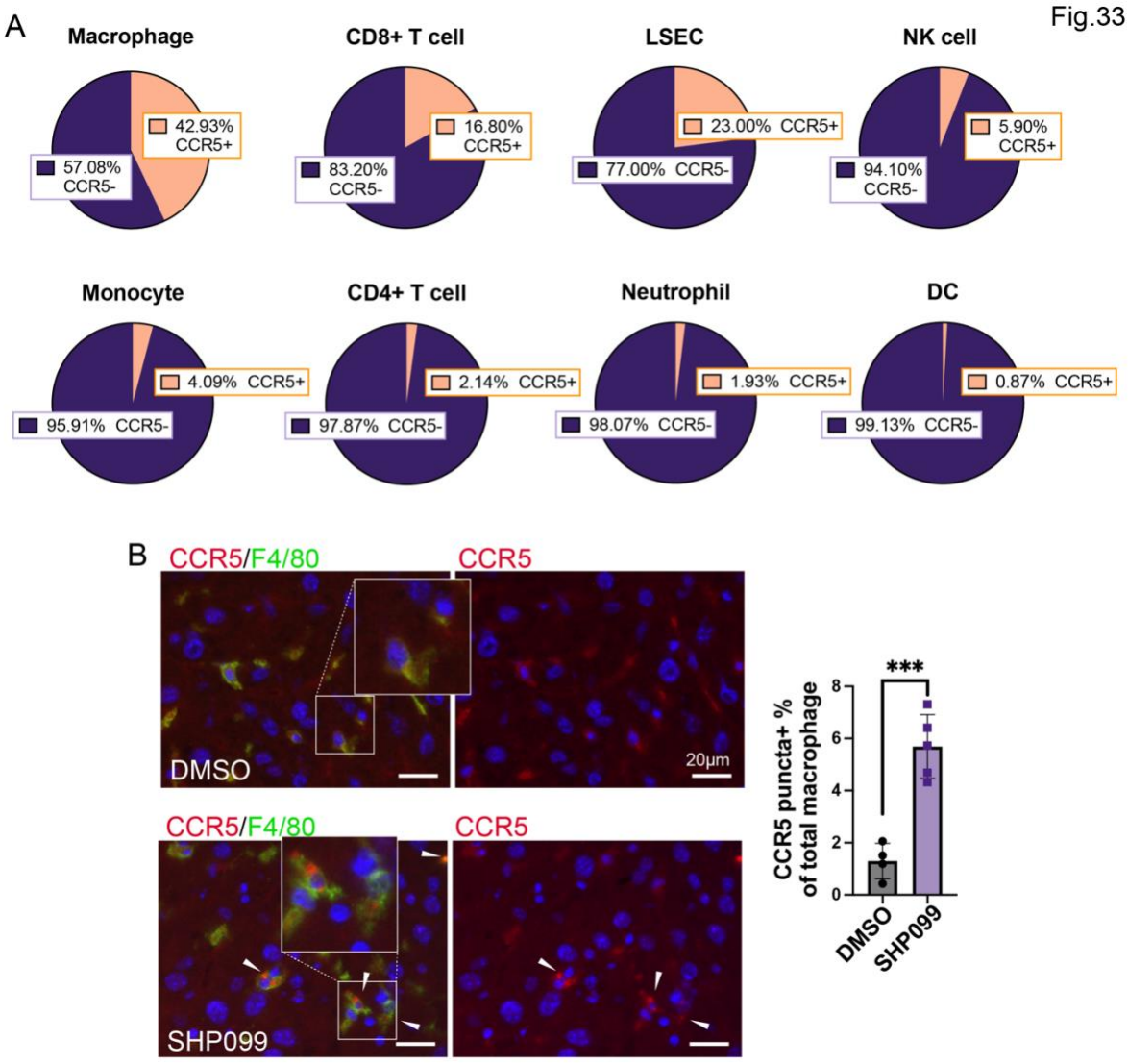

Figure 33. SHP099 alters expression pattern of CCR5 in hepatic macrophage

A. Cell surface CCR5^{+} percentage in annotated non-parenchymal cell subsets in *WT* liver on day-7 post MC38 transplantation.

B. Immunofluorescence staining of CCR5 (arrows: punctate CCR5 expression) and F4/80 in pretreated *WT* liver on day-9 post MC38 transplantation. Punctate CCR5^{+} F4/80^{+} cells were quantified based on six randomly selected microscopic fields of view for each biological sample. n=4(DMSO), 5(SHP099). Data are mean values ± SD. Statistical analysis was performed by unpaired two-tailed Student's T-test. ***P < 0.001.

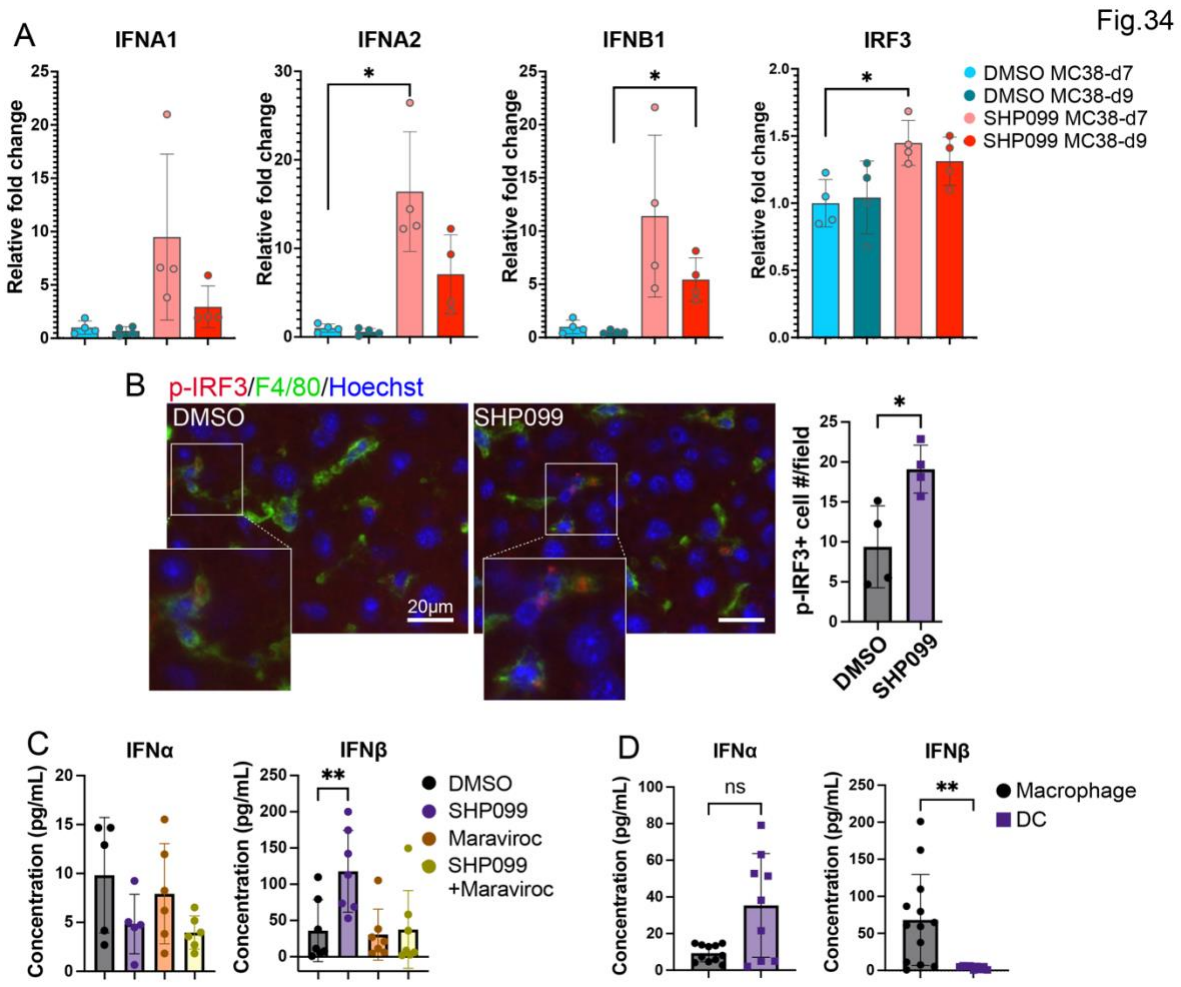

Figure 34. SHP099 stimulates type I interferons in liver

A. Transcript levels of type I interferons and IRF3 in NPCs isolated from pretreated *WT* liver.

B. Immunofluorescence staining of p-IRF3 and F4/80 in pretreated *WT* liver on day-7 post MC38 transplantation. p-IRF3^{+} cells were quantified based on six randomly selected microscopic fields of view for each biological sample. n=4.

C-D. ELISA measurement of secreted IFNα and IFNβ level in culture supernatants of (C)isolated liver macrophages treated with compounds, or (D)untreated isolated liver macrophage versus isolated liver dendritic cells (DC).

Fig.35

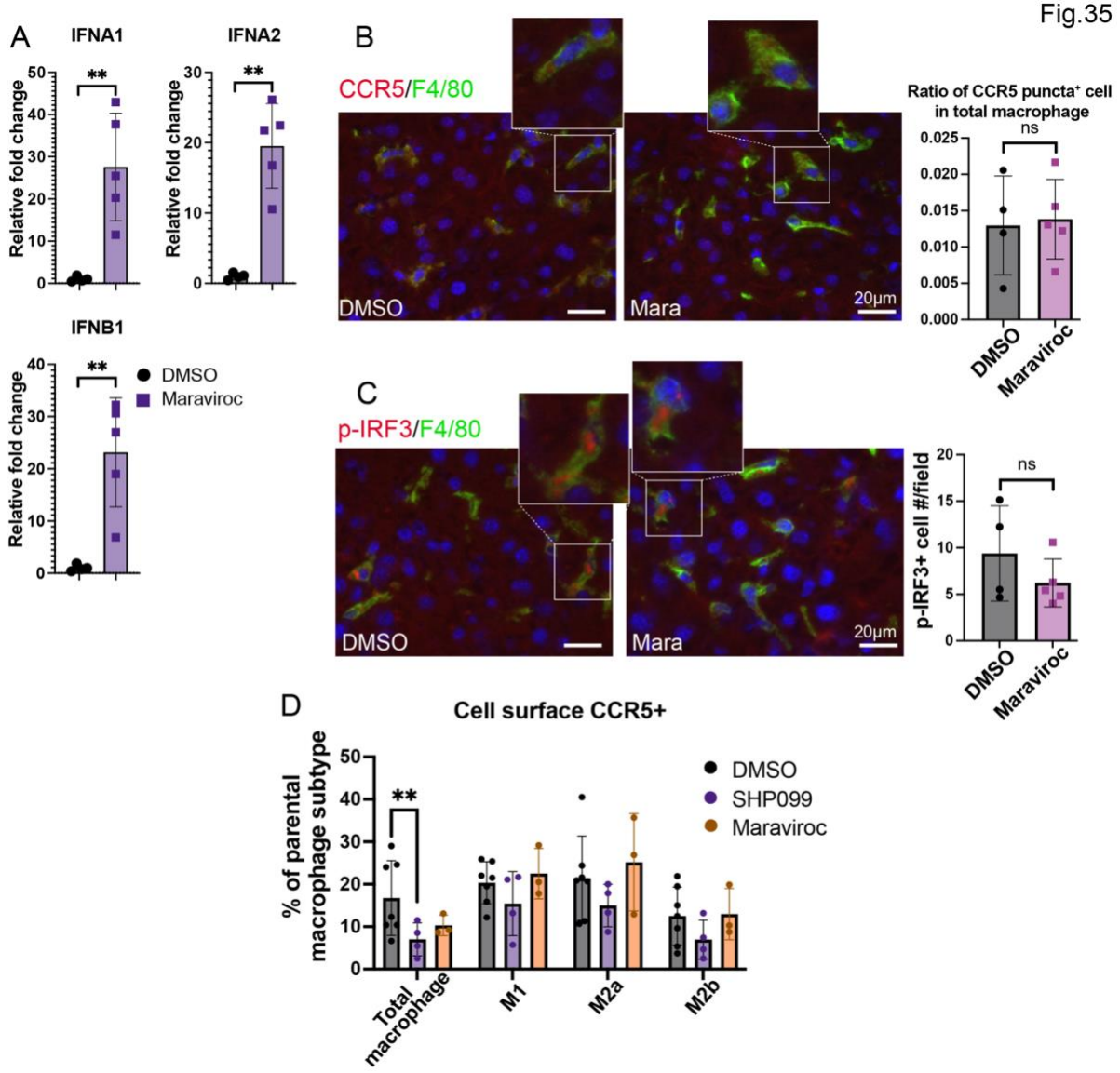

Figure 35. Effects of Maraviroc on type I interferon stimulation and CCL5/CCR5 axis

A. qRT-PCR measurement of mRNA levels of IFNA1, IFNA2, and IFNB1 in NPCs isolated from treated *WT* liver on day-7 post MC38 transplantation.

B-C. Immunofluorescence staining of (B)CCR5 and F4/80; (C)p-IRF3 and F4/80 in sections of treated *WT* liver on day-9 post MC38 transplantation. Quantification was based on six randomly selected microscopic fields of view for each biological sample.

D. Cell surface $CCR5^+$ cell percentage in each polarized macrophage subset or total macrophage.

Data are mean values ± SD and P values were calculated by unpaired two-tailed Student's T-test. ns or no annotation, not significant, **P < 0.01.

Fig.36

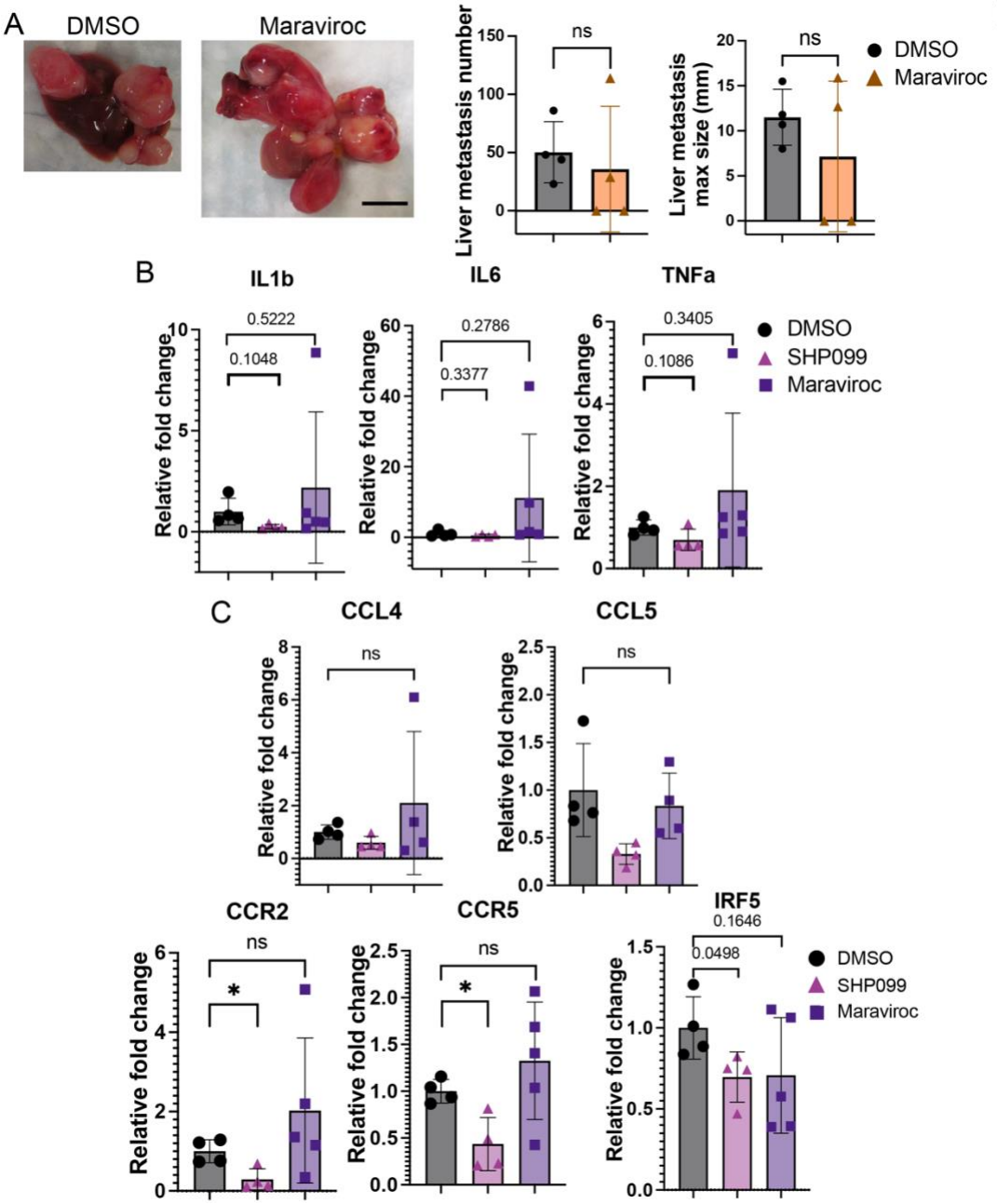

Figure 36. Maraviroc fails to confer hepatoprotective effect against metastasized liver tumor

A. Representative macroscopic images and quantification of metastasized tumors in *WT* livers treated with DMSO or Maraviroc. Experiments were terminated on day-25 post intrasplenic MC38 transplantation (7,000 cells per mouse). n=4. Scale bar: 1 cm.

B-C. Transcript levels of (B)pro-inflammatory factors and (C)CCL5/CCR5 axis-related genes in non-parenchymal cells isolated from treated *WT* liver on day-7 of MC38 metastasis.

Data are mean values ± SD and P values were calculated by unpaired two-tailed Student's T-test. ns or no annotation, not significant, *P < 0.05.

Fig.37

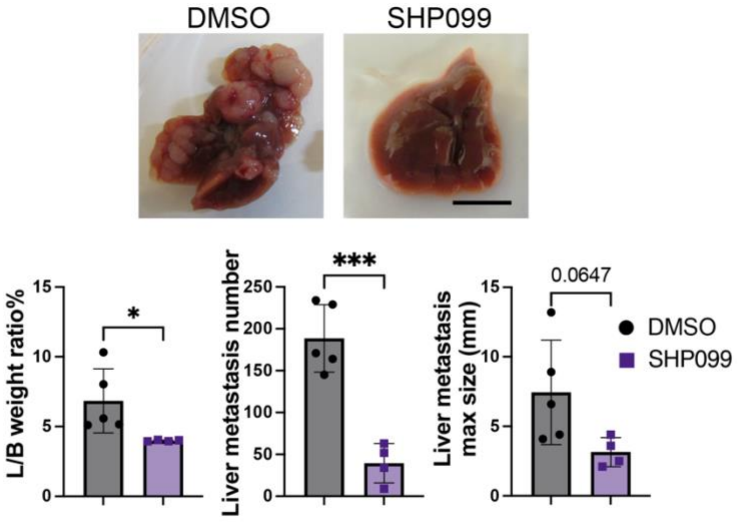

Figure 37. Anti-tumor effect of SHP099 treatment started post MC38 transplantation

Representative macroscopic images and quantification of metastasized tumor in *WT* livers. n=5(DMSO), 4(SHP099). Scale bar: 1cm. Data are mean values ± SD and P values were calculated by unpaired two-tailed Student's T-test. *P < 0.05, ***P < 0.001.

2.14. Shp2 inhibition had minimal influence on primary splenic tumor

We also investigated an effect of systemic SHP099 treatment in the spleen. Impaired phosphorylated Shp2 level, the indicator for Shp2 activity, was detected in SHP099-treated group right after SHP099 withdrawal (Figure 38A). However, the decrease in p-Shp2 level was reversed 8 days after SHP099 withdrawal (Figure 38B), which indicated SHP099 can exert its inhibitory function on spleen cells, however, in a reversible manner. SHP099 reduced both total macrophage percentage and M2b polarized macrophage ratios in the spleen (Figure 39A-B). However, given the low abundance of macrophages in spleen (<0.04% of total immune cells), SHP099-mediated regulation of macrophages might be marginal in the splenic microenvironment. In the lymphocyte compartment, unlike its effect in the liver, SHP099 failed to promote proliferation of T cells and NK cells in the spleen (Figure 39C). Moreover, SHP099's impact on pro-inflammatory response, CCR5 pathway and type I interferon response was blunted compared to that in liver (Figure 40). Collectively, these results indicated SHP099 failed to reshape tumor microenvironment in spleen as it did in liver. As a result, SHP099 had therapeutic efficacy on liver metastasized tumors but not MC38 tumors at transplantation site spleen (Figure 40).

2.15. Acknowledgement

This dissertation from Chapter 1 through Chapter 5, in part, is a reprint of the material as it appears in Shp2 deletion in hepatocytes suppresses hepatocarcinogenesis driven by oncogenic β-Catenin, PIK3CA and MET. Jacey Jijun Liu, Yanjie Li, Wendy Chen, Yan Liang, Gaowei Wang, Min Zong, Kota Kaneko, Ruiyun Xu, Michael Karin, Gen-Sheng Feng, Journal

of Hepatology, 2018. The dissertation author was the primary investigator and author of this paper.

This dissertation from Chapter 1 through Chapter 5, in part, has been accepted for publication of the material as it may appear in Pharmaceutical Shp2 Inhibition Suppresses Primary and Metastasized Liver Tumors by Provoking Hepatic Innate Immunity, Jacey Jijun Liu, Bing Xin, Li Du, Lydia Chen, Yanyan Long, Gen-Sheng Feng, Hepatology, 2022. The dissertation author was the primary investigator and author of this paper.

Figure 38

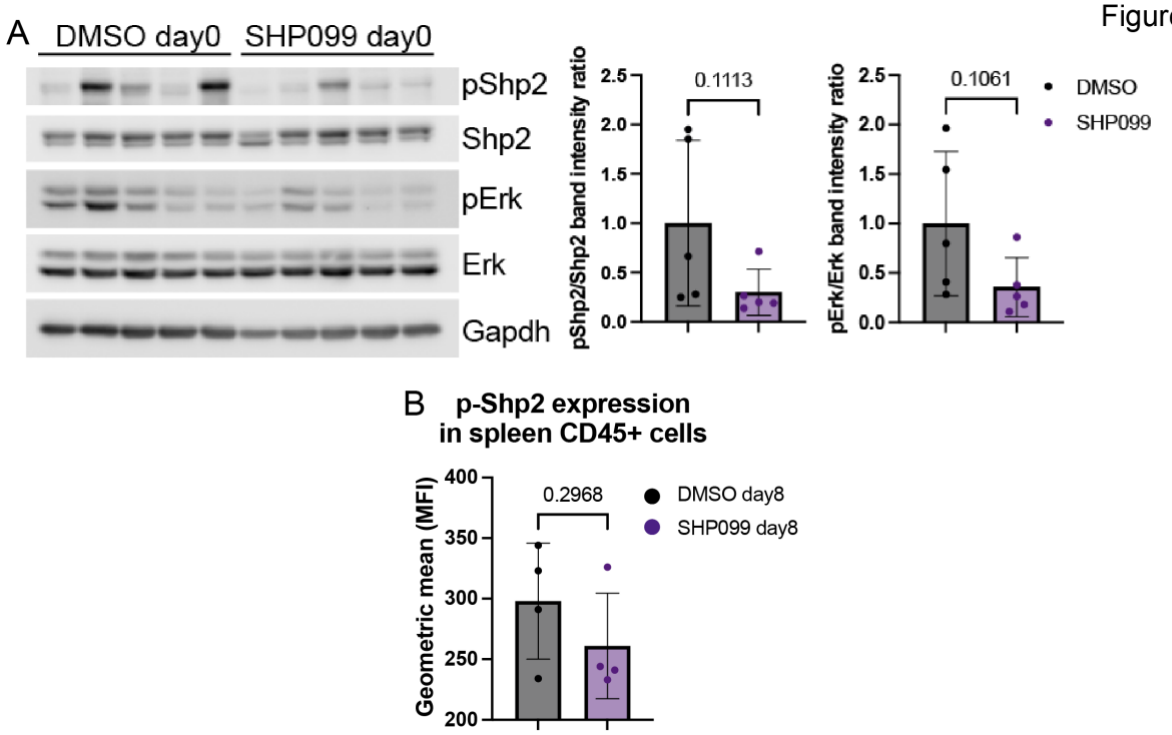

Figure 38. Inhibitory effect of SHP099 in spleen

A. Immunoblotting of p-Shp2 and quantification in whole spleen lysate of treated spleen.

B. Flow cytometry measurement of p-Shp2 expression CD45+ cells in treated spleen.

Figure 39

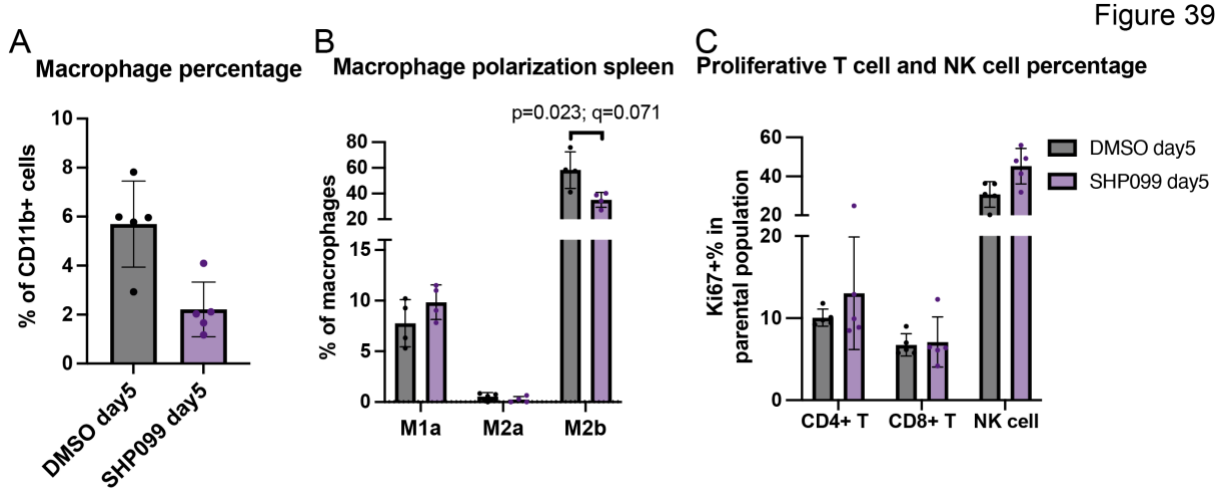

Figure 39. Effect of SHP099 on spleen immune profile

A-C. Percentages of indicated immune cell subsets in treated spleen on day 5 of MC38 transplantation.

Figure 40

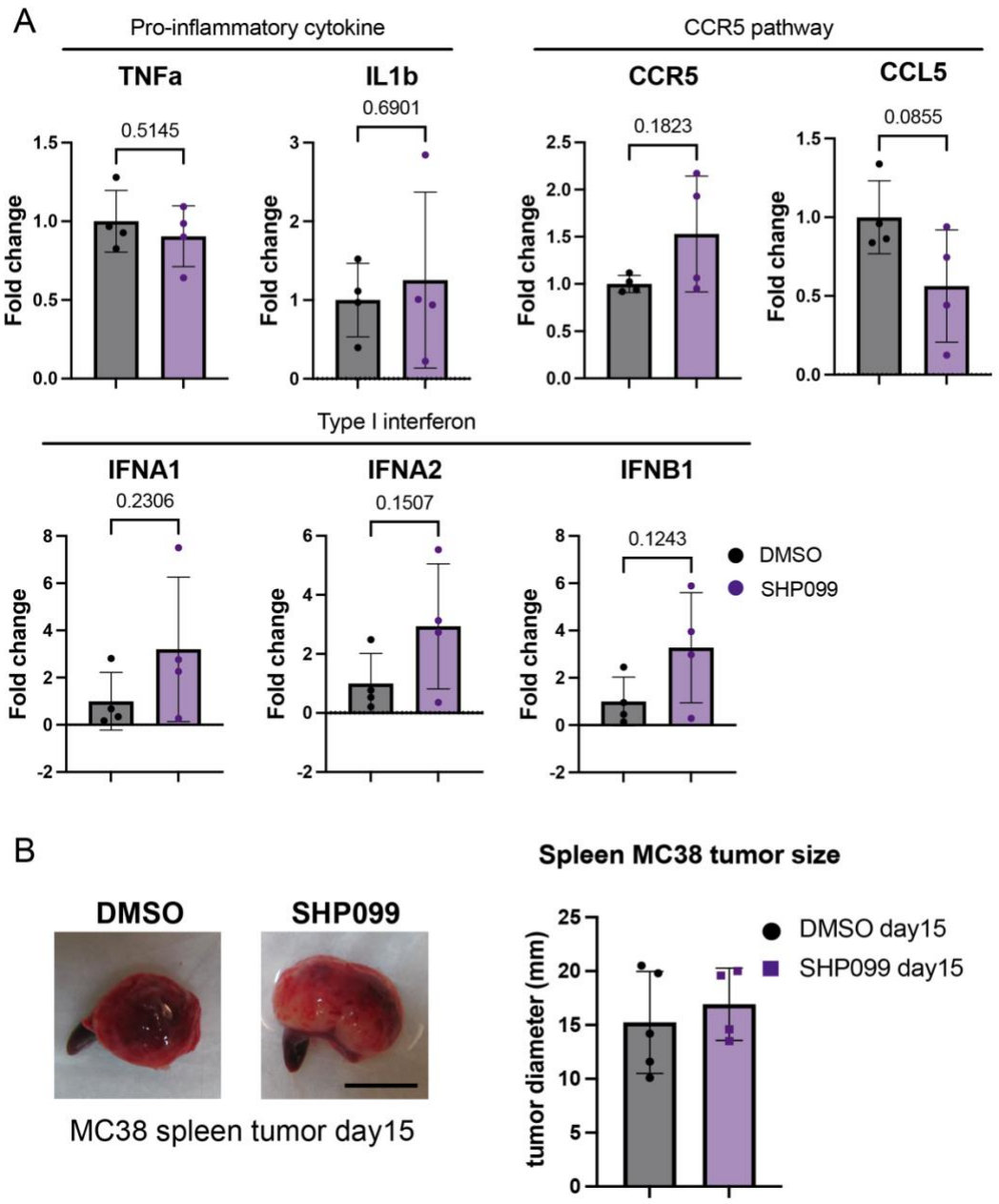

Figure 40. Lack of therapeutic effect by SHP099 on splenic MC38 tumor
A. mRNA level of indicated genes in whole spleen.
B. Macroscopic images of day-15 MC38 tumor in spleen pretreated by DMSO or SHP099. Scale bar: 1cm.

Chapter 3. Discussion

3.1. Discussion

By combined use of genetic and pharmaceutical approaches, we deciphered Shp2 function and mechanism in hepato-oncogenesis driven by RTK and other oncogenes and also identified Shp2 as a promising therapeutic target in liver cancer. Using a mutant mouse line with Shp2 selectively deleted in hepatocytes, we showed previously that Shp2 is critically required for development of autochthonous liver tumors driven by Met and β-Catenin (125), although the underlying molecular mechanism was unclear. In extending the previous observation, this study demonstrated that the catalytic activity of Shp2 was essential for its function in oncogenic signaling initiated from Met. In interrogating the biochemical mechanism, we identified Socs3 as a molecule involved in downregulation of Met-emanated oncogenic signaling and Met degradation. Socs3 consists of an SH2 domain, which enables its binding to phosphotyrosine-containing target protein, as well as a SOCS box which recruits ubiquitin ligase for ubiquitination and degradation of target proteins (100). The SH2 domain of Socs3 shares similar binding specificity with that of Shp2 and thus the two molecules compete for binding molecular partners/targets (101, 102, 104); Socs3 is likely to compete with Shp2 for Met binding in control of Met stability. Indeed, we observed restoration of Met/Cat-induced tumor formation and steady Met expression by abrogating Socs3 function or expressing an undegradable Met mutant in the absence of Shp2 in hepatocyte (Figure 16A,B,D; Figure 17A,C). The partial rescue by inhibiting Socs3 function also suggest two separate mechanisms for Shp2 function in Met signaling, i.e. sustaining Met expression and promoting Met-Ras-Erk signaling.

This study also unveiled variable effects of hepatocyte-specific Shp2 removal on liver tumorigenesis driven by different oncogenes, which revealed cell-intrinsic and extrinsic

mechanisms of Shp2 functions. Despite its stringent requirement for Met-induced oncogenic signaling, Shp2 is dispensable for HCC development driven by mutant β-catenin and PI3K (Cat/Pik), Ras/Cat and Ras/Myc (Figure 11A; Figure 12A; Figure 13A). Further, this and previous experiments showed that deleting Shp2 in hepatocytes even aggravated liver tumorigenesis driven by Ras and other cytoplasmic/nuclear oncogenes, by inducing a tumor-promoting microenvironment (Figure 12; Figure 13). Collectively, these data revealed a tumor-suppressive role of Shp2 in shaping the microenvironment, in sharp contrast to its critical mediatory role in cell-autonomous oncogenic pathway (125, 126).

Great efforts are being devoted to advancing Shp2-targeted oncological treatment in pharmaceutical industry, which has been facilitated by the discovery of an allosteric Shp2 inhibitor (SHP099) that robustly suppressed proliferation of RTK-dependent cancer cells (77). Furthermore, several groups have demonstrated additive or synergistic tumor-inhibiting effects of Shp2 inhibitor and Mek or other oncogenic kinase inhibitors in a variety of cancer cell lines and animal tumor models (84, 127-129). However, the paradoxical pro- and anti-oncogenic effects of Shp2 in HCC raised a caution on inhibiting Shp2 in liver cancer treatment. In particular, the tumor-promoting hepatic microenvironment formed in *Shp2*$^{hep-/-}$ mice would even argue against Shp2 as a pharmaceutical target.

To address this serious concern, we compared effects of genetic deletion and chemical inhibition of Shp2 in primary and metastasized liver tumors. Consistent with the gene deletion data, SHP099 treatment significantly suppressed progression of Met/Cat-induced liver tumors, validating a critical role of Shp2 in relay of cell-intrinsic oncogenic signal initiated by Met (Figure 19). Moreover, we found that chemical inhibition of Shp2 even exerted a tumor-suppressive effect on metastasized liver tumors (Figure 21A,B), opposite to the pro-tumorigenic

effect observed in *Shp2*$^{hep-/-}$ liver. Mechanistically, Shp2 deletion in hepatocytes led to upregulation of inflammatory cytokines, increased immune cell infiltration, fibrosis and cholestasis, constituting a tumor-promoting hepatic niche (Figure 22; Figure 25A-C). In contrast, pharmaceutical Shp2 inactivation remedied the inflammatory environment by controlling immune population infiltration (Figure 25A-C) and reducing proinflammatory cytokine expressions, including IL-1β, TNFα and IL-6 (Figure 30A). We performed detailed analysis on the impact of Shp2 inactivation on hepatic immune cell subpopulations. Of note, only modest changes in adaptive immune subset composition were observed in SHP099-treated liver, which were not significant enough to illustrate the anti-tumorigenic effect (Figure 23A,B; Figure 27A,B). However, there was a significant upregulation of T cell and NK cell proliferation but not activation (Figure 28), indicating that SHP099 treatment triggered partial activation of anti-tumor adaptive immunity in response to liver metastasis stress. Although Shp2 was reported to interact with PD-1 in T cells, and Shp2 deficiency was shown to enhance T cell-mediated anti-tumor immunity (130, 131), we did not observe significant changes in immunosuppressive mechanisms as evaluated by PD-L1 levels and $CD8^+$ T/Treg ratio in the liver following Shp2 inhibition (Figure 26; Figure 27E).

These data prompted us to shift attention to potential roles and regulation of myeloid cells. In an unbiased search, we found that SHP099 selectively attenuated mRNA expression of the CCL5/CCR5 axis components in non-parenchymal cells, concomitant with impaired expression of proinflammatory factors (Figure 30A,C). In agreement with our data shown here, several groups reported that the CCL5/CCR5 signaling promoted hepatic fibrosis (132) and inflammation-associated HCC (133), and a possible Shp2 function in this axis (134). In specifying the immune cell subpopulation that is primarily impacted by Shp2 inhibition and

responsible for enhanced anti-tumor immunity, we found that macrophages constituted a largest portion that expressed CCR5 among all hepatic immune cell subpopulations (Figure 33A), suggesting that the CCR5 axis in macrophages is prone to be influenced by SHP099 treatment. Indeed, SHP099 treatment enhanced internalization and retention of CCR5 in sub-cellular perinuclear punctate structure in liver macrophages (Figure 33B), which hindered the activity of CCR5 signaling. Previous studies have also suggested that Shp2 plays a critical role in macrophages to regulate their polarization and inflammation-related secretory profiles (135-137). CCR5 pathway stimulation leading to inflammation was reportedly dependent on MAPK pathway (138), implying Shp2 inhibition could impede CCR5 pathway activation directly through influencing MAPK pathway.

In this study, we observed a significant effect of type I IFN induction by SHP099, especially upregulated IFNβ secretion from macrophages (Figure 34A,C). Consistent with this observation, we showed previously that polyIC, a potent IFN inducer, effectively prevented HCC initiation and also suppressed tumor progression in combination with anti-PD-L1 antibody (122-124). We believe that the tumor suppressive role of Shp2 inhibitor is associated with multiple effects and mechanisms, including downregulation of inflammatory cytokines, suppression of the CCR5 axis and upregulation of IFN signaling, which work in concert to enhance the hepatic anti-tumor innate immunity. In conclusion, this study demonstrates an encouraging therapeutic benefit of targeting Shp2 in primary and metastasized liver tumors.

3.2. Acknowledgement

This dissertation from Chapter 1 through Chapter 5, in part, is a reprint of the material as it appears in Shp2 deletion in hepatocytes suppresses hepatocarcinogenesis driven by

oncogenic β-Catenin, PIK3CA and MET. Jacey Jijun Liu, Yanjie Li, Wendy Chen, Yan Liang, Gaowei Wang, Min Zong, Kota Kaneko, Ruiyun Xu, Michael Karin, Gen-Sheng Feng, Journal of Hepatology, 2018. The dissertation author was the primary investigator and author of this paper.

This dissertation from Chapter 1 through Chapter 5, in part, has been accepted for publication of the material as it may appear in Pharmaceutical Shp2 Inhibition Suppresses Primary and Metastasized Liver Tumors by Provoking Hepatic Innate Immunity, Jacey Jijun Liu, Bing Xin, Li Du, Lydia Chen, Yanyan Long, Gen-Sheng Feng, Hepatology, 2022. The dissertation author was the primary investigator and author of this paper.

Chapter 4. Summary and future direction

4.1. Summary

Here is a graphical abstract to summarize the important findings in this study (Figure 41). In this study, we revealed the dual roles of Shp2 in the liver, which are its tumor promoting role in mediating intrinsic RTK/Ras/MAPK pathway, and its tumor suppressive role in maintaining hepatic environment homeostasis. Depending on the actual oncogenic drivers and environmental cues, one role may overweight its counterpart and lead to opposing tumorigenic result. We unveiled a possible mechanism for Shp2's mediatory function for RTK/Ras/MAPK pathway, in which Shp2 competes with Socs3 for the binding to intracellular domain of Met to prevent Socs3-mediated Met degradation.

Consistent with Shp2's tumor promoting role, Shp2 pharmacological inhibition impairs RTK/Ras pathway to suppress hepatic tumor growth. Meanwhile, Shp2 inhibition also affects hepatic tumor microenvironment, whereas Shp2 genetic deletion in hepatocyte also causes tumor microenvironmental impacts but in a opposite direction as pharmacological inhibition. Shp2 genetic deletion embarks inflammation in liver microenvironment, which is reflected by increased immune cell infiltration and upregulation of M1-type polarization of macrophage, resulting in exacerbation of oncogene-driven Shp2-independent primary liver tumor and liver metastasized tumor. In sharp contrast, Shp2 pharmacological inhibition suppresses metastasized tumor formation. Mechanistic study showed that Shp2 inhibition has neglectable effect on lymphocyte cell composition and adaptive immunity. However, in myeloid compartment, Shp2 inhibition significantly alters polarization of hepatic Kupffer cells by downregulating M2b polarization and impedes activation of CCR5 pathway in macrophage,

collectively to alleviate inflammation. Shp2 inhibition also provokes type I interferon mediated anti-tumor immunity.

Overall, multiple effects conveyed by Shp2 on liver microenvironment work in concert to enhance the hepatic anti-tumor innate immunity. All in all, Shp2 inhibitor has impacts on both intrinsic oncogenic pathway and tumor microenvironment to achieve its anti-tumor activity. More experiments are warranted to elucidate the complex molecular and cellular mechanisms and to further improve the efficacy, but this study has demonstrated an encouraging therapeutic benefit of targeting Shp2 in primary and metastasized liver tumors. Further, the solid discrepancy in environmental outcomes caused by genetic and pharmacological disturbance of Shp2 indicates a limitation of cell type-specific gene deletion data in predicting possible outcomes of pharmaceutical inhibition of the same gene product.

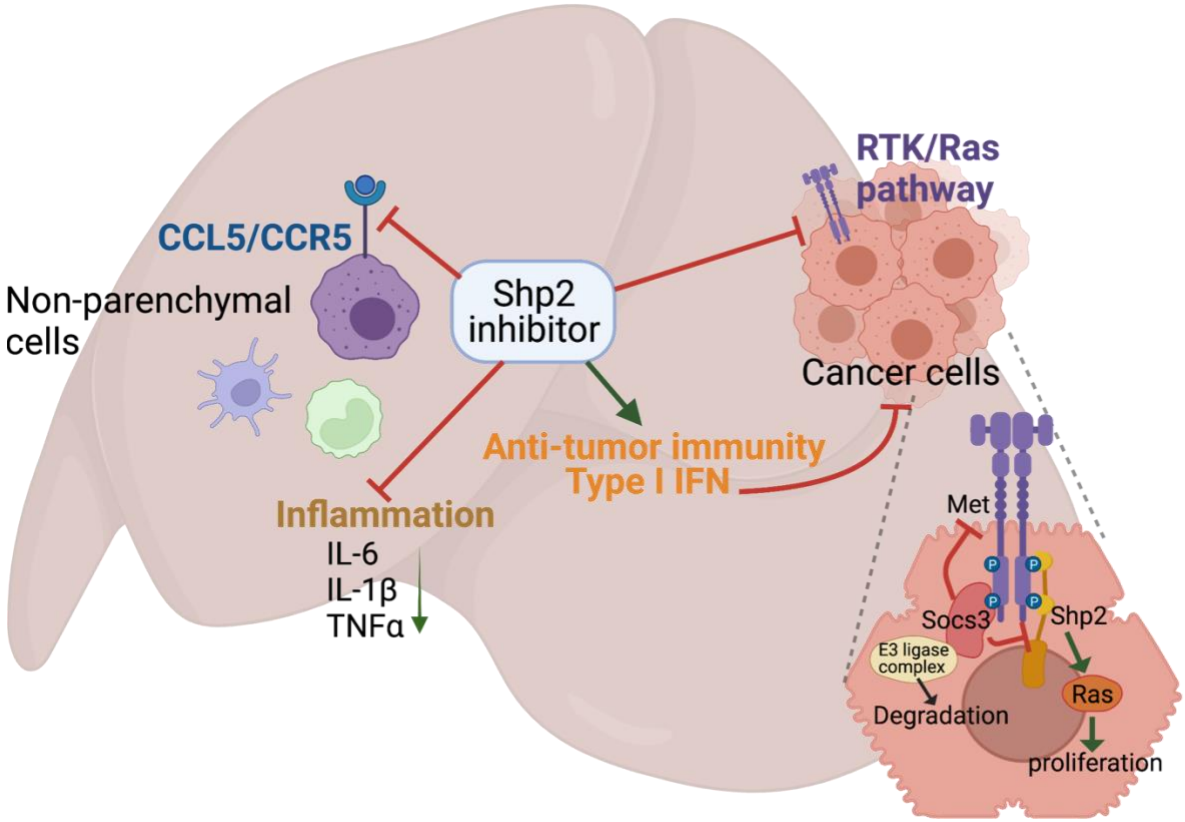

Figure 41. Graphical abstract

4.2. Future direction

The existing data generated more questions that await answers. First, we observed that Shp2 inhibitor treatment altered hepatic macrophage ratio and M2b polarization. However, it is likely that only one specific proinflammatory subset within M2b macrophages that is prone to regulation by Shp2. We are interested in further characterizing of this specific subset in the future, through identifying markers for this subset, and through determining the subset's contribution to liver tumor. Also, we wonder if there are any other molecular targets beside Shp2 that can be exploited to downregulate this subset to further alleviate inflammation.

Another future direction is to optimize anti-HCC therapeutic strategies by combining inhibition of Shp2 and another target. One staple candidate is immune checkpoint inhibitor. The idle adaptive immunity and increased regulatory T cell ratio upon Shp2 inhibitor treatment implies potential efficacy of combined treatment with immune checkpoint inhibitor. Second candidate is Ras/MAPK pathway inhibitors such as MEK inhibitor and ERK inhibitor. It was proven in other solid cancers that Shp2 inhibition combats the acquired resistance to MEKi or ERKi. Meanwhile, MEKi or ERKi have greater anti-tumor potency that can compensate for Shp2 inhibitor's mild potency. Therefore, it is a worthwhile therapeutic combination to examine in HCC.

4.3. Acknowledgement

This dissertation from Chapter 1 through Chapter 5, in part, is a reprint of the material as it appears in Shp2 deletion in hepatocytes suppresses hepatocarcinogenesis driven by oncogenic β-Catenin, PIK3CA and MET. Jacey Jijun Liu, Yanjie Li, Wendy Chen, Yan Liang,

Gaowei Wang, Min Zong, Kota Kaneko, Ruiyun Xu, Michael Karin, Gen-Sheng Feng, Journal of Hepatology, 2018. The dissertation author was the primary investigator and author of this paper.

This dissertation from Chapter 1 through Chapter 5, in part, has been accepted for publication of the material as it may appear in Pharmaceutical Shp2 Inhibition Suppresses Primary and Metastasized Liver Tumors by Provoking Hepatic Innate Immunity, Jacey Jijun Liu, Bing Xin, Li Du, Lydia Chen, Yanyan Long, Gen-Sheng Feng, Hepatology, 2022. The dissertation author was the primary investigator and author of this paper.

Chapter 5. Materials and methods

5.1. Experimental mice

The *Shp2*$^{hep-/-}$ (Shp2$^{fl/fl}$;Alb-Cre^{+}) mouse line in C57BL/6 background was generated by breeding Shp2$^{fl/fl}$ mouse with Albumin-Cre transgenic mice, as previously described (27, 63). All animal studies were conducted on male Shp2$^{fl/fl}$ (*WT*) or Shp2$^{fl/fl}$;Alb-Cre(*Shp2*$^{hep-/-}$) mice at age of 6-23 weeks. Mice were group-housed (2-5 mice per cage) expect for less than 5% of mice were single-housed in later time period due to the death of cage-mates. All mice were maintained under a 12 h light/dark cycle with free access to water and standard mouse chow. The animal protocol (S09108) and the experimental procedures were approved by the Institutional Animal Care and Use Committee (IACUC) of the University of California San Diego.

5.2. *In vivo* small molecule treatment

SHP099 (Chemietek, Indianapolis, IN), Trametinib (GSK1120212, APExBIO, Houston, Texas) and Maraviroc (UK-427857, Irvine, CA) were administrated to experimental mice. SHP099, Trametinib and Maraviroc were all dissolved in DMSO to make stock solutions at 100mg/ml, 10mg/ml and 90mg/ml, respectively. SHP099 was diluted (1:24) in Ringer's solution as delivery vehicle and delivered through intraperitoneal injection. Trametinib was diluted (1:29) in Ringer's solution as delivery vehicle and delivered through intraperitoneal injection at the dose of 0.25mg/kg BW(pre-treatment) or 3mg/kg BW(treatment for Nras/Myc tumor). Maraviroc was diluted in olive oil (1:8) as delivery vehicle and delivered through intraperitoneal injection. Pre-treatment of small molecules was performed on 2-3month-old male mice. SHP099 pre-treatment lasted for 14 days at 100mg/kg/q.d.. SHP099 treatment on post-MC38 transplantation mouse, Met/Cat- and Nras/Myc-tumor bearing mouse lasted for 10,

21 and 21 days respectively at at 100mg/kg/q.d.. Trametinib pre-treatment lasted for 14 days at 0.25mg/kg/q.d.. Trametinib treatment on Nras/Myc-tumor bearing mouse lasted for 21 days at at 3mg/kg/q.d.. Maraviroc treatment on Met/Cat tumor was given at 30mg/kg, q.d. for first 7 days and q.o.d. for the next 14 days. Maraviroc given to post-MC38 transplantation mouse was at 30mg/kg/q.d. from day-4 to day-8, and then q.o.d for the next 10 days. In SHP099/Maraviroc combo treatment given to Met/Cat, Nras/Myc or post-MC38 transplantation mouse, both drugs were administrated every other day on alternative days at 100 mg/kg (SHP099) and 30 mg/kg (Maraviroc) for 21, 21and 14 days, respectively.

5.3. Hydrodynamic injection

Oncogene-expressing constructs were delivered by hydrodynamic tail vein injection into mice at 6-8 weeks of age, as described in this article (139). Plasmids: *met*: PT3EF1aH-hMet; *ctnnb1/β-catenin*: PT3EF1aH-β-catenin; *pik3ca*: PIK3CA-H1047RΔf-PT3EF5a; *sleeping beauty transposase(SB)*: pCMV/SB were gifts from Dr. Xin Chen (Addgene plasmid # 86498, #86499). Plasmid encoding for $nras^{G12V}$ (pT/Caggs-NRASV12) was a gift from Dr. John Ohlfest (Addgene plasmid # 20205). Plasmids encoding for other genes (*ptpn11/Shp2; socs1; socs3;* met^{Y1003F}) were constructed by cloning cDNA, which was reversely transcribed from HEK293T or MC38 cell, into pT3 vector under EF-1α promotor. Point mutations of genes to hydrodynamically deliver were made by Q5 Site-Directed Mutagenesis Kit (E0554S, New England Biolabs, Ipswich, MA). DNA plasmids were extracted from DH5α cells using GenElute HP Endotoxin-Free Plasmid Maxiprep Kit (NA0410, Sigma-Aldrich, St. Louis, MO). All constructs were diluted together with Sleeping Beauty transposase construct (*SB*) in PBS to final concentrations as below: Cat/Pik model: *β-catenin*: 10 μg/ml, *pik3ca*: 10 μg/ml, *SB*: 0.8 μg/ml; $Nras^{G12V}$/Cat model: *β-catenin*: 5 μg/ml, $nras^{G12V}$: 5 μg/ml, *SB*: 0.4 μg/ml;

Nras^{G12V}/Myc model: *myc*: 0.25 μg/ml, *nras^{G12V}*: 4.75 μg/ml, *SB*: 0.2 μg/ml; Nras^{G12V}/Pik model: *nras^{G12V}*: 10 μg/ml, *pik3ca*: 10 μg/ml, *SB*: 0.8 μg/ml; Nras^{G12V} model: *nras^{G12V}*: 10 μg/ml, *SB*: 0.4 μg/ml; Met/Cat/Shp2(WT or mutant) model: *met*: 5 μg/ml, *β-catenin*: 5 μg/ml, *shp2*: 10μg/ml, *SB*: 0.8 μg/ml; Met/Pik/Shp2(WT or mutant) model: *met*: 10 μg/ml, *pik3ca*: 10 μg/ml, *shp2*: 20 μg/ml, *SB*: 1.6 μg/ml; Met/Cat/Socs1(F59D) model: *met*: 5 μg/ml, *β-catenin*: 5 μg/ml, *socs1^{F59D}*: 5μg/ml, *SB*: 0.6 μg/ml; Met/Cat/Socs3(F25A) model: *met*: 5 μg/ml, *β-catenin*: 5 μg/ml, *socs3^{F25A}*: 5μg/ml, *SB*: 0.6 μg/ml; Cat/Socs3(F25A) model: *β-catenin*: 5 μg/ml, *socs3^{F25A}*: 5μg/ml, *SB*: 0.4 μg/ml; Met^{Y1003F}/Cat model: *met^{Y1003F}*: 5 μg/ml, *β-catenin*: 5 μg/ml, *SB*: 0.4 μg/ml; Met^{Y1003F}/Cat/Shp2(C463S) model: *met^{Y1003F}*: 5 μg/ml, *β-catenin*: 5 μg/ml, *shp2^{C463S}*: 5 μg/ml, *SB*: 0.6 μg/ml. Plasmid DNA-containing PBS solution was injected at 0.1 ml/g body weight through tail vein in 5-7 seconds.

5.4. Intraportal vein injection

Intraportal vein injection was performed on mice under anesthesia with isoflurane after 6 hours of fasting. The mouse abdominal cavity was widely opened with portal vein exposed, and then ligand dissolved in sterile PBS was injected into portal vein in a 20-second interval. The mouse was then euthanized in 15 minutes and liver samples were snap-frozen on dry ice. Ligands and dose used: human Wnt3a (R&D, 5036-WN-010), 2 μg per mouse; mouse HGF (Sigma, SRP3300), 3.3 μg per mouse; mouse R-spondin 1 (R&D,7150-RS-025), 2 μg per mouse.

5.5. Intrasplenic injection of MC38 cells and hemi-splenectomy

MC38 cells were suspended in PBS and kept on ice. 50μl (Intrasplenic injection only) or 150μl (hemi-splenectomy+intrasplenic injection) PBS followed by 50μl MC38 suspension

were drawn into 1ml syringe (309628, BD, Franklin Lakes, NJ) through 30g needle (26437, EXELINT international, Redondo Beach, CA) immediately before intrasplenic injection. Mice were put under anesthesia and shaved at left subcostal area. For intrasplenic injection only, a left subcostal incision in line with left ear was made through skin and peritoneum. Then inferior half of spleen was expressed through the incision. Then injection of 100μl MC38 cell-containing PBS solution was performed through the inferior end of spleen over a 1-2 minute time period. For hemi-splenectomy+injection, the procedure was performed as described in this article (140), except for minor modifications in the choice of materials mentioned elsewhere in this section. In all survival surgeries, mice were anesthetized with 2-3% isoflurane (502017, VetOne, Boise, ID) and were given Ethiqa XR (Fidelis Pharmaceuticals, North Brunswick Township, NJ) at 15μl/20g BW as analgesic. At the end of surgeries including laparotomy and intrasplenic injection, incision was closed by suture (5-0 Perma Hand silk suture, 682G, Ethicon, Bridgewater, NJ), followed by stapling skin (9mm Autoclip wound clip, 427631, BD).

5.6. Laparotomy

Laparotomy was performed to inspect liver tumor development. Mice were put under anesthesia and shaved at most of the abdominal surface. A 2cm incision was made down the middle of the abdomen through skin and linea alba. Liver was then expressed by applying gentle pressure downwards on both sides of the incision. After tumor inspection, liver was gently placed back to peritoneal cavity using moisturized (Ringer's solution, 2B2324X, Baxter, Deerfield, IL) cotton applicator. The incision was then closed by suture.

5.7. Hepatic non-parenchymal cell isolation and staining

Mouse liver was perfused with collagenase H (11074059001, Millipore Sigma, Burlington, MA) and then the perfused liver was passed through 100 micron cell strainer (431752, Fisher Scientific, Waltham, MA). The resulting cell suspension was centrifuged at 50g for 5 minutes at 4°C and the supernatant containing hepatic non-parenchymal cells (NPCs) was saved. After one PBS wash, the NPCs were pelleted by centrifuging at 300g for 5 minutes at 4°C. NPCs were then resuspended in PBS and after ACK lysing buffer (A1049201, Thermo Fisher Scientific) treatment for 10 minutes at RT. NPCs were stained with 1:100 dilution of Live/Dead cell stain (L34957, Invitrogen, Waltham, WA) in PBS, washed with PBS and then stained with various surface marker antibodies (Table. 1) in staining buffer (PBS containing 2% FBS) for 30 minutes at 4°C. Stained cells were washed with staining buffer for twice, and then resuspended in PBS for FACS, or permeabilized with Foxp3 / Transcription Factor Staining Buffer Set (00-5523-00, Invitrogen), followed by staining with various intracellular target antibodies (Table. 1) at 4°C overnight. After two permeabilization buffer washes, NPCs were resuspended in PBS for FACS analysis.

5.8. Flow cytometry and culture of sorted cells

Flow cytometry analysis was run on BD LSRFortessa™ X-20 Cell analyzer (BD, Franklin Lakes, NJ). Cell sorting was run on BD FACS Aria II and BD FACS Aria Fusion. Sorted hepatic macrophage and dendritic cells were collected in pure heat inactivated FBS in 15ml tube. Sorted cells were later transferred to 10% FBS RPMI culture medium and plated in 96-well plate at 20k cells/well. SHP099 (20μM), Maraviroc(10μM) or CCL5(20ng/ml) were

then added to sorted cell culture. Cell culture supernatant for ELISA as well as cultured cells was collected after 16hr of treatment.

5.9. *In vitro* stimulation of hepatocytes

Primary hepatocytes were isolated from mice at the age of 2 months the day before stimulation, then cultured in collagen-coated tissue culture plate. The same ligands as the ones used in *in vivo* stimulation, HGF (20 ng/ml), Wnt3a (40 ng/ml) and R-Spondin1(40 ng/ml), were added into serum-free cell culture medium and remained in cell medium until harvest of cells.

5.10. Cell culture and transfection

MC38 cells were a gift from Karin Lab, UC San Diego. HEK293T cells were obtained from ATCC (CRL-3216, ATCC, Manassas, VA). MC38 and HEK293T cells were cultured in 10% FBS DMEM (10313021, Gibco, Waltham, MA) supplemented by GlutaMax (35050-061, Gibco), Non-essential Amino Acid (M7145, Sigma-Aldrich) and Penicillin-Streptomycin (15140122, Gibco). DNA plasmid transfection of HEK293T cells was performed with Lipofectamine 3000 (L3000015, Invitrogen) in Opti-MEM (31985062, Gibco).

5.11. Special staining

Fresh liver tissues were embedded in Tissue-Tek OCT compound (Sakura Finetek, Torrance, CA) and frozen to tissue blocks for sectioning. Oil Red O staining was performed on fresh frozen tissue sections using Oil Red O solution (O1516, Sigma-Aldrich). For SA-β-galactosidase staining, fresh frozen tissue sections were fixed by 4% Paraformaldehyde at 4°C for 24hr and then stained with freshly-made staining solution, which was 1x PBS at pH6.0

containing 1 g/L X-gal (ab144388, Abcam, Cambridge, United Kingdom), 1mM potassium ferrocyanide [$K_4Fe(CN)_6$], 5 mM potassium ferricyanide [$K_3Fe(CN)_6$], 2 mM $MgCl_2$, overnight at 37°C. Sirius Red staining was performed on z-fix fixed paraffin-embedded sections using Picro-Sirius Red Staining kit (Statlab, Mckinney, Texas) according to manufacturer's instruction.

5.12. Immunoblotting and immunostaining

Immunoblotting was performed on liver tissue lysates or cultured whole cell lysates using standard protocols. Primary antibodies to human Met (8198, Cell Signaling Technology, Danvers, MA), p-Met (3126, CST), Akt (9272, CST), p-Akt^{S473} (9271, CST), p-Erk (4370, CST), Erk (4695, CST), c-Myc (ab32072, Abcam), p-β-Catenin (9561, CST), GSK3β (9315, CST), p-GSK3α/β (9331, CST), GAPDH (60004, Proteintech, Rosemont, IL), PI3K p110α (21890, Proteintech), β-Actin (A1978, Sigma-Aldrich), β-catenin (sc-7199, Santa Cruz Biotechnology, Dallas, Texas), Glutamine Synthetase (sc-74430, Santa Cruz Biotechnology), Nras (sc-31, Santa Cruz Biotechnology), Socs3 (sc-9023, Santa Cruz Biotechnology) and Socs1 (sc-9021, Santa Cruz Biotechnology) were used. Blots were washed three times with 1x TBS with 0.1% Tween-20 and then incubated with secondary antibody (Sheep anti-mouse 84-848, Donkey anti-rabbit 20-303, Genesee Scientific, San Diego, CA). Blots were developed with ProSignal Pico ECL Reagent (20-300, Genesee Scientific) and imaged using Bio-rad ChemiDoc system. Immunohistochemical staining was performed on z-fix fixed paraffin-embedded tissue sections using antibodies for Glutamine Synthetase (sc-74430, Santa Cruz Biotechnology), p-Erk (4370, CST). Immunofluorescence was performed on fresh frozen tissue sections fixed with 4% Paraformaldehyde or ice-cold methanol. Primary antibodies to F4/80

(14-4801-82, Invitrogen, Waltham, MA), CCR5 (bs-2514R, Bioss Antibodies, Woburn, MA), HNF4α (sc-8987, Santa Cruz Biotechnology), Ki67 (14-5698-80, Invitrogen), CD133 (14-1331-80, Invitrogen), c-Myc (ab32072, Abcam), Met (8198, CST), p-IRF3 (29047, CST) and secondary antibody (Goat anti-rat A11007, Donkey anti-rat A21208, Goat anti-rabbit A11012, Donkey anti-rabbit A21206, Invitrogen) were used. Staining was finished by nuclear counterstain with Hoechst 33342 (H3570, Invitrogen) and mounting with Anti-Fade fluorescence mounting medium (ab104135, Abcam).

5.13. RNA extraction and real-time qPCR analysis

Total RNAs were extracted from snap frozen hepatic non-parenchymal cells using Trizol reagent (15596018, Thermo Fisher Scientific, Waltham, MA) and a purity (A260/A280 value) over 1.9 was ensured before reverse transcription using MultiScribe Reverse Transcriptase (4311235, Applied Biosystems, Waltham, MA). Real-time qPCR was performed using PowerUp SYBR green master mix (A35776, Thermo Fisher Scientific). Primer sequences were summarized in Table. 2. Thermal profile used was: segment 1:50°C(2min)-95°C(2min); segment 2 (40 cycles):95°C(15s)-60°C(30s); segment 3 (Dissociation curve): 95°C(15s)-60°C(1min)-95°C(15s). Results of real-time qPCR were normalized to *ubc* cDNA concentration in each sample. Each control or experimental group contained 3 or more biological samples.

5.14. ELISA

Expression level of IFNα (luex-mifnav2, InvivoGen, San Diego, CA), IFNβ (luex-mifnbv2, InvivoGen), TNFα (430904, Biolegend, San Diego, CA), IL-1β (432604, Biolegend),

IL-6 (431301, Biolegend) and CCL5/RANTES(88-56009-22, Invitrogen) were measured by ELISA kits according to manufacturer's instruction.

5.15. RNA-sequencing analysis

Total RNAs were extracted from mouse livers using RNeasy Microarray Tissue Mini Kit (73304, QIAGEN, Germantown, MD), and at least three mice were included for each group. RNA-sequencing (RNA-seq) was conducted at the IGM Genomics Center, University of California, San Diego. cDNA library was constructed using Illumina TruSeq Stranded mRNA Library Prep Kit (RS-122-2101, Illumina, San Diego CA) for day-0 and day-3 samples, and by Illumina TruSeq RNA Library Prep Kit v2 (15025062) for day-7 samples, and deep sequencing was performed using Illumina HiSeq 4000. All the RNA-seq raw data were aligned using STAR. We performed gene differential expression analysis using Cuffdiff and R package extraction of differential gene expression (EDGE), respectively. Gene Set Enrichment Analysis (GSEA), Preranked tool and Ingenuity pathway analysis (IPA, Ingenuity® Systems) softwares were used for pathway analysis. All of the sequencing data have been deposited to GEO (GEO Accession: GSE97996, GSE109544). Significant differences in gene expression were identified by FDR<0.05, and enriched pathways or gene sets were identified by $P<0.05$ or FDR-q<0.05.

5.16. Statistical analysis

Statistical analysis was done using GraphPad Prism 9. Statistical significance between means was calculated by Student's T-test if not specified otherwise (*P<0.05; **P<0.01; ***P<0.001). If the experiment involved two independent variables placing influences on dependent variable, statistical analysis was performed by two-way ANOVA together with

multiple comparisons by Two-stage linear step-up procedure of Benjamini, Krieger and Yekutieli. P value <0.05 was considered significant ($^{\#}P<0.05$; $^{\#\#}P<0.01$; $^{\#\#\#}P<0.001$).

5.17. Acknowledgement

This dissertation from Chapter 1 through Chapter 5, in part, is a reprint of the material as it appears in Shp2 deletion in hepatocytes suppresses hepatocarcinogenesis driven by oncogenic β-Catenin, PIK3CA and MET. Jacey Jijun Liu, Yanjie Li, Wendy Chen, Yan Liang, Gaowei Wang, Min Zong, Kota Kaneko, Ruiyun Xu, Michael Karin, Gen-Sheng Feng, Journal of Hepatology, 2018. The dissertation author was the primary investigator and author of this paper.

This dissertation from Chapter 1 through Chapter 5, in part, has been accepted for publication of the material as it may appear in Pharmaceutical Shp2 Inhibition Suppresses Primary and Metastasized Liver Tumors by Provoking Hepatic Innate Immunity, Jacey Jijun Liu, Bing Xin, Li Du, Lydia Chen, Yanyan Long, Gen-Sheng Feng, Hepatology, 2022. The dissertation author was the primary investigator and author of this paper.

Table 1. Antibodies used in flow cytometry

Target	Conjugate	Manufacturer	Cat. No.
Mouse CD45	PerCP-Cy5.5	Biolegend	147706
Mouse Granzyme B	FITC	Biolegend	515403
Mouse NK1.1	APC	Biolegend	108710
Mouse CD8α	PE-Cy7	Biolegend	100722
Mouse CD19	APC-Cy7	Biolegend	115530
Mouse CD4	BV605	Biolegend	100548
Mouse CD69	BV711	Biolegend	104537
Mouse Ly6c	FITC	Biolegend	128006
Mouse F4/80	PB	Biolegend	123124
Mouse CD11c	APC	Biolegend	117310
Mouse CD206	PE-Cy7	Biolegend	141720
Mouse MHCII	APC-Cy7	Biolegend	107628
Mouse CD11b	BV605	Biolegend	101257
Mouse B220	BV711	Biolegend	103255
Mouse CD44	APC	Biolegend	103012
Mouse CD3e	FITC	Biolegend	100204
Mouse CD19	PE	Biolegend	115508
Mouse CCR5	PE	Invitrogen	12-1951-81
Mouse Ki67	PB	Invitrogen	48-5698-82
Mouse CD3e	PE-Cy5	Invitrogen	15-0031-81
Mouse Ly6G	PE-Cy5	Invitrogen	15-9668-82
Mouse SIRPα	SB645	Invitrogen	64-1721-80
Mouse Foxp3	APC	Invitrogen	17-5773-82
Mouse PD-1	APC-Cy7	Invitrogen	47-9985-80
Mouse CD62L	PE	Invitrogen	12-0621-82

Table 2. Primer sequences

Target (all mouse genes)	Sequence (5'-3')
UBC-F	CCCAGTGACACCATAGAGAATG
UBC-R	CTGGATGTTGTAGTCTGACAGG
CXCL2-F	GCCAAGGGTTGACTTCAAGA
CXCL2-R	CTTCAGGGTCAAGGCAAACT
CXCL3-F	CAGTGCCTGAACACCCTAC
CXCL3-R	GCAAACTTCTTGACCATCCTTG
CXCL4-F	CTTAGCTGTGTGTGTGTGAAGA
CXCL4-R	CCATTCTTCAGGGTGGCTATG
CXCL5-F	CTACGGTGGAAGTCATAGCTAAA
CXCL5-R	GCATTCCGCTTAGCTTTCTTT
CXCL7-F	GCGCTGCAGATGTACGAATA
CXCL7-R	CCATTCTTCAGTGTGGCTATCA
CXCL9-F	GGCAAATGTGAAGAAGCTGATG
CXCL9-R	TGAACGACGACGACTTTGG
CXCL10-F	CAGTGAGAATGAGGGCCATAG
CXCL10-R	GGATTCAGACATCTCTGCTCAT
CXCL11-F	CGGGATGAAAGCCGTCAAA
CXCL11-R	CCAGGCACCTTTGTCGTTTA
CXCL12-F	CCGAAATTAAAGTGGATCCAAGAG
CXCL12-R	GGCAGCCTTTCTCTTCTTCT
CXCL13-F	TGTTGTCGGTCTAAACATCATAGA
CXCL13-R	GGCACGAGGATTCACACATA
CXCL14-F	CTGCGAGGAGAAGATGGTTATC
CXCL14-R	CTTCTCGTTCCAGGCATTGTA
CXCL15-F	ATTTGGGAGACCTGAGAACAAG

Table 2. Primer sequences, continued

Target (all mouse genes)	Sequence (5'-3')
CXCL15-R	TCACTGGAGTCCCGTAGAAA
CXCL16-F	GAGGCTGAGGCAAATGAGAA
CXCL16-R	CTGCAGTGAGGAAGAAGACAA
CXCL17-F	GTCCCTGTGATCACGTCAAG
CXCL17-R	CCAGGTGACATCGTTTGAGAA
CCL3-F	ACTCTGCAACCAAGTCTTCTC
CCL3-R	GATCTGCCGGTTTCTCTTAGTC
CCL2-F	AGTAGGCTGGAGAGCTACAA
CCL2-R	GTATGTCTGGACCCATTCCTTC
CCL4-F	ACTATGAGACCAGCAGTCTTTG
CCL4-R	AACTCCAAGTCACTCATGTACTC
CCL5-F	GCCCACGTCAAGGAGTATTT
CCL5-R	CTTGAACCCACTTCTTCTCTGG
CCL17-F	GAGTGCTGCCTGGATTACTT
CCL17-R	ACCAATCTGATGGCCTTCTTC
CCL7-F	CAAGAGCTACAGAAGGATCACC
CCL7-R	TCCTCGACCCACTTCTGAT
CCL11-F	CCAACACACTACTGAAGAGCTAC
CCL11-R	ATCCTGGACCCACTTCTTCT
CCL12-F	GATCTTCAGGACCATACTGGATAAG
CCL12-R	GAAGGTTCAAGGATGAAGGTTTG
CCL19-F	TGCCTGCTGTTGTGTTCA
CCL19-R	GCTGTTGCCTTTGTTCTTGG
CCL20-F	TTCCAGAGCTATTGTGGGTTTC
CCL20-R	GGATCAGCGCACACAGATT

Table 2. Primer sequences, continued

Target (all mouse genes)	Sequence (5'-3')
CCL22-F	GGAGTTCTTCTGGACCTCAAA
CCL22-R	GAGTAGCTTCTTCACCCAGAC
CCL24-F	CATCACCAAGAAGGGCCATAA
CCL24-R	ACTTGGTTCTCACTGCCTTG
CCL27a-F	ATGTCGCGATTGAGGAGATAC
CCL27a-R	TCTGGCTTGTTGGAGACATC
CCR5-F	TCCGGAGTTATCTCTCAGTGT
CCR5-R	TCTCCTGTGGATCGGGTATAG
CCR2-F	GGCTATTGTTCATGCTGTGTTT
CCR2-R	ATAAGGGCCACAGGTGTAATG
IL1b F	ATCCCAAGCAATACCCAAAGA
IL1b R	GCTTGTGAGGTGCTGATGTA
LIGHT F	TCCTGGGAGAAGCTGATACA
LIGHT R	CCATAACAGAGGTCCACCAATAC
IRF3 F	GTCTTAAGGAGCTGTTAGAGATGG
IRF3 R	TGGTCAGAGGTAAGGGAGATAG
IRF5 F	AGGAGCAAGTGGAACTCTTTG
IRF5 R	CATCTAGCAGCTGGTTCGTATAG
IFNA1 F	CTGCTGGCTGTGAGGAAATA
IFNA1 R	CACATTGGCAGAGGAAGACA
IFNA2 F	CTTTCCTCGTGATGCTGATAGT
IFNA2 R	CCTTCAAGGCCCTCTTGTT
IFNB1 F	GATGACGGAGAAGATGCAGAAG
IFNB1 R	CATCCAGGAGACGTACAACAATAG
TNFa F	AATGGCCTCCCTCTCATCAGTT
TNFa R	CCACTTGGTGGTTTGCTACGA

Table 2. Primer sequences, continued

Target (all mouse genes)	Sequence (5'-3')
IL6 F	GAACAACGATGATGCACTTGC
IL6 R	TCCAGGTAGCTATGGTACTCC

Chapter 6. References

1. Bray F, Ferlay J, Soerjomataram I, Siegel RL, Torre LA, Jemal A. Global cancer statistics 2018: GLOBOCAN estimates of incidence and mortality worldwide for 36 cancers in 185 countries. CA Cancer J Clin. 2018;68(6):394-424.

2. Yang JD, Hainaut P, Gores GJ, Amadou A, Plymoth A, Roberts LR. A global view of hepatocellular carcinoma: trends, risk, prevention and management. Nat Rev Gastroenterol Hepatol. 2019;16(10):589-604.

3. Cancer Genome Atlas Research Network. Electronic address wbe, Cancer Genome Atlas Research N. Comprehensive and Integrative Genomic Characterization of Hepatocellular Carcinoma. Cell. 2017;169(7):1327-41 e23.

4. Calderaro J, Couchy G, Imbeaud S, Amaddeo G, Letouze E, Blanc JF, Laurent C, Hajji Y, Azoulay D, Bioulac-Sage P, Nault JC, Zucman-Rossi J. Histological subtypes of hepatocellular carcinoma are related to gene mutations and molecular tumour classification. J Hepatol. 2017;67(4):727-38.

5. Llovet JM, De Baere T, Kulik L, Haber PK, Greten TF, Meyer T, Lencioni R. Locoregional therapies in the era of molecular and immune treatments for hepatocellular carcinoma. Nat Rev Gastroenterol Hepatol. 2021;18(5):293-313.

6. Llovet JM, Ricci S, Mazzaferro V, Hilgard P, Gane E, Blanc JF, de Oliveira AC, Santoro A, Raoul JL, Forner A, Schwartz M, Porta C, Zeuzem S, Bolondi L, Greten TF, Galle PR, Seitz JF, Borbath I, Haussinger D, Giannaris T, Shan M, Moscovici M, Voliotis D, Bruix J, Group SIS. Sorafenib in advanced hepatocellular carcinoma. N Engl J Med. 2008;359(4):378-90.

7. Cheng AL, Kang YK, Chen Z, Tsao CJ, Qin S, Kim JS, Luo R, Feng J, Ye S, Yang TS, Xu J, Sun Y, Liang H, Liu J, Wang J, Tak WY, Pan H, Burock K, Zou J, Voliotis D, Guan Z. Efficacy and safety of sorafenib in patients in the Asia-Pacific region with advanced hepatocellular carcinoma: a phase III randomised, double-blind, placebo-controlled trial. Lancet Oncol. 2009;10(1):25-34.

8. Kudo M, Finn RS, Qin S, Han KH, Ikeda K, Piscaglia F, Baron A, Park JW, Han G, Jassem J, Blanc JF, Vogel A, Komov D, Evans TRJ, Lopez C, Dutcus C, Guo M, Saito K, Kraljevic S, Tamai T, Ren M, Cheng AL. Lenvatinib versus sorafenib in first-line treatment of patients with unresectable hepatocellular carcinoma: a randomised phase 3 non-inferiority trial. Lancet. 2018;391(10126):1163-73.

9. Sangro B, Sarobe P, Hervas-Stubbs S, Melero I. Advances in immunotherapy for hepatocellular carcinoma. Nat Rev Gastroenterol Hepatol. 2021;18(8):525-43.

10. Finn RS, Qin S, Ikeda M, Galle PR, Ducreux M, Kim TY, Kudo M, Breder V, Merle P, Kaseb AO, Li D, Verret W, Xu DZ, Hernandez S, Liu J, Huang C, Mulla S, Wang Y, Lim HY, Zhu AX, Cheng AL, Investigators IM. Atezolizumab plus Bevacizumab in Unresectable Hepatocellular Carcinoma. N Engl J Med. 2020;382(20):1894-905.

11. Alonso A, Pulido R. The extended human PTPome: a growing tyrosine phosphatase family. FEBS J. 2016;283(11):2197-201.

12. Tautz L, Critton DA, Grotegut S. Protein tyrosine phosphatases: structure, function, and implication in human disease. Methods Mol Biol. 2013;1053:179-221.

13. Andersen JN, Mortensen OH, Peters GH, Drake PG, Iversen LF, Olsen OH, Jansen PG, Andersen HS, Tonks NK, Moller NP. Structural and evolutionary relationships among protein tyrosine phosphatase domains. Mol Cell Biol. 2001;21(21):7117-36.

14. Barr AJ, Ugochukwu E, Lee WH, King ON, Filippakopoulos P, Alfano I, Savitsky P, Burgess-Brown NA, Muller S, Knapp S. Large-scale structural analysis of the classical human protein tyrosine phosphatome. Cell. 2009;136(2):352-63.

15. Barford D, Neel BG. Revealing mechanisms for SH2 domain mediated regulation of the protein tyrosine phosphatase SHP-2. Structure. 1998;6(3):249-54.

16. Pluskey S, Wandless TJ, Walsh CT, Shoelson SE. Potent stimulation of SH-PTP2 phosphatase activity by simultaneous occupancy of both SH2 domains. J Biol Chem. 1995;270(7):2897-900.

17. Eck MJ, Pluskey S, Trub T, Harrison SC, Shoelson SE. Spatial constraints on the recognition of phosphoproteins by the tandem SH2 domains of the phosphatase SH-PTP2. Nature. 1996;379(6562):277-80.

18. Hof P, Pluskey S, Dhe-Paganon S, Eck MJ, Shoelson SE. Crystal structure of the tyrosine phosphatase SHP-2. Cell. 1998;92(4):441-50.

19. Zhang ZY. Mechanistic studies on protein tyrosine phosphatases. Prog Nucleic Acid Res Mol Biol. 2003;73:171-220.

20. Chan RJ, Feng GS. PTPN11 is the first identified proto-oncogene that encodes a tyrosine phosphatase. Blood. 2007;109(3):862-7.

21. Tartaglia M, Kalidas K, Shaw A, Song X, Musat DL, van der Burgt I, Brunner HG, Bertola DR, Crosby A, Ion A, Kucherlapati RS, Jeffery S, Patton MA, Gelb BD. PTPN11 mutations in Noonan syndrome: molecular spectrum, genotype-phenotype correlation, and phenotypic heterogeneity. Am J Hum Genet. 2002;70(6):1555-63.

22. Hanafusa H, Torii S, Yasunaga T, Nishida E. Sprouty1 and Sprouty2 provide a control mechanism for the Ras/MAPK signalling pathway. Nat Cell Biol. 2002;4(11):850-8.

23. Tefft D, Lee M, Smith S, Crowe DL, Bellusci S, Warburton D. mSprouty2 inhibits FGF10-activated MAP kinase by differentially binding to upstream target proteins. Am J Physiol Lung Cell Mol Physiol. 2002;283(4):L700-6.

24. Tefft D, De Langhe SP, Del Moral PM, Sala F, Shi W, Bellusci S, Warburton D. A novel function for the protein tyrosine phosphatase Shp2 during lung branching morphogenesis. Dev Biol. 2005;282(2):422-31.

25. Agazie YM, Hayman MJ. Molecular mechanism for a role of SHP2 in epidermal growth factor receptor signaling. Mol Cell Biol. 2003;23(21):7875-86.

26. Montagner A, Yart A, Dance M, Perret B, Salles JP, Raynal P. A novel role for Gab1 and SHP2 in epidermal growth factor-induced Ras activation. J Biol Chem. 2005;280(7):5350-60.

27. Bard-Chapeau EA, Yuan J, Droin N, Long S, Zhang EE, Nguyen TV, Feng GS. Concerted functions of Gab1 and Shp2 in liver regeneration and hepatoprotection. Mol Cell Biol. 2006;26(12):4664-74.

28. Cunnick JM, Meng S, Ren Y, Desponts C, Wang HG, Djeu JY, Wu J. Regulation of the mitogen-activated protein kinase signaling pathway by SHP2. J Biol Chem. 2002;277(11):9498-504.

29. Ren Y, Meng S, Mei L, Zhao ZJ, Jove R, Wu J. Roles of Gab1 and SHP2 in paxillin tyrosine dephosphorylation and Src activation in response to epidermal growth factor. J Biol Chem. 2004;279(9):8497-505.

30. Zhang SQ, Yang W, Kontaridis MI, Bivona TG, Wen G, Araki T, Luo J, Thompson JA, Schraven BL, Philips MR, Neel BG. Shp2 regulates SRC family kinase activity and Ras/Erk activation by controlling Csk recruitment. Mol Cell. 2004;13(3):341-55.

31. Bunda S, Burrell K, Heir P, Zeng L, Alamsahebpour A, Kano Y, Raught B, Zhang ZY, Zadeh G, Ohh M. Inhibition of SHP2-mediated dephosphorylation of Ras suppresses oncogenesis. Nat Commun. 2015;6:8859.

32. Bennett AM, Tang TL, Sugimoto S, Walsh CT, Neel BG. Protein-tyrosine-phosphatase SHPTP2 couples platelet-derived growth factor receptor beta to Ras. Proc Natl Acad Sci U S A. 1994;91(15):7335-9.

33. Mussig K, Staiger H, Fiedler H, Moeschel K, Beck A, Kellerer M, Haring HU. Shp2 is required for protein kinase C-dependent phosphorylation of serine 307 in insulin receptor substrate-1. J Biol Chem. 2005;280(38):32693-9.

34. Yang W, Klaman LD, Chen B, Araki T, Harada H, Thomas SM, George EL, Neel BG. An Shp2/SFK/Ras/Erk signaling pathway controls trophoblast stem cell survival. Dev Cell. 2006;10(3):317-27.

35. Tajan M, de Rocca Serra A, Valet P, Edouard T, Yart A. SHP2 sails from physiology to pathology. Eur J Med Genet. 2015;58(10):509-25.

36. Chan G, Cheung LS, Yang W, Milyavsky M, Sanders AD, Gu S, Hong WX, Liu AX, Wang X, Barbara M, Sharma T, Gavin J, Kutok JL, Iscove NN, Shannon KM, Dick JE, Neel BG, Braun BS. Essential role for Ptpn11 in survival of hematopoietic stem and progenitor cells. Blood. 2011;117(16):4253-61.

37. Nguyen TV, Ke Y, Zhang EE, Feng GS. Conditional deletion of Shp2 tyrosine phosphatase in thymocytes suppresses both pre-TCR and TCR signals. J Immunol. 2006;177(9):5990-6.

38. Salmond RJ, Huyer G, Kotsoni A, Clements L, Alexander DR. The src homology 2 domain-containing tyrosine phosphatase 2 regulates primary T-dependent immune responses and Th cell differentiation. J Immunol. 2005;175(10):6498-508.

39. Sharma N, Everingham S, Ramdas B, Kapur R, Craig AW. SHP2 phosphatase promotes mast cell chemotaxis toward stem cell factor via enhancing activation of the Lyn/Vav/Rac signaling axis. J Immunol. 2014;192(10):4859-66.

40. Mazharian A, Mori J, Wang YJ, Heising S, Neel BG, Watson SP, Senis YA. Megakaryocyte-specific deletion of the protein-tyrosine phosphatases Shp1 and Shp2 causes abnormal megakaryocyte development, platelet production, and function. Blood. 2013;121(20):4205-20.

41. Lima MH, Ueno M, Thirone AC, Rocha EM, Carvalho CR, Saad MJ. Regulation of IRS-1/SHP2 interaction and AKT phosphorylation in animal models of insulin resistance. Endocrine. 2002;18(1):1-12.

42. Choi E, Kikuchi S, Gao H, Brodzik K, Nassour I, Yopp A, Singal AG, Zhu H, Yu H. Mitotic regulators and the SHP2-MAPK pathway promote IR endocytosis and feedback regulation of insulin signaling. Nat Commun. 2019;10(1):1473.

43. Matsuo K, Delibegovic M, Matsuo I, Nagata N, Liu S, Bettaieb A, Xi Y, Araki K, Yang W, Kahn BB, Neel BG, Haj FG. Altered glucose homeostasis in mice with liver-specific deletion of Src homology phosphatase 2. J Biol Chem. 2010;285(51):39750-8.

44. Princen F, Bard E, Sheikh F, Zhang SS, Wang J, Zago WM, Wu D, Trelles RD, Bailly-Maitre B, Kahn CR, Chen Y, Reed JC, Tong GG, Mercola M, Chen J, Feng GS. Deletion of Shp2 tyrosine phosphatase in muscle leads to dilated cardiomyopathy, insulin resistance, and premature death. Mol Cell Biol. 2009;29(2):378-88.

45. Tartaglia M, Mehler EL, Goldberg R, Zampino G, Brunner HG, Kremer H, van der Burgt I, Crosby AH, Ion A, Jeffery S, Kalidas K, Patton MA, Kucherlapati RS, Gelb BD. Mutations in PTPN11, encoding the protein tyrosine phosphatase SHP-2, cause Noonan syndrome. Nat Genet. 2001;29(4):465-8.

46. Ogata T, Yoshida R. PTPN11 mutations and genotype-phenotype correlations in Noonan and LEOPARD syndromes. Pediatr Endocrinol Rev. 2005;2(4):669-74.

47. Tartaglia M, Martinelli S, Stella L, Bocchinfuso G, Flex E, Cordeddu V, Zampino G, Burgt I, Palleschi A, Petrucci TC, Sorcini M, Schoch C, Foa R, Emanuel PD, Gelb BD. Diversity and functional consequences of germline and somatic PTPN11 mutations in human disease. Am J Hum Genet. 2006;78(2):279-90.

48. Kontaridis MI, Swanson KD, David FS, Barford D, Neel BG. PTPN11 (Shp2) mutations in LEOPARD syndrome have dominant negative, not activating, effects. J Biol Chem. 2006;281(10):6785-92.

49. Bonetti M, Paardekooper Overman J, Tessadori F, Noel E, Bakkers J, den Hertog J. Noonan and LEOPARD syndrome Shp2 variants induce heart displacement defects in zebrafish. Development. 2014;141(9):1961-70.

50. Chen PC, Wakimoto H, Conner D, Araki T, Yuan T, Roberts A, Seidman C, Bronson R, Neel B, Seidman JG, Kucherlapati R. Activation of multiple signaling pathways causes developmental defects in mice with a Noonan syndrome-associated Sos1 mutation. J Clin Invest. 2010;120(12):4353-65.

51. Nakamura T, Gulick J, Pratt R, Robbins J. Noonan syndrome is associated with enhanced pERK activity, the repression of which can prevent craniofacial malformations. Proc Natl Acad Sci U S A. 2009;106(36):15436-41.

52. Strullu M, Caye A, Lachenaud J, Cassinat B, Gazal S, Fenneteau O, Pouvreau N, Pereira S, Baumann C, Contet A, Sirvent N, Mechinaud F, Guellec I, Adjaoud D, Paillard C, Alberti C, Zenker M, Chomienne C, Bertrand Y, Baruchel A, Verloes A, Cave H. Juvenile myelomonocytic leukaemia and Noonan syndrome. J Med Genet. 2014;51(10):689-97.

53. Kratz CP, Franke L, Peters H, Kohlschmidt N, Kazmierczak B, Finckh U, Bier A, Eichhorn B, Blank C, Kraus C, Kohlhase J, Pauli S, Wildhardt G, Kutsche K, Auber B, Christmann A, Bachmann N, Mitter D, Cremer FW, Mayer K, Daumer-Haas C, Nevinny-Stickel-Hinzpeter C, Oeffner F, Schluter G, Gencik M, Uberlacker B, Lissewski C, Schanze I, Greene MH, Spix C, Zenker M. Cancer spectrum and frequency among children with Noonan, Costello, and cardio-facio-cutaneous syndromes. Br J Cancer. 2015;112(8):1392-7.

54. Keilhack H, David FS, McGregor M, Cantley LC, Neel BG. Diverse biochemical properties of Shp2 mutants. Implications for disease phenotypes. J Biol Chem. 2005;280(35):30984-93.

55. Niihori T, Aoki Y, Ohashi H, Kurosawa K, Kondoh T, Ishikiriyama S, Kawame H, Kamasaki H, Yamanaka T, Takada F, Nishio K, Sakurai M, Tamai H, Nagashima T, Suzuki Y, Kure S, Fujii K, Imaizumi M, Matsubara Y. Functional analysis of PTPN11/SHP-2 mutants identified in Noonan syndrome and childhood leukemia. J Hum Genet. 2005;50(4):192-202.

56. Loh ML, Vattikuti S, Schubbert S, Reynolds MG, Carlson E, Lieuw KH, Cheng JW, Lee CM, Stokoe D, Bonifas JM, Curtiss NP, Gotlib J, Meshinchi S, Le Beau MM, Emanuel PD, Shannon KM. Mutations in PTPN11 implicate the SHP-2 phosphatase in leukemogenesis. Blood. 2004;103(6):2325-31.

57. Nomdedeu J, Carricondo MT, Lasa A, Perea G, Aventin A, Sierra J. Low frequency of exon 3 PTPN11 mutations in adult de novo acute myeloid leukemia. Analysis of a consecutive series of 173 patients. Haematologica. 2005;90(3):412-3.

58. Bentires-Alj M, Paez JG, David FS, Keilhack H, Halmos B, Naoki K, Maris JM, Richardson A, Bardelli A, Sugarbaker DJ, Richards WG, Du J, Girard L, Minna JD, Loh ML, Fisher DE, Velculescu VE, Vogelstein B, Meyerson M, Sellers WR, Neel BG. Activating mutations of the noonan syndrome-associated SHP2/PTPN11 gene in human solid tumors and adult acute myelogenous leukemia. Cancer Res. 2004;64(24):8816-20.

59. Lee IO, Kim JH, Choi YJ, Pillinger MH, Kim SY, Blaser MJ, Lee YC. Helicobacter pylori CagA phosphorylation status determines the gp130-activated SHP2/ERK and JAK/STAT signal transduction pathways in gastric epithelial cells. J Biol Chem. 2010;285(21):16042-50.

60. Lazzara MJ, Lane K, Chan R, Jasper PJ, Yaffe MB, Sorger PK, Jacks T, Neel BG, Lauffenburger DA. Impaired SHP2-mediated extracellular signal-regulated kinase activation contributes to gefitinib sensitivity of lung cancer cells with epidermal growth factor receptor-activating mutations. Cancer Res. 2010;70(9):3843-50.

61. Gu J, Han T, Ma RH, Zhu YL, Jia YN, Du JJ, Chen Y, Jiang XJ, Xie XD, Guo X. SHP2 promotes laryngeal cancer growth through the Ras/Raf/Mek/Erk pathway and serves as a prognostic indicator for laryngeal cancer. Int J Oncol. 2014;44(2):481-90.

62. Aceto N, Sausgruber N, Brinkhaus H, Gaidatzis D, Martiny-Baron G, Mazzarol G, Confalonieri S, Quarto M, Hu G, Balwierz PJ, Pachkov M, Elledge SJ, van Nimwegen E, Stadler MB, Bentires-Alj M. Tyrosine phosphatase SHP2 promotes breast cancer progression and maintains tumor-initiating cells via activation of key transcription factors and a positive feedback signaling loop. Nat Med. 2012;18(4):529-37.

63. Bard-Chapeau EA, Li S, Ding J, Zhang SS, Zhu HH, Princen F, Fang DD, Han T, Bailly-Maitre B, Poli V, Varki NM, Wang H, Feng GS. Ptpn11/Shp2 acts as a tumor suppressor in hepatocellular carcinogenesis. Cancer Cell. 2011;19(5):629-39.

64. Luo X, Liao R, Hanley KL, Zhu HH, Malo KN, Hernandez C, Wei X, Varki NM, Alderson N, Chu C, Li S, Fan J, Loomba R, Qiu SJ, Feng GS. Dual Shp2 and Pten Deficiencies Promote Non-alcoholic Steatohepatitis and Genesis of Liver Tumor-Initiating Cells. Cell Rep. 2016;17(11):2979-93.

65. Hanley KL, Liang Y, Wang G, Lin X, Yang M, Karin M, Fu W, Feng GS. Concurrent Disruption of the Ras/MAPK and NF-kappaB Pathways Induces Circadian Deregulation and Hepatocarcinogenesis. Mol Cancer Res. 2021.

66. Birchmeier C, Birchmeier W, Gherardi E, Vande Woude GF. Met, metastasis, motility and more. Nat Rev Mol Cell Biol. 2003;4(12):915-25.

67. Takami T, Kaposi-Novak P, Uchida K, Gomez-Quiroz LE, Conner EA, Factor VM, Thorgeirsson SS. Loss of hepatocyte growth factor/c-Met signaling pathway accelerates early stages of N-nitrosodiethylamine induced hepatocarcinogenesis. Cancer Res. 2007;67(20):9844-51.

68. Nejak-Bowen KN, Thompson MD, Singh S, Bowen WC, Jr., Dar MJ, Khillan J, Dai C, Monga SP. Accelerated liver regeneration and hepatocarcinogenesis in mice overexpressing serine-45 mutant beta-catenin. Hepatology. 2010;51(5):1603-13.

69. Zhang XF, Tan X, Zeng G, Misse A, Singh S, Kim Y, Klaunig JE, Monga SP. Conditional beta-catenin loss in mice promotes chemical hepatocarcinogenesis: role of oxidative stress and platelet-derived growth factor receptor alpha/phosphoinositide 3-kinase signaling. Hepatology. 2010;52(3):954-65.

70. Lee H, Herrmann A, Deng JH, Kujawski M, Niu G, Li Z, Forman S, Jove R, Pardoll DM, Yu H. Persistently activated Stat3 maintains constitutive NF-kappaB activity in tumors. Cancer Cell. 2009;15(4):283-93.

71. Wang H, Lafdil F, Wang L, Park O, Yin S, Niu J, Miller AM, Sun Z, Gao B. Hepatoprotective versus oncogenic functions of STAT3 in liver tumorigenesis. Am J Pathol. 2011;179(2):714-24.

72. Hui L, Zatloukal K, Scheuch H, Stepniak E, Wagner EF. Proliferation of human HCC cells and chemically induced mouse liver cancers requires JNK1-dependent p21 downregulation. J Clin Invest. 2008;118(12):3943-53.

73. Das M, Garlick DS, Greiner DL, Davis RJ. The role of JNK in the development of hepatocellular carcinoma. Genes Dev. 2011;25(6):634-45.

74. Feng GS. Conflicting roles of molecules in hepatocarcinogenesis: paradigm or paradox. Cancer Cell. 2012;21(2):150-4.

75. He R, Zeng LF, He Y, Zhang S, Zhang ZY. Small molecule tools for functional interrogation of protein tyrosine phosphatases. FEBS J. 2013;280(2):731-50.

76. Zhang ZY. Drugging the Undruggable: Therapeutic Potential of Targeting Protein Tyrosine Phosphatases. Acc Chem Res. 2017;50(1):122-9.

77. Chen YN, LaMarche MJ, Chan HM, Fekkes P, Garcia-Fortanet J, Acker MG, Antonakos B, Chen CH, Chen Z, Cooke VG, Dobson JR, Deng Z, Fei F, Firestone B, Fodor M, Fridrich C, Gao H, Grunenfelder D, Hao HX, Jacob J, Ho S, Hsiao K, Kang ZB, Karki R, Kato M, Larrow J, La Bonte LR, Lenoir F, Liu G, Liu S, Majumdar D, Meyer MJ, Palermo M, Perez L, Pu M, Price E, Quinn C, Shakya S, Shultz MD, Slisz J, Venkatesan K, Wang P, Warmuth M, Williams S, Yang G, Yuan J, Zhang JH, Zhu P, Ramsey T, Keen NJ, Sellers WR, Stams T, Fortin PD. Allosteric inhibition of SHP2 phosphatase inhibits cancers driven by receptor tyrosine kinases. Nature. 2016;535(7610):148-52.

78. Garcia Fortanet J, Chen CH, Chen YN, Chen Z, Deng Z, Firestone B, Fekkes P, Fodor M, Fortin PD, Fridrich C, Grunenfelder D, Ho S, Kang ZB, Karki R, Kato M, Keen N, LaBonte LR, Larrow J, Lenoir F, Liu G, Liu S, Lombardo F, Majumdar D, Meyer MJ, Palermo M, Perez L, Pu M, Ramsey T, Sellers WR, Shultz MD, Stams T, Towler C, Wang P, Williams SL, Zhang JH, LaMarche MJ. Allosteric Inhibition of SHP2: Identification of a Potent, Selective, and Orally Efficacious Phosphatase Inhibitor. J Med Chem. 2016;59(17):7773-82.

79. Nichols RJ, Haderk F, Stahlhut C, Schulze CJ, Hemmati G, Wildes D, Tzitzilonis C, Mordec K, Marquez A, Romero J, Hsieh T, Zaman A, Olivas V, McCoach C, Blakely CM, Wang Z, Kiss G, Koltun ES, Gill AL, Singh M, Goldsmith MA, Smith JAM, Bivona TG. RAS nucleotide cycling underlies the SHP2 phosphatase dependence of mutant BRAF-, NF1- and RAS-driven cancers. Nat Cell Biol. 2018;20(9):1064-73.

80. Ruess DA, Heynen GJ, Ciecielski KJ, Ai J, Berninger A, Kabacaoglu D, Gorgulu K, Dantes Z, Wormann SM, Diakopoulos KN, Karpathaki AF, Kowalska M, Kaya-Aksoy E, Song L, van der Laan EAZ, Lopez-Alberca MP, Nazare M, Reichert M, Saur D, Erkan MM, Hopt UT, Sainz B, Jr., Birchmeier W, Schmid RM, Lesina M, Algul H. Mutant KRAS-driven cancers depend on PTPN11/SHP2 phosphatase. Nat Med. 2018;24(7):954-60.

81. Hao HX, Wang H, Liu C, Kovats S, Velazquez R, Lu H, Pant B, Shirley M, Meyer MJ, Pu M, Lim J, Fleming M, Alexander L, Farsidjani A, LaMarche MJ, Moody S, Silver SJ, Caponigro G, Stuart DD, Abrams TJ, Hammerman PS, Williams J, Engelman JA, Goldoni S, Mohseni M. Tumor Intrinsic Efficacy by SHP2 and RTK Inhibitors in KRAS-Mutant Cancers. Mol Cancer Ther. 2019;18(12):2368-80.

82. Liu C, Lu H, Wang H, Loo A, Zhang X, Yang G, Kowal C, Delach S, Wang Y, Goldoni S, Hastings WD, Wong K, Gao H, Meyer MJ, Moody SE, LaMarche MJ, Engelman JA, Williams JA, Hammerman PS, Abrams TJ, Mohseni M, Caponigro G, Hao HX. Combinations with Allosteric SHP2 Inhibitor TNO155 to Block Receptor Tyrosine Kinase Signaling. Clin Cancer Res. 2021;27(1):342-54.

83. Dardaei L, Wang HQ, Singh M, Fordjour P, Shaw KX, Yoda S, Kerr G, Yu K, Liang J, Cao Y, Chen Y, Lawrence MS, Langenbucher A, Gainor JF, Friboulet L, Dagogo-Jack I, Myers DT, Labrot E, Ruddy D, Parks M, Lee D, DiCecca RH, Moody S, Hao H, Mohseni M, LaMarche M, Williams J, Hoffmaster K, Caponigro G, Shaw AT, Hata AN, Benes CH, Li F, Engelman JA. SHP2 inhibition restores sensitivity in ALK-rearranged non-small-cell lung cancer resistant to ALK inhibitors. Nat Med. 2018;24(4):512-7.

84. Wong GS, Zhou J, Liu JB, Wu Z, Xu X, Li T, Xu D, Schumacher SE, Puschhof J, McFarland J, Zou C, Dulak A, Henderson L, Xu P, O'Day E, Rendak R, Liao WL, Cecchi F, Hembrough T, Schwartz S, Szeto C, Rustgi AK, Wong KK, Diehl JA, Jensen K, Graziano F, Ruzzo A, Fereshetian S, Mertins P, Carr SA, Beroukhim R, Nakamura K, Oki E, Watanabe M, Baba H, Imamura Y, Catenacci D, Bass AJ. Targeting wild-type KRAS-amplified gastroesophageal cancer through combined MEK and SHP2 inhibition. Nat Med. 2018;24(7):968-77.

85. Lu H, Liu C, Velazquez R, Wang H, Dunkl LM, Kazic-Legueux M, Haberkorn A, Billy E, Manchado E, Brachmann SM, Moody SE, Engelman JA, Hammerman PS, Caponigro G, Mohseni M, Hao HX. SHP2 Inhibition Overcomes RTK-Mediated Pathway Reactivation in KRAS-Mutant Tumors Treated with MEK Inhibitors. Mol Cancer Ther. 2019;18(7):1323-34.

86. Zhao M, Guo W, Wu Y, Yang C, Zhong L, Deng G, Zhu Y, Liu W, Gu Y, Lu Y, Kong L, Meng X, Xu Q, Sun Y. SHP2 inhibition triggers anti-tumor immunity and synergizes with PD-1 blockade. Acta Pharm Sin B. 2019;9(2):304-15.

87. Ramesh A, Kumar S, Nandi D, Kulkarni A. CSF1R- and SHP2-Inhibitor-Loaded Nanoparticles Enhance Cytotoxic Activity and Phagocytosis in Tumor-Associated Macrophages. Adv Mater. 2019;31(51):e1904364.

88. Quintana E, Schulze CJ, Myers DR, Choy TJ, Mordec K, Wildes D, Shifrin NT, Belwafa A, Koltun ES, Gill AL, Singh M, Kelsey S, Goldsmith MA, Nichols R, Smith JAM. Allosteric Inhibition of SHP2 Stimulates Antitumor Immunity by Transforming the Immunosuppressive Environment. Cancer Res. 2020;80(13):2889-902.

89. Migliore C, Giordano S. Molecular cancer therapy: can our expectation be MET? Eur J Cancer. 2008;44(5):641-51.

90. Tavian D, De Petro G, Benetti A, Portolani N, Giulini SM, Barlati S. u-PA and c-MET mRNA expression is co-ordinately enhanced while hepatocyte growth factor mRNA is down-regulated in human hepatocellular carcinoma. Int J Cancer. 2000;87(5):644-9.

91. Osada S, Kanematsu M, Imai H, Goshima S. Clinical significance of serum HGF and c-Met expression in tumor tissue for evaluation of properties and treatment of hepatocellular carcinoma. Hepatogastroenterology. 2008;55(82-83):544-9.

92. Daveau M, Scotte M, Francois A, Coulouarn C, Ros G, Tallet Y, Hiron M, Hellot MF, Salier JP. Hepatocyte growth factor, transforming growth factor alpha, and their receptors as combined markers of prognosis in hepatocellular carcinoma. Mol Carcinog. 2003;36(3):130-41.

93. Kaposi-Novak P, Lee JS, Gomez-Quiroz L, Coulouarn C, Factor VM, Thorgeirsson SS. Met-regulated expression signature defines a subset of human hepatocellular carcinomas with poor prognosis and aggressive phenotype. J Clin Invest. 2006;116(6):1582-95.

94. Wang R, Ferrell LD, Faouzi S, Maher JJ, Bishop JM. Activation of the Met receptor by cell attachment induces and sustains hepatocellular carcinomas in transgenic mice. J Cell Biol. 2001;153(5):1023-34.

95. Marx-Stoelting P, Borowiak M, Knorpp T, Birchmeier C, Buchmann A, Schwarz M. Hepatocarcinogenesis in mice with a conditional knockout of the hepatocyte growth factor receptor c-Met. Int J Cancer. 2009;124(8):1767-72.

96. Decaens T, Barone C, Assenat E, Wermke M, Fasolo A, Merle P, Blanc JF, Grando V, Iacobellis A, Villa E, Trojan J, Straub J, Bruns R, Berghoff K, Scheele J, Raymond E, Faivre S. Phase 1b/2 trial of tepotinib in sorafenib pretreated advanced hepatocellular carcinoma with MET overexpression. Br J Cancer. 2021;125(2):190-9.

97. Ryoo BY, Cheng AL, Ren Z, Kim TY, Pan H, Rau KM, Choi HJ, Park JW, Kim JH, Yen CJ, Lim HY, Zhou D, Straub J, Scheele J, Berghoff K, Qin S. Randomised Phase 1b/2 trial of tepotinib vs sorafenib in Asian patients with advanced hepatocellular carcinoma with MET overexpression. Br J Cancer. 2021;125(2):200-8.

98. Kubo M, Hanada T, Yoshimura A. Suppressors of cytokine signaling and immunity. Nat Immunol. 2003;4(12):1169-76.

99. Bergamin E, Wu J, Hubbard SR. Structural basis for phosphotyrosine recognition by suppressor of cytokine signaling-3. Structure. 2006;14(8):1285-92.

100. Rui L, Yuan M, Frantz D, Shoelson S, White MF. SOCS-1 and SOCS-3 block insulin signaling by ubiquitin-mediated degradation of IRS1 and IRS2. J Biol Chem. 2002;277(44):42394-8.

101. Nicholson SE, De Souza D, Fabri LJ, Corbin J, Willson TA, Zhang JG, Silva A, Asimakis M, Farley A, Nash AD, Metcalf D, Hilton DJ, Nicola NA, Baca M. Suppressor of cytokine signaling-3 preferentially binds to the SHP-2-binding site on the shared cytokine receptor subunit gp130. Proc Natl Acad Sci U S A. 2000;97(12):6493-8.

102. Schmitz J, Weissenbach M, Haan S, Heinrich PC, Schaper F. SOCS3 exerts its inhibitory function on interleukin-6 signal transduction through the SHP2 recruitment site of gp130. J Biol Chem. 2000;275(17):12848-56.

103. De Souza D, Fabri LJ, Nash A, Hilton DJ, Nicola NA, Baca M. SH2 domains from suppressor of cytokine signaling-3 and protein tyrosine phosphatase SHP-2 have similar binding specificities. Biochemistry. 2002;41(29):9229-36.

104. Forrai A, Boyle K, Hart AH, Hartley L, Rakar S, Willson TA, Simpson KM, Roberts AW, Alexander WS, Voss AK, Robb L. Absence of suppressor of cytokine signalling 3 reduces self-renewal and promotes differentiation in murine embryonic stem cells. Stem Cells. 2006;24(3):604-14.

105. Riehle KJ, Campbell JS, McMahan RS, Johnson MM, Beyer RP, Bammler TK, Fausto N. Regulation of liver regeneration and hepatocarcinogenesis by suppressor of cytokine signaling 3. J Exp Med. 2008;205(1):91-103.

106. Gui Y, Yeganeh M, Donates YC, Tobelaim WS, Chababi W, Mayhue M, Yoshimura A, Ramanathan S, Saucier C, Ilangumaran S. Regulation of MET receptor tyrosine kinase signaling by suppressor of cytokine signaling 1 in hepatocellular carcinoma. Oncogene. 2015;34(46):5718-28.

107. Chen X, Calvisi DF. Hydrodynamic transfection for generation of novel mouse models for liver cancer research. Am J Pathol. 2014;184(4):912-23.

108. Thorpe LM, Yuzugullu H, Zhao JJ. PI3K in cancer: divergent roles of isoforms, modes of activation and therapeutic targeting. Nat Rev Cancer. 2015;15(1):7-24.

109. Wang C, Che L, Hu J, Zhang S, Jiang L, Latte G, Demartis MI, Tao J, Gui B, Pilo MG, Ribback S, Dombrowski F, Evert M, Calvisi DF, Chen X. Activated mutant forms of PIK3CA cooperate with RasV12 or c-Met to induce liver tumour formation in mice via AKT2/mTORC1 cascade. Liver Int. 2016;36(8):1176-86.

110. Gao C, Xiao G, Hu J. Regulation of Wnt/beta-catenin signaling by posttranslational modifications. Cell Biosci. 2014;4(1):13.

111. Lu X, Qu CK, Shi ZQ, Feng GS. Downregulation of platelet-derived growth factor receptor-beta in Shp-2 mutant fibroblast cell lines. Oncogene. 1998;17(4):441-8.

112. Zhu HH, Ji K, Alderson N, He Z, Li S, Liu W, Zhang DE, Li L, Feng GS. Kit-Shp2-Kit signaling acts to maintain a functional hematopoietic stem and progenitor cell pool. Blood. 2011;117(20):5350-61.

113. Zeller KI, Jegga AG, Aronow BJ, O'Donnell KA, Dang CV. An integrated database of genes responsive to the Myc oncogenic transcription factor: identification of direct genomic targets. Genome Biol. 2003;4(10):R69.

114. Boutros R, Lobjois V, Ducommun B. CDC25 phosphatases in cancer cells: key players? Good targets? Nat Rev Cancer. 2007;7(7):495-507.

115. Junttila MR, Evan GI. p53--a Jack of all trades but master of none. Nat Rev Cancer. 2009;9(11):821-9.

116. Huen MS, Sy SM, Chen J. BRCA1 and its toolbox for the maintenance of genome integrity. Nat Rev Mol Cell Biol. 2010;11(2):138-48.

117. Jeong WJ, Yoon J, Park JC, Lee SH, Lee SH, Kaduwal S, Kim H, Yoon JB, Choi KY. Ras stabilization through aberrant activation of Wnt/beta-catenin signaling promotes intestinal tumorigenesis. Sci Signal. 2012;5(219):ra30.

118. Wang LX, Zhang SX, Wu HJ, Rong XL, Guo J. M2b macrophage polarization and its roles in diseases. J Leukoc Biol. 2019;106(2):345-58.

119. Kitade H, Sawamoto K, Nagashimada M, Inoue H, Yamamoto Y, Sai Y, Takamura T, Yamamoto H, Miyamoto K, Ginsberg HN, Mukaida N, Kaneko S, Ota T. CCR5 plays a critical role in obesity-induced adipose tissue inflammation and insulin resistance by regulating both macrophage recruitment and M1/M2 status. Diabetes. 2012;61(7):1680-90.

120. Weiss M, Byrne AJ, Blazek K, Saliba DG, Pease JE, Perocheau D, Feldmann M, Udalova IA. IRF5 controls both acute and chronic inflammation. Proc Natl Acad Sci U S A. 2015;112(35):11001-6.

121. Halama N, Zoernig I, Berthel A, Kahlert C, Klupp F, Suarez-Carmona M, Suetterlin T, Brand K, Krauss J, Lasitschka F, Lerchl T, Luckner-Minden C, Ulrich A, Koch M, Weitz J, Schneider M, Buechler MW, Zitvogel L, Herrmann T, Benner A, Kunz C, Luecke S, Springfeld C, Grabe N, Falk CS, Jaeger D. Tumoral Immune Cell Exploitation in Colorectal Cancer Metastases Can Be Targeted Effectively by Anti-CCR5 Therapy in Cancer Patients. Cancer Cell. 2016;29(4):587-601.

122. Lee J, Liao R, Wang G, Yang BH, Luo X, Varki NM, Qiu SJ, Ren B, Fu W, Feng GS. Preventive Inhibition of Liver Tumorigenesis by Systemic Activation of Innate Immune Functions. Cell Rep. 2017;21(7):1870-82.

123. Wen L, Xin B, Wu P, Lin CH, Peng C, Wang G, Lee J, Lu LF, Feng GS. An Efficient Combination Immunotherapy for Primary Liver Cancer by Harmonized Activation of Innate and Adaptive Immunity in Mice. Hepatology. 2019;69(6):2518-32.

124. Xin B, Yang M, Wu P, Du L, Deng X, Hui E, Feng GS. Enhancing the therapeutic efficacy of programmed death ligand 1 antibody for metastasized liver cancer by overcoming hepatic immunotolerance in mice. Hepatology. 2021.

125. Liu JJ, Li Y, Chen WS, Liang Y, Wang G, Zong M, Kaneko K, Xu R, Karin M, Feng GS. Shp2 deletion in hepatocytes suppresses hepatocarcinogenesis driven by oncogenic beta-Catenin, PIK3CA and MET. J Hepatol. 2018;69(1):79-88.

126. Chen WS, Liang Y, Zong M, Liu JJ, Kaneko K, Hanley KL, Zhang K, Feng GS. Single-cell transcriptomics reveals opposing roles of Shp2 in Myc-driven liver tumor cells and microenvironment. Cell Rep. 2021;37(6):109974.

127. Mainardi S, Mulero-Sanchez A, Prahallad A, Germano G, Bosma A, Krimpenfort P, Lieftink C, Steinberg JD, de Wit N, Goncalves-Ribeiro S, Nadal E, Bardelli A, Villanueva A, Bernards R. SHP2 is required for growth of KRAS-mutant non-small-cell lung cancer in vivo. Nat Med. 2018;24(7):961-7.

128. Valencia-Sama I, Ladumor Y, Kee L, Adderley T, Christopher G, Robinson CM, Kano Y, Ohh M, Irwin MS. NRAS Status Determines Sensitivity to SHP2 Inhibitor Combination Therapies Targeting the RAS-MAPK Pathway in Neuroblastoma. Cancer Res. 2020;80(16):3413-23.

129. Ahmed TA, Adamopoulos C, Karoulia Z, Wu X, Sachidanandam R, Aaronson SA, Poulikakos PI. SHP2 Drives Adaptive Resistance to ERK Signaling Inhibition in Molecularly Defined Subsets of ERK-Dependent Tumors. Cell Rep. 2019;26(1):65-78 e5.

130. Hui E, Cheung J, Zhu J, Su X, Taylor MJ, Wallweber HA, Sasmal DK, Huang J, Kim JM, Mellman I, Vale RD. T cell costimulatory receptor CD28 is a primary target for PD-1-mediated inhibition. Science. 2017;355(6332):1428-33.

131. Wang B, Zhang W, Jankovic V, Golubov J, Poon P, Oswald EM, Gurer C, Wei J, Ramos I, Wu Q, Waite J, Ni M, Adler C, Wei Y, Macdonald L, Rowlands T, Brydges S, Siao J, Poueymirou W, MacDonald D, Yancopoulos GD, Sleeman MA, Murphy AJ, Skokos D. Combination cancer immunotherapy targeting PD-1 and GITR can rescue CD8(+) T cell dysfunction and maintain memory phenotype. Sci Immunol. 2018;3(29).

132. Seki E, De Minicis S, Gwak GY, Kluwe J, Inokuchi S, Bursill CA, Llovet JM, Brenner DA, Schwabe RF. CCR1 and CCR5 promote hepatic fibrosis in mice. J Clin Invest. 2009;119(7):1858-70.

133. Barashi N, Weiss ID, Wald O, Wald H, Beider K, Abraham M, Klein S, Goldenberg D, Axelrod J, Pikarsky E, Abramovitch R, Zeira E, Galun E, Peled A. Inflammation-induced hepatocellular carcinoma is dependent on CCR5 in mice. Hepatology. 2013;58(3):1021-30.

134. Ganju RK, Brubaker SA, Chernock RD, Avraham S, Groopman JE. Beta-chemokine receptor CCR5 signals through SHP1, SHP2, and Syk. J Biol Chem. 2000;275(23):17263-8.

135. Tao B, Jin W, Xu J, Liang Z, Yao J, Zhang Y, Wang K, Cheng H, Zhang X, Ke Y. Myeloid-specific disruption of tyrosine phosphatase Shp2 promotes alternative activation of macrophages and predisposes mice to pulmonary fibrosis. J Immunol. 2014;193(6):2801-11.

136. Xiao P, Zhang H, Zhang Y, Zheng M, Liu R, Zhao Y, Zhang X, Cheng H, Cao Q, Ke Y. Phosphatase Shp2 exacerbates intestinal inflammation by disrupting macrophage responsiveness to interleukin-10. J Exp Med. 2019;216(2):337-49.

137. Wang S, Yao Y, Li H, Zheng G, Lu S, Chen W. Tumor-associated macrophages (TAMs) depend on Shp2 for their anti-tumor roles in colorectal cancer. Am J Cancer Res. 2019;9(9):1957-69.

138. Li M, Sun X, Zhao J, Xia L, Li J, Xu M, Wang B, Guo H, Yu C, Gao Y, Wu H, Kong X, Xia Q. CCL5 deficiency promotes liver repair by improving inflammation resolution and liver regeneration through M2 macrophage polarization. Cell Mol Immunol. 2020;17(7):753-64.

139. Chen X, Calvisi DF. Hydrodynamic transfection for generation of novel mouse models for liver cancer research. Am J Pathol. 2014;184(4):912-23.

140. Soares KC, Foley K, Olino K, Leubner A, Mayo SC, Jain A, Jaffee E, Schulick RD, Yoshimura K, Edil B, Zheng L. A preclinical murine model of hepatic metastases. J Vis Exp. 2014(91):51677.